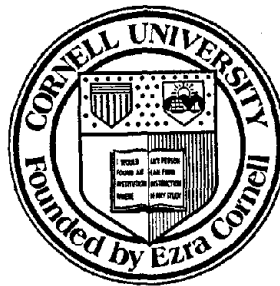


# Surface Faulting and Its Effect On Buried Pipelines

by

Michael A. McCaffrey

Thomas D. O'Rourke



Report to

National Science Foundation

Washington, DC

Grant Number CME 8022427

by

School of Civil and Environmental Engineering

Cornell University

Ithaca, New York

November, 1983

GEOTECHNICAL ENGINEERING REPORT 83-10



SURFACE FAULTING AND  
ITS EFFECT ON  
BURIED PIPELINES

by

Michael A. McCaffrey  
Thomas D. O'Rourke

Report to

National Science Foundation  
Washington, D. C.  
Grant Number CME 8022427

by

School of Civil and Environmental Engineering  
Cornell University  
Ithaca, New York  
November, 1983

Geotechnical Engineering  
Report 83-10

Any opinions, findings, conclusions  
or recommendations expressed in this  
publication are those of the author(s)  
and do not necessarily reflect the views  
of the National Science Foundation.



<b>REPORT DOCUMENTATION PAGE</b>		<b>1. REPORT NO.</b> NSF/CEE-83222	<b>2.</b>	<b>3. Recipient's Accession No.</b> PB84 15283 4
<b>4. Title and Subtitle</b> Surface Faulting and Its Effect on Buried Pipelines			<b>5. Report Date</b> November 1983	
<b>7. Author(s)</b> M.A. McCaffrey, T.D. O'Rourke			<b>6.</b>	
<b>9. Performing Organization Name and Address</b> Cornell University School of Civil and Environmental Engineering Ithaca, NY 14853			<b>8. Performing Organization Rept. No.</b> Geotech. Eng. 83-10	
<b>12. Sponsoring Organization Name and Address</b> Directorate for Engineering (ENG) National Science Foundation 1800 G Street, N.W. Washington, DC 20550			<b>10. Project/Task/Work Unit No.</b>	
			<b>11. Contract(C) or Grant(G) No.</b> (C) (G) CEE8022427	
<b>15. Supplementary Notes</b>			<b>13. Type of Report &amp; Period Covered</b>	
<b>16. Abstract (Limit: 200 words)</b> Results are presented of a study undertaken to evaluate the ground movements associated with various types of faulting and to assess the response of pipelines to these fault movements. Fault types and the patterns and dimensions of surface ruptures that occur during an earthquake are described. Correlations are developed between surface fault rupture length, maximum displacement, and earthquake magnitude. Historic strike-slip faulting in the United States is investigated and the relation between strike-slip faults and global plate boundaries is discussed. The effects of surface faulting on gas distribution and transmission pipelines during the 1971 San Fernando earthquake are examined. It is concluded that surface faulting is not likely to occur at earthquake magnitudes less than 5.5. Coseismic slip is said to be the most damaging type of movement for buried pipelines because it allows little chance for stress relaxation or redistribution of soil pressures.			<b>14.</b>	
<b>17. Document Analysis a. Descriptors</b>				
Pipelines Earthquakes Hazards		Displacement Earthquake resistant structures Dynamic structural response		
<b>b. Identifiers/Open-Ended Terms</b>				
Surface faulting San Fernando (California)		T.D. O'Rourke, /PI		
<b>c. COSATI Field/Group</b>				
<b>18. Availability Statement</b>		<b>19. Security Class (This Report)</b>		<b>21. No. of Pages</b>
NTIS		<b>20. Security Class (This Page)</b>		<b>22. Price</b>



## PREFACE

This report presents the results of research performed by Cornell University for the National Science Foundation (NSF) under Grant Number CME-8022427. The NSF Program Managers for this research were Drs. William Hakala, Chi Liu, and K. T. Thirumalai.

The main body of this report represents the M.S. Thesis research of Michael A. McCaffrey. Thomas D. O'Rourke of Cornell University was Principal Investigator for the research. Fred H. Kulhawy and Mircea D. Grigoriu were Associate Investigators, who assisted with and reviewed various aspects of the research investigations.



## ABSTRACT

Surface faulting is one of the most damaging types of earthquake-induced ground movement for buried pipelines. It is important to recognize the location, distribution, and potential maximum displacement associated with fault rupture, and the influence of this movement on buried pipelines crossing active faults.

Data on faults and surface fault rupture were obtained from an extensive literature review in addition to discussions with researchers who had made field investigations of surface rupture events. Correlations between fault rupture length, maximum displacement, and Richter magnitude were developed from these data. Pipeline response to fault creep was studied by means of a statistical evaluation of repair records for water distribution pipelines crossing and adjacent to the Hayward fault. In addition, a detailed investigation of pipeline performance in zones of reverse faulting during the 1971 San Fernando earthquake was made.

Linear regression analyses performed in this work provide a means of estimating surface rupture length and maximum displacement on the basis of earthquake magnitude. The linear regressions with the highest degree of statistical significance pertain to strike-

slip faulting, whereas those with the lowest statistical significance pertain to reverse faulting.

The distribution of strike-slip fault displacement was investigated for several earthquakes. The distribution of movements along the length of faulting was found to be skewed, and a model was developed to approximate this distribution. For purposes of analysis, coseismic slip can be modeled as an abrupt planar displacement. This modeling assumption is consistent with the worst field conditions, and generally will provide for a moderate degree of conservatism in the analysis.

A hyperbolic function was found to provide a good representation of the pattern of ground displacement across zones of fault creep. Using this function, recurrence intervals for damage to a cast iron pipeline were estimated at 18 to 73 years.

The highest concentration of pipeline damage during the 1971 San Fernando earthquake occurred within zones of fault displacement. Sixty-seven percent of the length of gas distribution pipelines within the Sylmar segment of the San Fernando fault zone was replaced. Based partially on field observations, a simplified model is proposed for choosing the optimal orientation of a pipeline intersecting a reverse-oblique fault.

## ACKNOWLEDGMENTS

The help and advice from Professors Ta Liang, Fred H. Kulhawy and Mircea D. Grigoriu of Cornell University are sincerely appreciated. Charles Trautmann and Jared Nedzel assisted the authors during the collection of data and references. The typing was done by Lorraine Donley and Marie Jones. Figures were drafted by the late Bill Sawbridge, and by Fong Lan Lin and Ali Avcisoy.

Many individuals gave their time, and shared data and comments during the course of this study. Thanks are extended to several people in the following organizations:

### Southern California Gas Company

D. Buchanan  
J. L. LePire  
M. Jones  
J. D. McNorgan  
J. E. Streich

### East Bay Municipal Utility District

W. B. Bode  
R. L. Kolm

### Alameda County Water District

C. N. Hill

### City of Hayward Water Department

L. R. Blair

### U.S. Geological Survey

M. G. Bonilla  
R. O. Burford  
M. M. Clark  
R. D. Nason  
R. V. Sharp

California Division of Mines and Geology

E. W. Hart

Woodward-Clyde Consultants of San Francisco

P. Kneugher  
D. P. Schwartz  
B. Swan  
C. L. Taylor

Agbabian Associates

R. T. Eguchi

California Institute of Technology

B. Kamb

## TABLE OF CONTENTS

	Page
PREFACE . . . . .	1
ABSTRACT. . . . .	ii
ACKNOWLEDGMENTS . . . . .	iv
TABLE OF CONTENTS . . . . .	vi
LIST OF TABLES. . . . .	viii
LIST OF FIGURES . . . . .	ix
LIST OF SYMBOLS . . . . .	xii
CHAPTER 1 INTRODUCTION . . . . .	1
1.1 Background. . . . .	1
1.2 Objectives. . . . .	6
1.3 Scope . . . . .	8
CHAPTER 2 CHARACTERISTICS OF SURFACE FAULTING. . . . .	11
2.1 Background. . . . .	11
2.2 Fault Types . . . . .	15
2.3 Distribution of Faulting. . . . .	22
2.4 Fault Length. . . . .	27
2.5 Fault Displacement. . . . .	32
2.6 Correlations Between Fault Length, Maximum Displacement, and Earthquake Magnitude . . . . .	33
2.6.1 Correlation of Fault Length and Earthquake Magnitude. . . . .	41
2.6.2 Correlation of Maximum Fault Dis- placement and Earthquake Magnitude. . . . .	48
2.6.3 Discussion of Fault Analyses. . . . .	55
2.7 Summary . . . . .	60
CHAPTER 3 STRIKE-SLIP FAULTING . . . . .	62
3.1 Tectonic Mechanism. . . . .	62
3.2 Geomorphology . . . . .	69
3.3 Fault Creep . . . . .	73

	Page
3.4 Distribution of Displacement. . . . .	75
3.4.1 Distribution of Displacement Along the Length of Surface Faulting. . . . .	76
3.4.2 Distribution of Displacement Across the Width of Surface Faulting . . . . .	84
3.5 Location of Fault Movement. . . . .	94
3.6 Summary . . . . .	97
CHAPTER 4 BURIED PIPELINE RESPONSE TO CREEP. . . . .	99
4.1 Introduction. . . . .	99
4.2 Pipeline Repair . . . . .	102
4.3 Modeling of Pipeline Response to Creep. . . . .	109
4.4 Summary . . . . .	115
CHAPTER 5 BURIED PIPELINE RESPONSE TO FAULTING DURING THE 1971 SAN FERNANDO EARTHQUAKE. . . . .	117
5.1 Introduction. . . . .	117
5.2 Pattern of Surface Faulting and Pipeline Damage . . . . .	120
5.3 Pipeline Repairs Relative to the Fault Zone Centerline . . . . .	126
5.4 Performance of Gas Transmission Pipelines . . . . .	130
5.5 Detailed Observation of Pipeline and Ground Deformation. . . . .	134
5.6 Effects of Pipeline Orientation . . . . .	142
5.7 Summary . . . . .	146
CHAPTER 6 CONCLUSIONS. . . . .	149
6.1 Characteristics of Surface Faulting . . . . .	149
6.2 Strike-Slip Faulting. . . . .	154
6.3 Long-Term Performance of Pipelines in Areas of Fault Creep . . . . .	157
6.4 Pipeline Response to Reverse Faulting. . . . .	159
REFERENCES. . . . .	163

## LIST OF TABLES

Table Number		Page
2.1	Summary of historic surface faulting information	36
2.2	Linear regressions for fault displacement data	56
2.3	Summary of maximum predicted displacements for strike-slip faults	58
3.1	Summary of geomorphic features associated with strike-slip faults	72
3.2	Summary of observed displacements for four surface faulting events	81
3.3	Fractions of maximum fault displacement associated with various fractions of surface fault length	83
5.1	Summary of information for gas transmission pipelines	131

## LIST OF FIGURES

Figure Number		Page
2.1	Block diagrams of fault types	18
2.2	Components of fault displacement for normal and reverse faults	19
2.3	Fault types defined by slip direction in the fault plane	21
2.4	Distribution of fault ruptures	23
2.5	Plot of fault length vs. magnitude	31
2.6	Plot of fault displacement vs. magnitude	34
2.7	Plot of length vs. magnitude for strike- slip faults	43
2.8	Plot of length vs. magnitude for normal and normal-oblique faults	44
2.9	Plot of length vs. magnitude for reverse and reverse-oblique faults	45
2.10	Plot of fault length vs. magnitude for strike-slip faults	47
2.11	Plot of fault length vs. magnitude for normal and normal-oblique faults	47
2.12	Plot of displacement vs. magnitude for strike-slip faults	49
2.13	Plot of displacement vs. magnitude for normal and normal-oblique faults	50
2.14	Plot of displacement vs. magnitude for reverse and reverse-oblique faults	51
2.15	Plot of fault displacement vs. magnitude for strike-slip faults	54
2.16	Plot for fault displacement vs. magni- tude for normal and normal-oblique faults	54

Figure Number		Page
3.1	Map showing global seismicity for the year 1966	63
3.2	Major faults in California and locations of historic surface rupture	66
3.3	Sketch map of northwestern North America showing major tectonic features along Pacific-North American plate boundary	67
3.4	Geomorphic features developed along active strike-slip faults	72
3.5	Plots of fractions of maximum fault displacement vs. fractions of surface fault length, comparing field observations with displacement model	78
3.6	Relation of slip, shift, and distortion	87
3.7	Fractions of surface rupture length vs. width of main and branch ruptures for the 1968 Borrego Mountain earthquake rupture	89
3.8	Distribution of displacement across the San Andreas Fault, determined from fence offsets, after the 1906 San Francisco earthquake	91
3.9	Plot showing distribution of fault displacement based on pipeline offset measurements for the 1979 Imperial Valley strike slip displacement	93
4.1	Locations of creep observations along the Hayward fault	100
4.2	Repair frequency for 1961-1981 time interval, for the EBMUD study area	105
4.3	Creep displacement and pipeline damage on the Hayward fault	107
4.4	Pipeline repair locations for a typical section of the EBMUD water distribution system study area along the Hayward fault	108

Figure Number		Page
4.5	Analysis of displacements within zones of fault creep	111
5.1	Plan view of surface faulting and re-placed gas distribution pipelines	121
5.2	Plan view of repairs to gas distribution pipelines	125
5.3	Plot showing number of pipeline repairs as a function of distance from the fault zone	128
5.4	Plan view of breaks and explosion craters for gas transmission pipelines	132
5.5	Cross-sectional view of pipeline welds	135
5.6	Plan view of ground ruptures and pipeline damage in the eastern Sylmar segment	136
5.7	Plan view of ground ruptures and pipeline damage in the western Sylmar segment	139
5.8	Three and two-dimensional views of pipeline deformation from reverse faulting with strike slip movement	143
5.9	Optimal pipeline orientation as a function of the ratio of fault slip components for a reverse fault	145

## LIST OF SYMBOLS

Symbol	Description
A	Constant for linearly increasing function
a	Constant for the equation of a line
B	Constant for a decaying exponential function
b	Constant for the equation of a line
C	Slope of a line
D	Fault displacement
d	Outside diameter of pipe
$\bar{D}_E$	Average observed displacement
$\bar{D}_M$	Average modeled displacement
$D_{max}$	Maximum displacement
$K_m$	Maximum curvature imposed on a pipeline by fault displacement
L	Length of surface fault rupture
$z$	Minimum distance of fault rupture to point of maximum displacement
M	Earthquake Richter magnitude
$M_L$	Local magnitude
$M_S$	Surface wave magnitude
n	Number of data points in a population set
P	Probability that a predicted value will be exceeded
$r^2$	Coefficient of determination
S	Values of half fault offset

Symbol	Description
$S_d$	Dip-slip fault displacement
$S_h$	Thrust fault displacement (heave)
$S_m$	Half maximum fault offset
$S_s$	Strike-slip fault displacement
$S_v$	Vertical fault displacement (throw)
$S_{90}$	90% of half fault offset
$W$	Distance from fault centerline
$W_{90}$	90% of half effective fault width
$x$	Distance along a fault
%	Percent
$\alpha$	Inclination angle of fault plane
$\beta$	Angle of pipeline/fault intersection
$\epsilon_m$	Maximum pipeline tensile strain
$\phi$	Angle between fault strike and net slip fault displacement

## CHAPTER 1

### INTRODUCTION

#### 1.1 BACKGROUND

Pipeline systems are built up over a vast area, and their exposure to seismic hazards usually is greater than that of individual facilities occupying small areas. Active faults may be several hundred kilometers long so that it often is impossible to locate pipelines to avoid such hazards. For example, Los Angeles depends on natural gas piped in from oil fields in the Texas and the San Joaquin Valley and on water that is conveyed through pipelines from the Owens Valley and the Colorado and Feather Rivers (Tugend, 1980). Virtually all major lifelines for Los Angeles cross the San Andreas fault. A similar situation exists in the San Francisco Bay Area. An earthquake planning scenario prepared by the California Division of Mines and Geology (Davis, et al., 1982) points out that the City of San Francisco and a number of municipal utilities in San Mateo, Santa Clara, and Alameda counties receive water via the Hetch Hetchy Aqueduct, which crosses the Hayward fault. Major gas and petroleum transmission lines also cross portions

of the Hayward and San Andreas faults.

Surface faulting not only affects populated areas, but also influences the delivery of expensive raw commodities in remote locations. During construction of the Trans Alaska Pipeline, considerable effort was devoted to pipeline design at known fault crossings, such as the Denali fault. The Trans Alaska Pipeline System transports approximately \$50 million of oil per day (Oil and Gas Journal, 1980), and thus the expense of one day's downtime is significant.

Studies that summarize data from surface faulting events include those by Richter (1958), Bonilla (1967, 1970, 1979), Bonilla and Buchanan (1970), Slemmons (1977), and Taylor and Cluff (1977). Correlations between surface rupture length, displacement, and earthquake magnitude have been made by Bonilla (1967, 1970, 1982), Bonilla and Buchanan (1970), Krinitzsky (1974), Slemmons (1977, 1982), and Taylor and Cluff (1977).

Most correlations involving fault length, displacement, and earthquake magnitude have been developed from worldwide data. The use of observations from different tectonic settings assumes that the mechanisms of crustal displacement are sufficiently

consistent that a general grouping of data will lead to statistically meaningful results. This assumption may not apply in all cases. Moreover, the grouping of observations with different degrees of accuracy means that variation in the data generally increase as the observations are collected from increasingly widespread sources. It should be emphasized that correlations between fault displacement and magnitude apply only for maximum fault movement. The variations in displacement along the length and across the width of surface faults are not taken into account by such correlations.

It would be interesting to develop correlations between surface fault length, maximum displacement, and earthquake magnitude, based on a more select choice of data within a given regional setting. A relatively large number of historic faulting observations have been obtained for California and adjoining western U.S. states. These observations provide an opportunity to develop correlations for a regionally integrated set of earthquake mechanisms. Furthermore, they provide a data base for which earthquake magnitude and offset measurements are defined in a relatively consistent manner.

A close examination of the distribution of displacement along the length and across the width of surface fault rupture would help refine estimates of displacement and establish a basis for predicting fault offset in a statistically significant manner. Several cases, e.g., the 1857 Fort Tejon (Sieh, 1978), 1906 San Francisco (Lawson, et al., 1908), 1968 Borrego Mountain (Clark, 1972), and 1979 Imperial Valley (Sharp, et al., 1982) earthquakes, provide observations of displacement which are distributed at sufficiently small distances to obtain a good sense of the distribution of movement.

Studies of fault creep are an important supplement to the research on fault rupture. Areas of active creep coincide with zones of previous coseismic slip (e.g., Burford and Harsh, 1980 and Nason, 1971b) so that creep observations can provide a means of locating principal ruptures during future faulting events. The cumulative creep displacements over many years may be equivalent in magnitude to the rapid offset imposed by faulting. Accordingly, a systematic study of pipeline response to creep can help clarify aspects of pipeline response to coseismic slip and provide a better understanding of the maintenance re-

quirements and residual risk associated with pipelines influenced by creep.

Previous studies of pipeline response to creep are limited. The deformation and offset of two Hetch Hetchy Aqueduct pipelines from creep on the Hayward fault have been described by Cluff and Steinbrugge (1966). O'Rourke and Trautmann (1980a) discuss gas pipeline response to creep on the Calaveras fault. A study of pipeline system response to fault creep requires access to utility repair records for a large number of mains. The Hayward fault occurs in a highly populated area, where it is crossed by numerous pipelines over a relatively long distance. Accordingly, it is a good location for studies regarding the long-term performance of pipelines subject to fault creep.

The 1971 San Fernando earthquake represents one of the most important events with respect to earthquake damage to buried pipelines. Surface faulting, which occurred in only 0.5% of the area affected by strong ground shaking (Housner and Jennings, 1972), was a principal cause of pipeline damage (Moran and Duke, 1971). More than 2,400 breaks in pipelines were reported in areas of fault displacements (Steinbrugge, et al., 1971). This event provides an opportunity to

investigate how pipeline damage was distributed with respect to the location of fault movement, and to determine what orientations, soil conditions, and mechanical features had the most significant impact on performance. In addition, it provides an opportunity to study measures which may be taken to mitigate future earthquake damage to pipelines.

## 1.2 OBJECTIVES

Pipeline response to surface fault rupture depends on the type of fault movements, the amount and distribution of these movements, the orientation of the pipeline/fault intersection, and the type and size of pipeline. The aims of this study are to evaluate the ground movements associated with various types of faulting and to assess the response of pipelines to these fault movements. The four main objectives set to accomplish these goals, are to:

1. Describe the general characteristics of surface faulting. A study of 42 selected historic surface faulting events is used to correlate the length of surface faulting and maximum displacement with earthquake magnitude. The strike-slip and normal surface faulting events were selected from a

specific tectonic region of the U.S., encompassing the San Andreas fault system and the Basin and Range Province. These correlations are compared with those of other researchers, and their statistical features are summarized.

2. Evaluate the characteristics of strike-slip fault displacement from coseismic slip along the length and across the width of the main rupture zone. Special attention is devoted to the amount and distribution of fault displacement for siting of a pipeline/fault intersection.
3. Investigate long-term pipeline performance in areas of fault creep. Damage is studied for individual pipelines and pipeline systems subject to creep along the Hayward fault. Pipeline damage is evaluated with respect to distance from the fault trace centerline, length of time subjected to creep, and variation in pipe material. A limit on the maximum fault creep offset that can be tolerated by buried, flexible mains is derived. Recurrence intervals for pipeline

damage are estimated from the limit.

4. Summarize the characteristics of pipeline response to surface faulting during the 1971 San Fernando earthquake. Surface fault displacements are studied in detail and correlated with repairs to the gas distribution system and high pressure gas transmission lines. The optimal orientation of a pipeline intersected by a reverse-oblique fault is discussed.

### 1.3 SCOPE

This report is composed of six chapters, of which the first chapter presents background information and describes the objectives and scope of the study.

Chapter 2 describes fault types, and the patterns and dimensions of surface ruptures that occur during an earthquake. Correlations are developed between surface fault rupture length, maximum displacement, and earthquake magnitude.

Chapter 3 investigates historic strike-slip faulting in the U.S. The relation between strike-slip faults and global plate boundaries is discussed, as are the geomorphic features which are caused by repetitive fault movements. The distribution of dis-

placement along the length and across the width of surface rupture is investigated, and models are developed which represent these distributions.

In Chapter 4 the distribution of creep movements and the long-term performance of buried pipelines crossing the Hayward fault are discussed. Mathematical functions are derived representing both the pattern of displacements across zones of creep and limiting offsets for buried, small diameter pipelines.

Chapter 5 deals with the effects of surface faulting on gas distribution and transmission pipelines during the 1971 San Fernando earthquake. The zones of surface faulting are identified and the damage to buried pipelines relative to these zones are discussed. A model is presented for siting a pipeline in an area of potential reverse and strike slip displacement.

Chapter 6 presents the summary and conclusions. It establishes a basis for evaluating the length of surface fault rupture and maximum displacement relative to earthquake magnitude, as well as the distribution of displacement along the length and across the width of the main fault rupture zone. The principal features of pipeline response to creep along the

Hayward fault and coseismic slip during the 1971 San Fernando earthquake are summarized.

## CHAPTER 2

### CHARACTERISTICS OF SURFACE FAULTING

This chapter describes the types, patterns, and dimensions of surface ruptures caused by earthquake faulting. Fault types are identified on the basis of relative movements of opposite sides of the fault. A system by Bonilla (1967, 1970) is described for classifying the distribution of surface ruptures commonly observed during faulting. Correlations between both the length of surface rupture and maximum displacement with respect to earthquake magnitude are discussed. Correlations are developed for U.S. events of all fault types, with reverse faults supplemented by worldwide data.

#### 2.1 BACKGROUND

Permanent differential displacement of the earth's crust that produces a roughly planar rupture or rupture zone is referred to as faulting. The term, fault, was originally used in connection with coal mining (De La Beche, 1851), where an abrupt offset in a coal seam was encountered. Because the coal could not be mined at its anticipated location, the miners found themselves "at fault". Faults of this type were

often single, distinct planes within the rock mass, and general models for classification were developed on the basis of simple, planar features. Surface faulting during an earthquake frequently results in a complex system of fissures, compression ridges, and relative offsets. Although traditional methods of describing faults do not account for these patterns, they nevertheless provide a framework for distinguishing different types of faulting and for evaluating the overall directions and magnitudes of movement.

Sudden, crustal displacement during an earthquake is referred to as coseismic slip. Sudden displacements are the most damaging for pipelines and other buried structures. When movements develop quickly, there is little chance for gradual redistribution of soil pressures. Iida (1965) estimates that the length of time over which coseismic slip takes place may vary from a fraction of a second, in the smallest earthquakes, to about 10 seconds in the largest. Displacement from coseismic slip can account for all or part of the fault displacement. Movement that occurs subsequent to coseismic slip is referred to as afterslip. It is generally characterized by a gradually increasing displacement, at a logarithmically decreasing rate

(Bonnilla, 1982). The rate, however, can be temporarily accelerated by additional earthquake activity. The time during which afterslip occurs may vary from a few hours to several months.

Bonilla (1970) discusses post-earthquake creep, or afterslip, and points out that, in most instances, it represents only a fraction of the coseismic slip. Of the seven California earthquakes for which afterslip has been recorded, post-earthquake displacements have generally amounted to less than 30% of the coseismic slip. Only in the case of the 1966 Parkfield-Cholame earthquake did the afterslip exceed the coseismic movement. In this instance, an afterslip of 200 mm was measured over a period of twelve months, which represents 250% of the maximum coseismic displacement. Another instance of significant afterslip involves the 1976 Guatemala earthquake, after which 0.31 m of afterslip was measured over 20 months at a location where 0.60 m of coseismic displacement had occurred (Bucknam, Plafker, and Sharp, 1978).

Although surface faulting is less likely to occur as the magnitude of the earthquake decreases, there is no clear relationship between the occurrence of surface faulting and a threshold magnitude at which

faulting is initiated. Indeed, many significant earthquakes are not even accompanied by surface faulting. Twenty-one earthquake shocks with land-based epicenters and magnitudes greater than 6.0 were recorded in California between 1932 and 1972 (Hileman, Allen, and Nordquist, 1973 and Bolt and Miller, 1975). Of these, only five were associated with surface faulting. Krinitzsky (1974) points out that surface faulting rarely occurs when the earthquake magnitude is less than 5.4. Slemmons (1977) summarizes 87 worldwide events after which surface fault displacements were observed. Of these, eight were earthquakes of magnitude between 5.1 and 5.9. With one exception, the instances of surface faulting correlate with earthquake magnitudes greater than 5.0. The only exception is the 1966 Imperial Valley earthquake of magnitude 3.6, in which 15 mm of surface movement was recorded in an area where creep had previously been noted (Brune and Allen, 1967).

Creep involves very small, episodic fault movements that are not associated with afterslip or directly triggered by perceptible earthquake activity. They are often averaged over several years and expressed in terms of an annual rate of displacement at

a given location. Creep has been observed on the San Andreas fault (Burford and Harsh, 1980 and Steinbrugge, et al., 1960), the Imperial fault and Brawley fault zones (Cohn, et al., 1982), the Hayward fault (Radbruch and Bonilla, 1966), and the Calaveras fault (Armstrong and Wagner, 1980). Although creep occurs in small increments, the cumulative displacement over a period of years may cause substantial offsets, thereby affecting pipeline performance at some fault crossings. Creep will be discussed in the forthcoming chapter on strike-slip faults since it occurs predominantly on this fault type.

## 2.2 FAULT TYPES

Methods for classifying faults are described by Billings (1972), based on geometric relations and relative and absolute displacement. Relative displacement is the most commonly used means of classifying faults for engineering purposes. For example, Krinitsky (1974) and Slemmons (1977) define the principal types of faulting on this basis.

Models of fault displacement involve simplifying assumptions, the most important of which is that displacement is confined to a single plane. Although this method of visualizing fault movement does not ac-

count for the complex surface patterns that are often observed, it nevertheless sets an upper bound on the severity of deformation for a given magnitude of total offset. Because pipeline deformations will often be confined to a local area, rotational fault movement is not likely to have a significant influence on pipeline performance.

The orientation of a fault plane is described by the strike and dip of the plane. The direction, or bearing, of the line of intersection between a fault plane and the horizontal plane is the strike of the fault. The angle between the horizontal plane and a fault plane is the dip. A fault trace is the expression of a fault plane intersecting the ground surface.

A strike-slip fault is one in which the predominant component of slip is a horizontal displacement parallel to the fault plane. This type of displacement is called strike slip. Displacement of two formerly adjacent points on opposite sides of a fault define the direction of relative slip. If the opposite side of the fault is offset from right to left, the fault is left-lateral, whereas left to right offset is right-lateral.

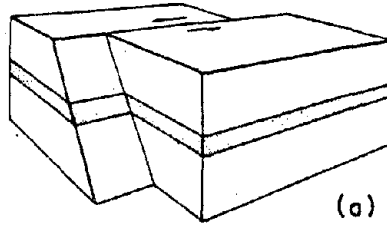
A reverse fault is one in which the side overlying the fault plane, or hanging wall, slips upward

relative to the side underlying the fault plane, or footwall. During reverse fault displacement, two formerly adjacent points on opposite sides of the fault are offset vertically and overlapped horizontally. The overlapping will result in compression or net shortening of a structure intersecting the fault. A thrust fault as defined by Billings (1972) is a reverse type fault with a dip of less than 45 degrees.

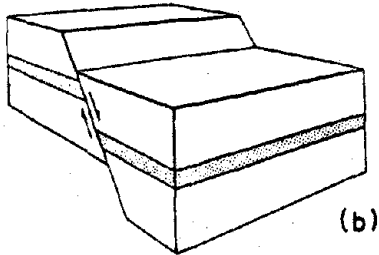
A normal fault is one in which the hanging wall has slipped downward relative to the footwall. During normal fault displacement, two formerly adjacent points on opposite sides of a fault are offset vertically and separated horizontally. The horizontal separation will subject a structure intersecting the fault to tension or net extension. Combinations of strike slip displacement with normal or reverse displacement are called normal-oblique or reverse-oblique faults, respectively. Diagrammatic sketches of fault types depicting their relative displacement across the fault plane are shown in Figure 2.1.

Fault displacements are subdivided into components of net slip, dip slip, and strike slip. Figure 2.2 shows the components of slip in block diagrams. Net slip is the total displacement, measured in the

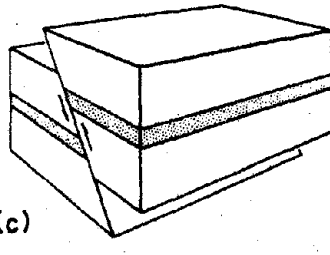
Strike slip fault  
(Left lateral)



Normal fault



Reverse fault

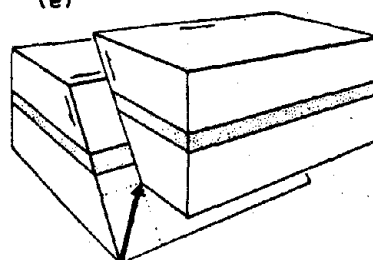
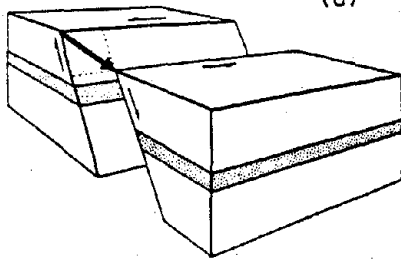


(b)

(c)

(d)

(e)



Left oblique normal fault

Left oblique reverse fault

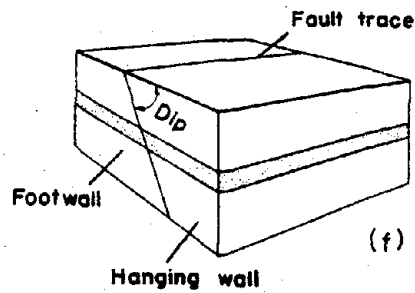


Figure 2.1. Block diagrams of fault types (modified from Clark & Hauge, 1977).

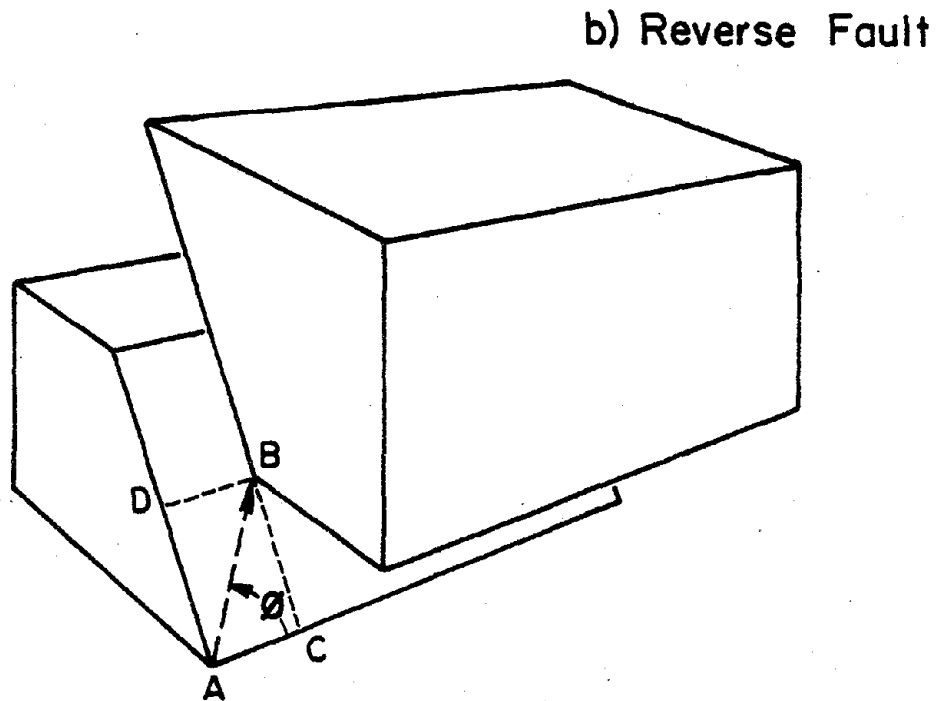
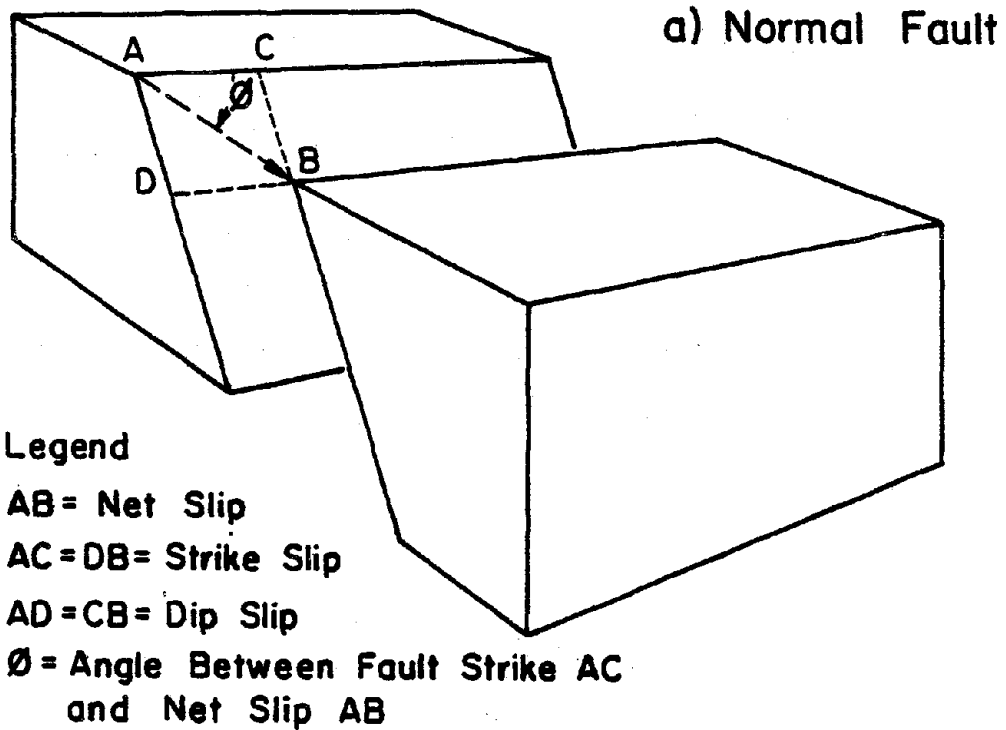


Figure 2.2. Components of fault displacement for normal and reverse faults.

fault plane, between two formerly adjacent points. Dip slip is the component of net slip parallel to the dip of the fault, and strike slip is the component of net slip parallel to the strike of the fault. The amount of horizontal overlapping or separation caused by fault displacement in the plane perpendicular to the fault is referred to as heave. The vertical offset measured in the same plane is referred to as throw.

Bonilla and Buchanan (1970) have classified fault types on the basis of direction and the ratio of strike to dip slip. Figure 2.3 represents the plane of a fault dipping toward the observer. Five fault types are denoted by letters A through E, designating the basic types of faults defined by Bonilla and Buchanan (1970): normal, reverse, strike-slip, normal-oblique, and reverse-oblique. Displacement by faulting of a point on the far side of the fault originally at the center of the circle, to the rim of the circle, produces the fault types indicated in the figure. The radial line generated by the displacement of the point makes an angle  $\phi$  with the strike of the fault. Figure 2.2 shows the measurement of  $\phi$  in the fault plane, measured between the net slip in the fault plane and

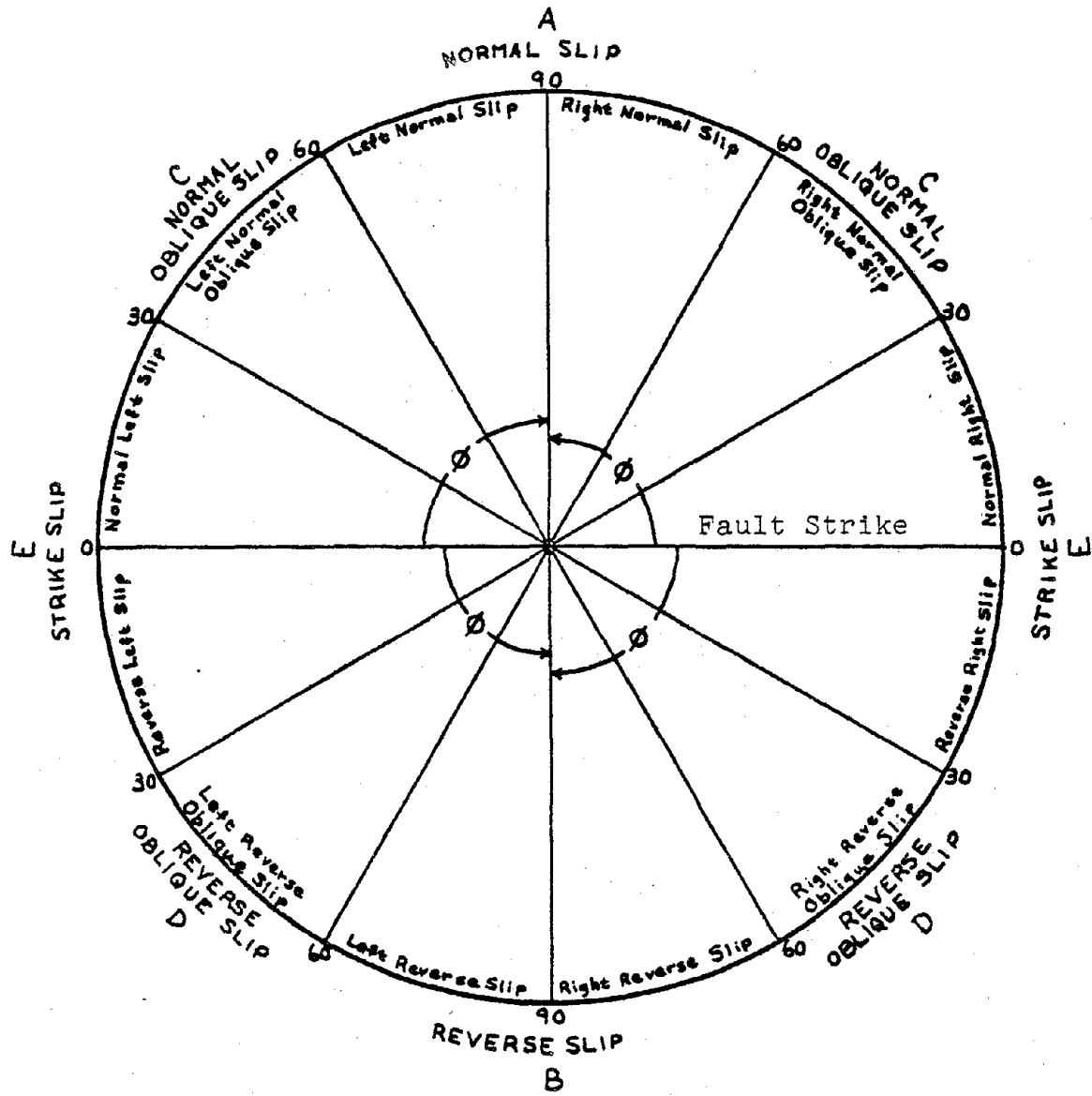


Figure 2.3. Fault types defined by slip direction in the fault plane (after Bonilla and Buchanan, 1970).

strike of the fault. The value  $\phi$  can be measured by striations on the fault plane indicating the net slip direction, or it can be calculated from values of strike slip, ( $S_s$ ), and dip slip, ( $S_d$ ), (Bonilla and Buchanan, 1970):

$$\text{cotangent } \phi = \frac{S_s}{S_d} \quad (2.1)$$

### 2.3 DISTRIBUTION OF FAULTING

Surface faulting may occur as a single narrow ground rupture, or as a complex pattern of ground ruptures forming a predominant rupture zone. The zone of principal movement may be accompanied by other ruptures at various distances and orientations from the main fault. The distribution of surface displacements will depend on the type and amount of main fault movement and on the geologic and topographic conditions surrounding the fault. Bonilla (1967, 1970) has proposed a system for classifying the distribution of ground ruptures associated with faulting. The system defines three categories or zones: the main fault zone (Zone I), zone of branch faults (Zone II), and zone of secondary faults (Zone III). A typical pattern of faulting is shown in Figure 2.4, which is used to

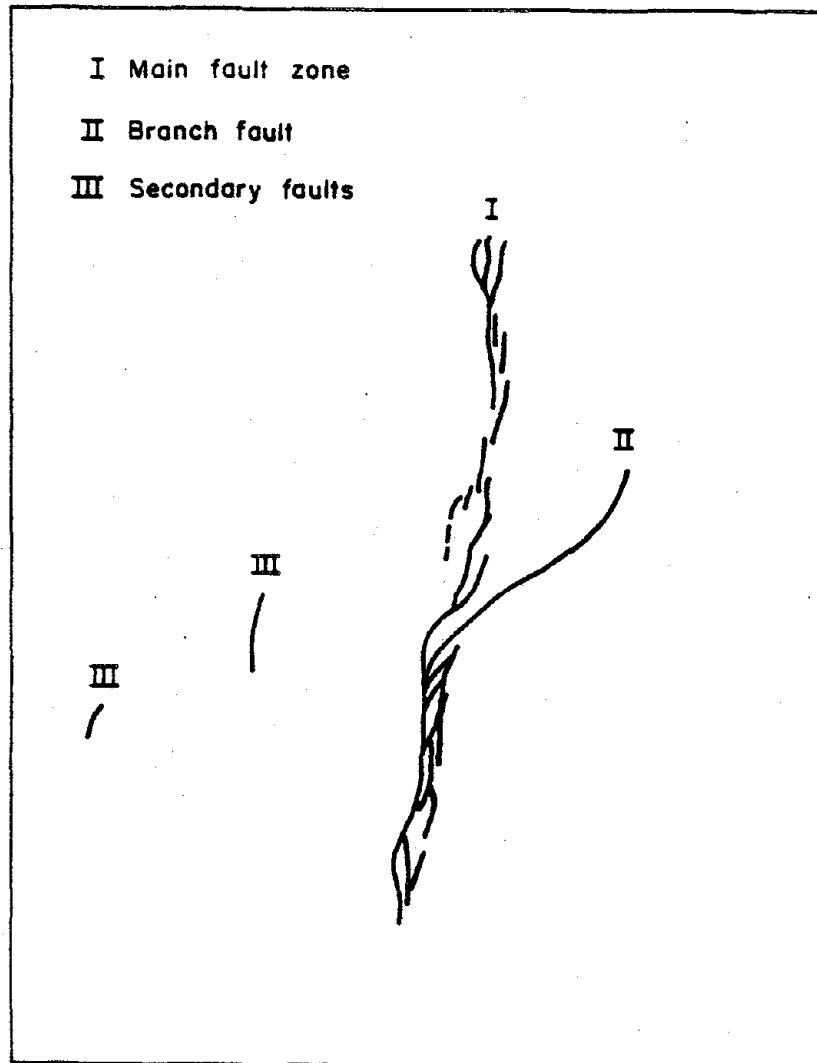


Figure 2.4. Distribution of fault ruptures (after Bonilla, 1967).

classify the various rupture zones.

The main fault is defined as the zone of ground breakage that predominates in terms of length, displacement, and continuity. Surface ruptures outside the main fault zone are regarded as subsidiary faults and include branch and secondary faults. Branch faults diverge from the main fault zone and extend a considerable distance from it. They intersect or can be inferred to intersect the main fault zone. Displacements are generally smaller, but of the same type, as those along the main zone and their lengths are shorter. Secondary faults do not intersect the main fault zone, and no inference regarding their intersection can be made. They usually are the same fault type, but smaller in terms of displacement and length, as the main fault zone.

In the case of reverse faulting, secondary faults may occur as normal faults on the upthrown block. These secondary features have been known to develop movements of comparable magnitude to those in the main fault zone. For example, the maximum scarp on the main reverse fault caused by the 1980 El-Asnam earthquake was 4.2 m, as compared with an ancillary normal fault scarp of 4 m (Leeds, 1983).

Of the more than 30 surface faulting events in North America studied by Bonilla (1967, 1970), at least half had subsidiary faulting, and in only about one-sixth of the events was there good evidence that subsidiary faulting did not occur. The cumulative length of all subsidiary faults, for 15 surface faulting events, ranged between about 5% and 95% of the length of the main fault. Of the nine normal faults included in the study, the cumulative lengths of subsidiary faults compared with the main fault length were 38%, as opposed to 7% for the five strike-slip faults.

Displacement on branch and secondary faults becomes smaller with increasing distance from the main fault zone. In general, strike-slip faults show the most rapid decay. Bonilla (1970) indicates that displacement on branch and secondary faults located more than 6 km from the main fault zone centerline is generally less than 20% of the main fault displacement.

The width of faulting as defined by Bonilla is the maximum distance from the centerline of the main zone to the outer edge of the main, branch, or secondary zone of faulting. The maximum width of the branch fault zone is 0.8 km for strike-slip faults and 2.6 km

to 4.8 km for normal and reverse faults. For secondary faults, the maximum width is 2.4 km for strike-slip faults, and 12.9 km to 13.7 km for normal and reverse faults.

Bonilla's system depends on the identification of the main fault zone. Main zone displacements on large, well-defined faults, such as the San Andreas fault, have occurred within relatively narrow boundaries. These zones have been easy to define, although variable widths have been observed for different earthquake magnitudes. For example, the principal displacements along the San Andreas fault were confined to zones with maximum widths of 60 m and 3 m for the 1906 San Francisco and 1966 Parkfield-Cholame earthquakes, respectively. In some cases, the zone of principal movement is virtually impossible to distinguish. Four distinct, subparallel surface faults were associated with the 1972 Managua earthquake, with two of these having similar lengths of 5.1 km and 5.9 km. The distances between these ruptures varied from 270 m to 500 m (Plafker and Brown, 1973). Surface ruptures caused by the 1980 Mammoth Lakes earthquakes were discontinuously distributed over a zone 20 km long and up to 10 km wide (Taylor and Bryant, 1980).

It should be recognized that the use of any system to classify surface faulting will be subject to oversimplifications, depending on the surficial geology, geologic structure, and regional tectonics. Nevertheless, a system such as Bonilla's provides a tool for visualizing general patterns, and for making qualitative judgments regarding the likelihood of displacement relative to the main fault trace. This classification system seems to work best for strike-slip faults which are discussed in the next chapter.

#### 2.4 FAULT LENGTH

As the length of surface faulting increases, so does the potential for intersecting pipelines and other lifeline structures that cross or are built in close proximity to the active fault. Accordingly, the length of faulting can be an important index with respect to earthquake damage. Reliability analyses of pipeline systems have been developed that account for the probability of pipeline damage by considering fault rupture length. Der Kiureghian and Ang (1977) stress the need to include fault length in the evaluation of seismic risk for structures built in close proximity to active faults. Ang and Mohammadi (1979) show that the probability of a fault rupture inter-

secting a pipeline is a function of surface rupture length and orientation of intersection. Greater lengths of rupture correlate with greater risk of pipeline damage.

Generally the length of surface displacement is only a fraction of the total fault length. Albee and Smith (1966) point out that the length of historic surface fault ruptures in southern California range between 20% and 50% of the fault length or fault system on which the earthquake occurred. Even great earthquakes on the San Andreas fault have produced movement on less than half of its mapped distance. The length of the San Andreas fault can be traced on land for a distance of approximately 970 km, extending from the San Francisco area to the Imperial Valley (Hart, 1980). The 1857 Fort Tejon earthquake, of inferred Richter magnitude 8.25, produced ground ruptures along 400 km of the central section of the San Andreas fault (Sieh, 1978), or 41% of the terrestrial fault length. Ground ruptures caused by the 1906 San Francisco earthquake, of Richter magnitude 8.25 (Gutenberg and Richter, 1954), extended for a distance of 435 km along the northern portion of the San Andreas fault (Lawson, et al., 1908), or 45% of the

terrestrial fault length.

Surface rupture length may be a fraction of the length of subsurface faulting. The fact that many earthquakes do not develop surface faults indicates that movement at depth is not always transmitted to the surface. Bonilla (1979) points out that subsurface displacements may be accompanied by one of four conditions at the surface: 1) no surface faulting, 2) regional tectonic uplift or subsidence, 3) surface rupture shorter than subsurface rupture, and 4) surface rupture approximately equal in length to subsurface rupture.

Subsurface faulting is often inferred from seismological evidence of aftershock locations and geodetic data on regional displacements. These multiple sources of evidence can lead to difficulties when developing a consistent basis for investigating fault length as a function of earthquake magnitude. Bonilla (1967, 1970), for example, bases his estimate of the Patton Bay fault length during the 1964 Alaska earthquake on the mapped length of breakage for both land and sea floor to obtain a total distance of 63 km (Plafker, 1967). Slemmons (1977), however, records the length of rupture as 800 km, which is consistent

with the evidence of regional uplift and subsidence. The two estimates of length differ by an order of magnitude and illustrate the difficulties associated with determining rupture distances for fault activity offshore.

Because earthquake magnitude is proportional to the energy released by faulting, greater lengths of faulting should relate to greater earthquake magnitudes. Tocher (1958) was the first to recognize this relationship and to plot earthquake magnitude as a function of surface fault length. Other researchers who have investigated earthquake magnitude as a function of surface fault length include Iida (1959), Otsuka (1964), King and Knopoff (1968), and Slemmons (1977). Fault length has also been correlated against earthquake magnitude by Iida (1965), Bonilla (1967, 1970, 1982), Bonilla and Buchanan (1970), and Taylor and Cluff (1977). A comprehensive study by Bonilla and Buchanan (1970) correlates surface fault length as a function of earthquake magnitude for 53 worldwide events.

Figure 2.5 summarizes surface fault length as a function of earthquake magnitude as reported by Taylor and Cluff (1977). Three linear regressions are shown

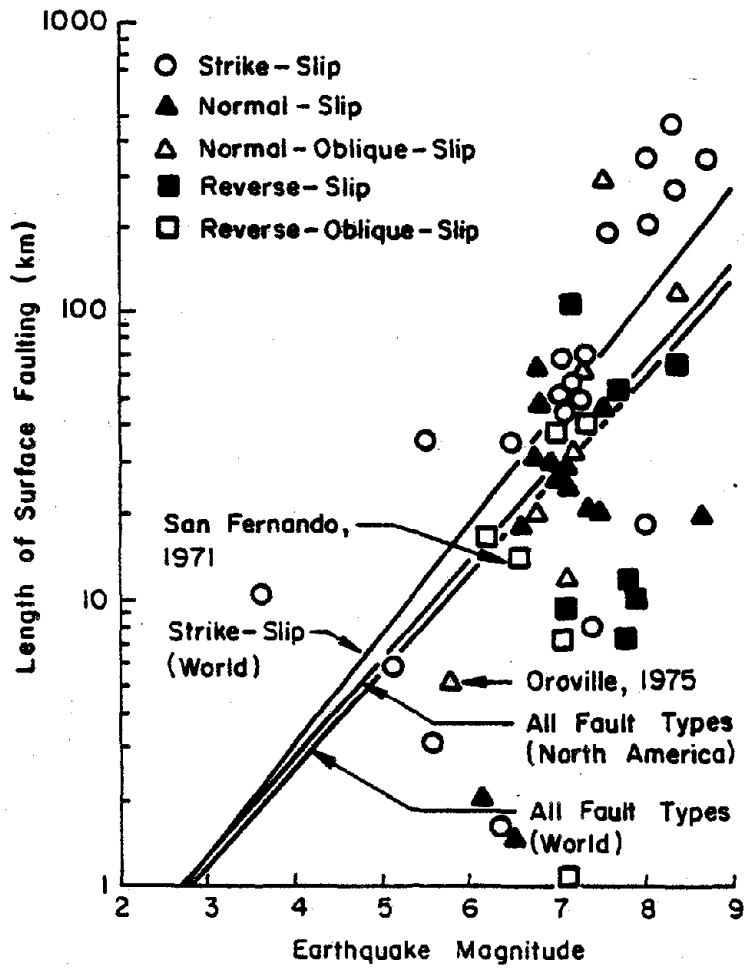


Figure 2.5. Plot of fault length vs. magnitude (after Taylor and Cluff, 1977).

in the figure, representing the best straight line fits for the data corresponding to worldwide and North American events of all fault types and for worldwide strike-slip faults. The data in the figure come principally from Bonilla and Buchanan (1970) with additional points introduced for the 1971 San Fernando and 1975 Oroville earthquakes.

## 2.5 FAULT DISPLACEMENT

Surface fault displacements may produce significant offsets in lifeline structures that intersect the fault. Accordingly, the extent of lifeline damage should correspond to the magnitude of fault offset for a constant angle of pipeline/fault intersection. The response of buried pipelines to abrupt fault movements has been investigated by Newmark and Hall (1975) and Kennedy, Chow, and Williamson (1977) for continuous, butt-welded lines and by O'Rourke and Trautmann (1981) for jointed pipelines.

Several researchers have investigated the relationship between fault displacement and earthquake magnitude and have plotted earthquake magnitude as a function of maximum surface fault displacement (e.g., Iida, 1965; Chinnery, 1969; and Slemmons, 1977). Maximum surface fault displacement has also been corre-

lated with earthquake magnitude by Bonilla (1967, 1970, 1982), Bonilla and Buchanan (1970), and Taylor and Cluff (1977). A comprehensive study by Bonilla and Buchanan (1970) correlates maximum surface fault displacement as a function of earthquake magnitude for 49 worldwide events.

Figure 2.6 summarizes maximum surface fault displacement as a function of earthquake magnitude reported by Bonilla and Buchanan (1970). Five linear regressions are shown in the figure, representing worldwide and North American events for all fault types and for strike-slip, normal, and reverse faults separately.

## 2.6 CORRELATIONS BETWEEN FAULT LENGTH, MAXIMUM DISPLACEMENT, AND EARTHQUAKE MAGNITUDE

As discussed in the previous two sections, fault length and displacement have been correlated with earthquake magnitude by various researchers. These correlations point out important trends and help in making quantitative judgments about rupture length and displacement for a given earthquake magnitude. Because the length of faulting and amount of displacement are critically important for evaluating the risk of pipeline damage, it is worthwhile to explore in de-

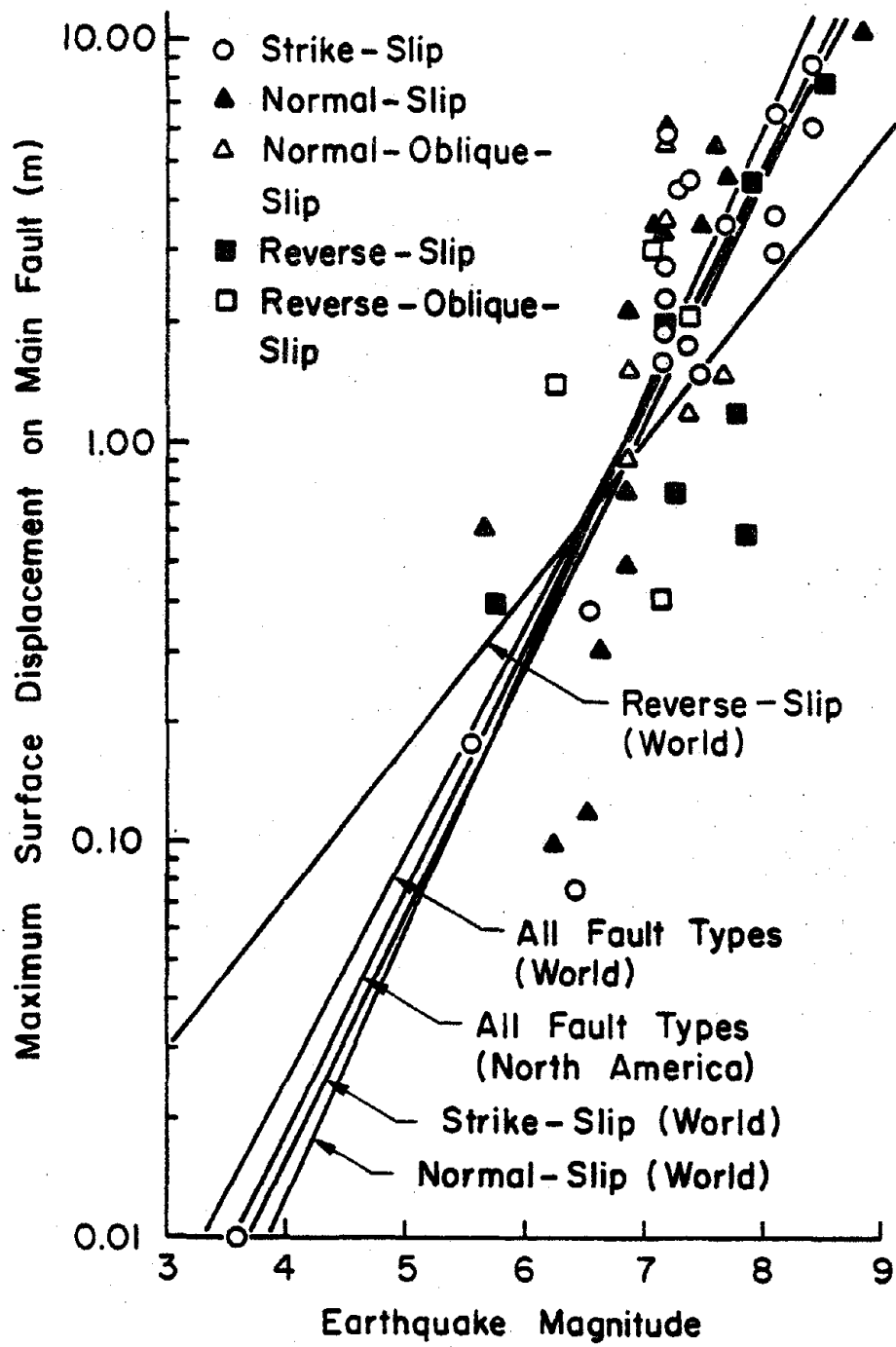


Figure 2.6. Plot of fault displacement vs. magnitude (after Bonilla and Buchanan, 1970).

tail correlations between fault length, maximum surface displacement, and earthquake magnitude.

Table 2.1 summarizes information associated with historic surface faulting. The data for strike-slip, normal, and normal-oblique faults pertain exclusively to earthquake events in the continental United States. The data for reverse and reverse-oblique faults pertain to worldwide events. The scarcity of information for reverse faults requires a data base developed from worldwide observations so that a sufficient number of data points can be used to make the correlations statistically significant.

The table list 42 events according to the years and names of the earthquakes for which there is information pertaining to magnitude, rupture length, and maximum displacement. It includes 14 strike-slip, 12 normal, and 16 reverse faults which are listed in two chronological groups of 29 and 13 events. The first group consists of all historic, surface faulting events in the continental U.S. The second group includes all historic, worldwide reverse faulting events. Reference numbers from 1 to 36 have been assigned to various events to identify data used in linear regression analyses. Fault types are denoted

Table 2.1. Summary of historic surface faulting information.

No.	Event	Fault Type	Magnitude	Surface Fault Length (km)	Maximum Displacement (m)	Fault	References
1	1857 Fort Tejon, CA	E	8.25 <sup>a</sup>	400.0	9.50	San Andreas	Sieh, 1978
2	1868 Hayward, CA	E	6.7	48.0	0.90	Hayward	Lawson, et al., 1908; Bonilla, 1970; Slemmons, 1977
3	1872 Owens Valley, NV	C	8.3	97.0 <sup>a</sup>	7.00	Owens Valley	Bonilla, 1970; Hobbe, 1910
4	1906 San Francisco, CA	E	8.25 <sup>b</sup>	435.0 <sup>a</sup>	6.40	San Andreas	Lawson, et al., 1908; Gutenberg and Richter, 1954
5	1915 Pleasant Valley, NV	A	7.75 <sup>b</sup>	48.0	4.90	NR	Jones, 1915; Page 1935; Gutenberg and Richter, 1954; Bonilla and Buchanan, 1970
6	1932 Cedar Mountain, NV	C	7.2	61.0	1.30	NR	Gianella and Callaghan, 1934; Gutenberg and Richter, 1954
7	1934 Excelsior Mountains, NV	A	6.3	1.4	0.13	Endowment Mine	Callaghan and Gianella, 1935; Gutenberg and Richter, 1954
8	1938 Hanceel Valley, UT	A	6.6	9.7	0.52	Kosmo	Neuman, 1936; Slemmons, 1977
9	1940 Imperial Valley, CA	E	7.1	64.0	5.79	Imperial	Buwald and Richter, 1941; Richter, 1958
10	1947 Mendocino, CA	E	6.4	1.6	0.08	NR	Richter, 1958
11	1950 Fort Sage, CA	A	5.6	8.9	0.20	NR	Gianella, 1957; Richter, 1958
12	1952 Kern County, CA	D	7.7	54.7	1.20	White Wolf	Buwald and St. Amand, 1951; Okeshott, 1955
13	1954 Fallon-Stillwater, NV	A	6.6	17.7	0.30	Rainbow Mtn.	Tocher, 1956; Richter, 1958
14	1954 Fallon-Stillwater, NV	A	6.8	30.6	0.76	Rainbow Mtn.	Tocher, 1956; Richter, 1958
15	1954 Fairview Peak, NV	C	7.3	58.0	5.70	NR	Slemmons, 1957; Richter, 1958; Bonilla, 1970; Slemmons, 1977
16	1954 Dixie Valley, NV	A	6.8	61.1	3.25	NR	Slemmons, 1957; Richter, 1958; Bonilla, 1970; Slemmons, 1977
17	1958 Alaska	E	8.0	200.0 <sup>a</sup>	6.60	Fairweather	Tocher, 1960
18	1959 Hebgen Lake, MT	A	7.1	24.1	6.10	NR	Murphy and Brases, 1964; Myres and Hamilton, 1964; Witkind, 1964
19	1964 Alaska	B	8.4	62.8 <sup>a</sup>	7.00	Patton Bay	Pfaffner, 1967, 1969
20	1966 Imperial Valley, CA	E	3.6	10.0	0.015	Imperial	Brune and Allen, 1967
21	1966 Parkfield-Cholame, CA	E	5.5	37.0	0.08	San Andreas	Brune and Vedder, 1967; Wallace and Roth, 1967
22	1968 Borrego Mountain, CA	E	6.4	33.0	0.38	Coyote Creek	Allen, et al., 1968; U. S. Geological Survey, 1972
23	1971 San Fernando, CA	D	6.4	15.0	1.00	San Fernando	U. S. Geological Survey Staff, 1971; Allen, Hanks, and Whitcomb, 1975
24	1975 Galway Lake, CA	E	5.2	6.8	0.02	Galway Lake	Hill and Beby, 1977
25	1975 Oroville, CA	E	5.7	3.0	0.05	Cleveland Hill	Hart, 1975
26	1979 Imperial Valley, CA	E	6.6	30.5	0.60	Imperial	Leeds, 1980; Sharp, et al., 1982
27	1979 Coyote Lake, CA	E	5.7	0.01	0.01	Calaveras	Keefer, Wilson, and Tannacl, 1980
28	1980 Livermore Valley, CA	E	5.5	5.0	0.02	Greenville	Hart, 1980
29	1980 Mammoth Lakes, CA	A	6.3	20.0	0.30	Hilton Creek	Taylor and Bryant, 1980
30	1929 West Nelson, NZ	B	7.8	11.2	4.50	White Creek	Pyfe, 1929; Henderson, 1977; Gutenberg and Richter, 1954; Richter, 1958
31	1931 Hawkes Bay, NZ	B	7.9	97.0	4.60	Poukawa Shear	Henderson, 1933; Richter, 1958
32	1944 San Juan, ARG	B	7.0	25.0	3.00	Chilhu	Richter, 1958; Slemmons, 1977
33	1945 Mikawa, JA	B	7.8	70.0	0.60	NR	Richter, 1958; Bonilla and Buchanan, 1970
34	1951 Taiwan	D	7.1	9.0	2.00	Fukoso	Richter, 1958
35	1951 Gobi-Altai, MO	D	7.3	7.0	2.30	Meiliu	Cheng, 1960; Bonilla and Buchanan, 1970
36	1962 Buyin-Zara, Iran	D	8.3	265.0	10.00	Sagdu Bogdo	Bonilla and Buchanan, 1970
37	1968 Inangahua, NZ	D	7.2	103.0	0.76	Ipak	Florenov and Solomonko, 1965; Bonilla and Buchanan, 1970
38	1968 Meckering, AUS	D	7.0	1.0	0.41	NR	Ambrasy, 1963, 1965
39	1969 Parícutina, Peru	D	6.2	16.0	1.85	Meckering	Adams and Lowry, 1971; Lensen and Olway, 1971
40	1980 El-Asnam, ALG	D	7.2	35.0	5.00	Oued Fodda	Everingham, Oregon, and Doyle, 1969; Gordon, 1971
41		D					Deza, 1971
42		D					Burford, Hersh, and Espinosa, 1981; Leeds, 1983

A = Normal  
 B = Reverse  
 C = Normal-Oblique  
 D = Reverse-Oblique  
 E = Strike-Slip  
 NR = not reported  
 a - value reported to nearest quarter magnitude by Sieh (1978)  
 b - value reported to nearest quarter magnitude by Gutenberg and Richter (1954)  
 NOTE: Fault lengths followed by a positive sign (+) indicate observations where additional distances of rupture are known to have occurred, but could not be measured directly.

by letters A, B, C, D, and E, representing normal, reverse, normal-oblique, reverse-oblique, and strike-slip faulting, respectively. This lettering system is the same as that used by both Bonilla and Buchanan (1970) and Slemmons (1977).

The reliability and accuracy of the observations vary, depending on the source of information and manner in which the measurements were made. For example, the strike-slip displacement of 0.9 m listed in Table 2.1 for the 1868 Hayward earthquake is taken from indirect evidence reported by Lawson, et al. (1908). In contrast, the maximum strike-slip displacement of 0.38 m for the 1968 Borrego Mountain earthquake was obtained as a result of organized field reconnaissance and detailed mapping. The records of the Borrego Mountain earthquake include a comprehensive account of how strike slip movements were distributed both along the length of faulting and throughout the width of the main fault zone (Clark, 1972).

In some instances, not all components of the fault movement are reported. This is especially true for many of the reverse faults. As a consequence, correlations have been devised for displacements representing maximum throw and oblique-slip, without dif-

ferentiation, so that the correlations are based on data that do not represent a consistent sense of movement.

As discussed previously, the length of faulting involving offshore displacements can differ significantly depending on whether direct observations or estimates from regional subsidence and uplift are used as the basis for measurement. In addition, the magnitude ascribed to worldwide earthquakes will vary depending on the locations of the recording stations, type of recording devices, and signal interpretation.

It is not possible to screen all sources of variation when interpreting the information from historic fault observations. Some residual uncertainty must be expected. Indeed, some degree of uncertainty is a direct consequence of incorporating observations obtained during the nineteenth and early twentieth centuries.

To the extent possible, fault displacements used for linear regression analyses in this study were taken from a specific tectonic setting. The strike slip and normal slip displacements are confined almost exclusively to the California and Nevada fault systems. As indicated by Hays (1980), these systems are

associated with a distinctive alignment of seismic activity and structurally linked with the right-lateral motion between the Pacific and North American plates. The 1959 Hebgen Lake and 1934 Hansel Valley earthquakes are the only instances of normal faulting included in the analyses that are not part of the California-Nevada systems. The geologic settings for these events are part of the overall fault-block mountain structure that involves the Nevada system, as well as the Wasatch fault zone and Intermountain Seismic Belt, so that sufficient similarities exist among the normal slip data to warrant a common grouping.

The fault displacements were selected to represent coseismic slip along lengths of faulting greater than 1.6 km (1 mile). Coseismic slip is of critical interest with respect to pipelines because abrupt, short-term displacements are the most damaging for buried structures. Accordingly, fault displacement data for the 1966 Imperial Valley and 1979 Coyote Lake earthquakes are not included in the regression analyses because they involve small displacements that cannot be clearly distinguished from afterslip or creep.

The data were also confined to cases where dis-

placements were linked to movements on the causative fault. Consequently, the movement observed during the 1947 Mannix earthquake is not used because there is strong evidence that the surface displacement was related to secondary faulting (Richter, 1958).

In this study, the length of faulting is taken as the distance of mappable, surface rupture. This establishes a consistent basis for defining length by relating it to features that have been identified and confirmed through direct observation. Because this distance is associated with abrupt surface movements, it is especially meaningful for pipelines and other lifeline structures that are constructed at or near the surface.

The data selected for regression analyses preclude offshore extrapolations of displacement based on evidence from regional uplift and subsidence. As such, the reverse fault length for the 1964 Alaska earthquake in Table 2.1 is consistent with the dimension reported by Bonilla (1970) and significantly less than that reported by Slemmons (1977). Likewise, the length of faulting for the 1906 San Francisco earthquake is a minimum length because movements on the San Andreas fault were traced offshore, north of Point

Arena (Lawson, et al., 1908).

The Richter magnitude used in this report and in studies by various researchers (e.g., Bonilla, 1967, 1970; Bonilla and Buchanan, 1970; and Slemmons, 1977) is consistent with the values and methods for estimating magnitude used by Richter (1958) and Gutenberg and Richter (1954). Richter magnitude draws from both local magnitude,  $M_L$ , and magnitude derived from surface waves, or teleseisms,  $M_S$ . In general, the Richter magnitude is equivalent to local magnitude for magnitudes less than 7. It is equivalent to surface wave magnitude for magnitudes greater than or equal to 7. Kanamori and Regan (1982) plot local against surface wave magnitudes for selected California earthquakes and show that local magnitudes may be substantially smaller than surface wave magnitudes for magnitudes greater than 7.

#### 2.6.1 Correlation of Fault Length and Earthquake Magnitude

The length of faulting is generally considered to be roughly proportional to earthquake energy. The rupture distance is therefore taken as an exponential function of magnitude, and linear regression analyses are performed using the following expression for

length of faulting, L:

$$\text{Log } L = a + bM \quad (2.2)$$

where M is the Richter magnitude and a and b are constants defining the best straight line fit of the data.

Figures 2.7, 2.8, and 2.9 show the length of faulting plotted against Richter magnitude on semi-log graphs for strike-slip, normal-slip, and reverse-slip faults, respectively. The plots for normal and reverse faults also include data for events with oblique displacements. The linear regression equation is given in each figure in the form of Equation 2.2. A straight line representing the equation is plotted relative to the data points, each of which is indexed with respect to the observations of surface faulting summarized in Table 2.1. The coefficient of determination,  $r^2$ , and the number of data points in each population set, n, are also shown in the figures. For each linear regression, standard tests were performed which shown that there is a statistically significant trend of increasing fault length with increasing Richter magnitude.

The linear regression with the highest degree of

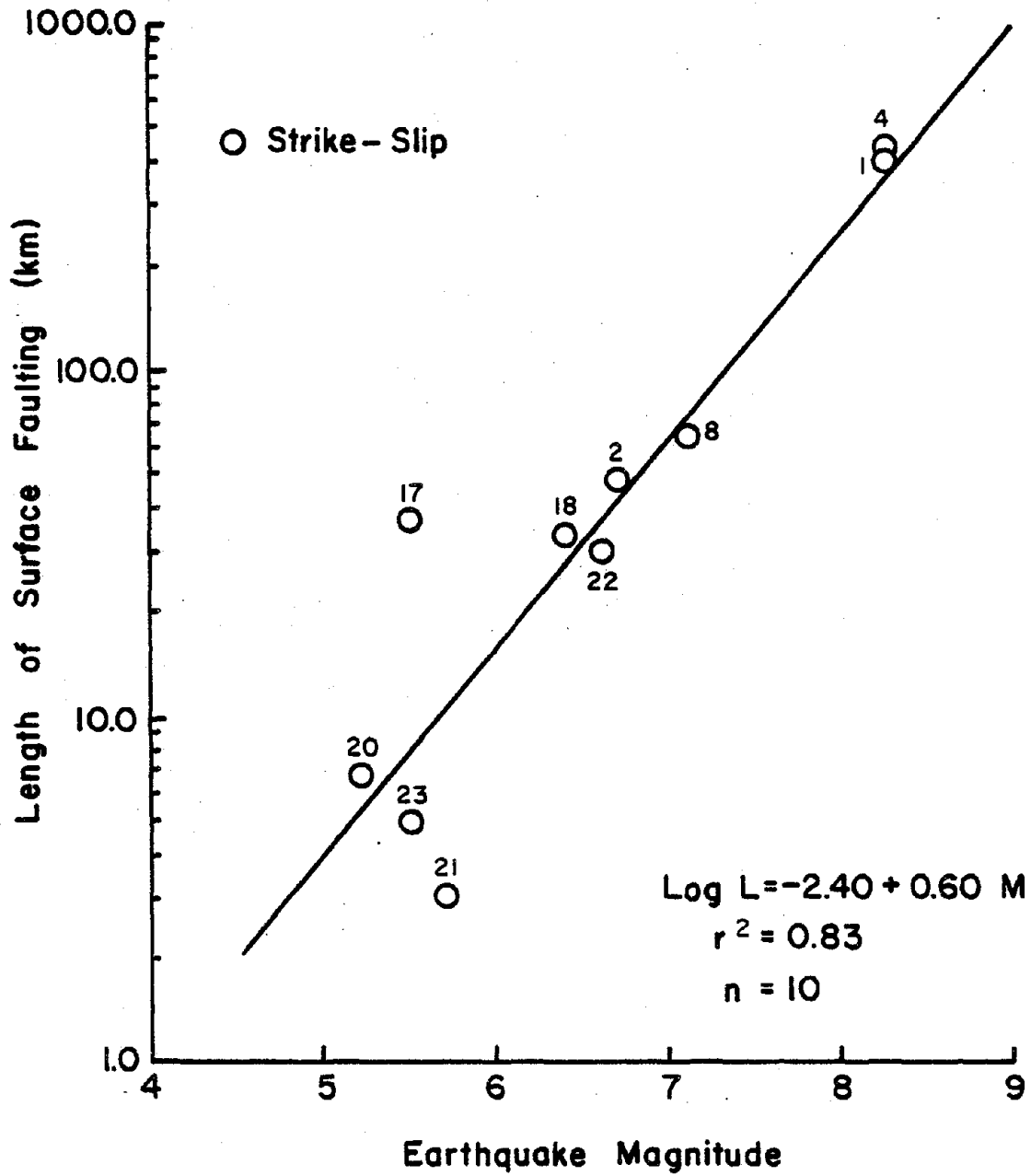


Figure 2.7. Plot of length vs. magnitude for strike-slip faults.

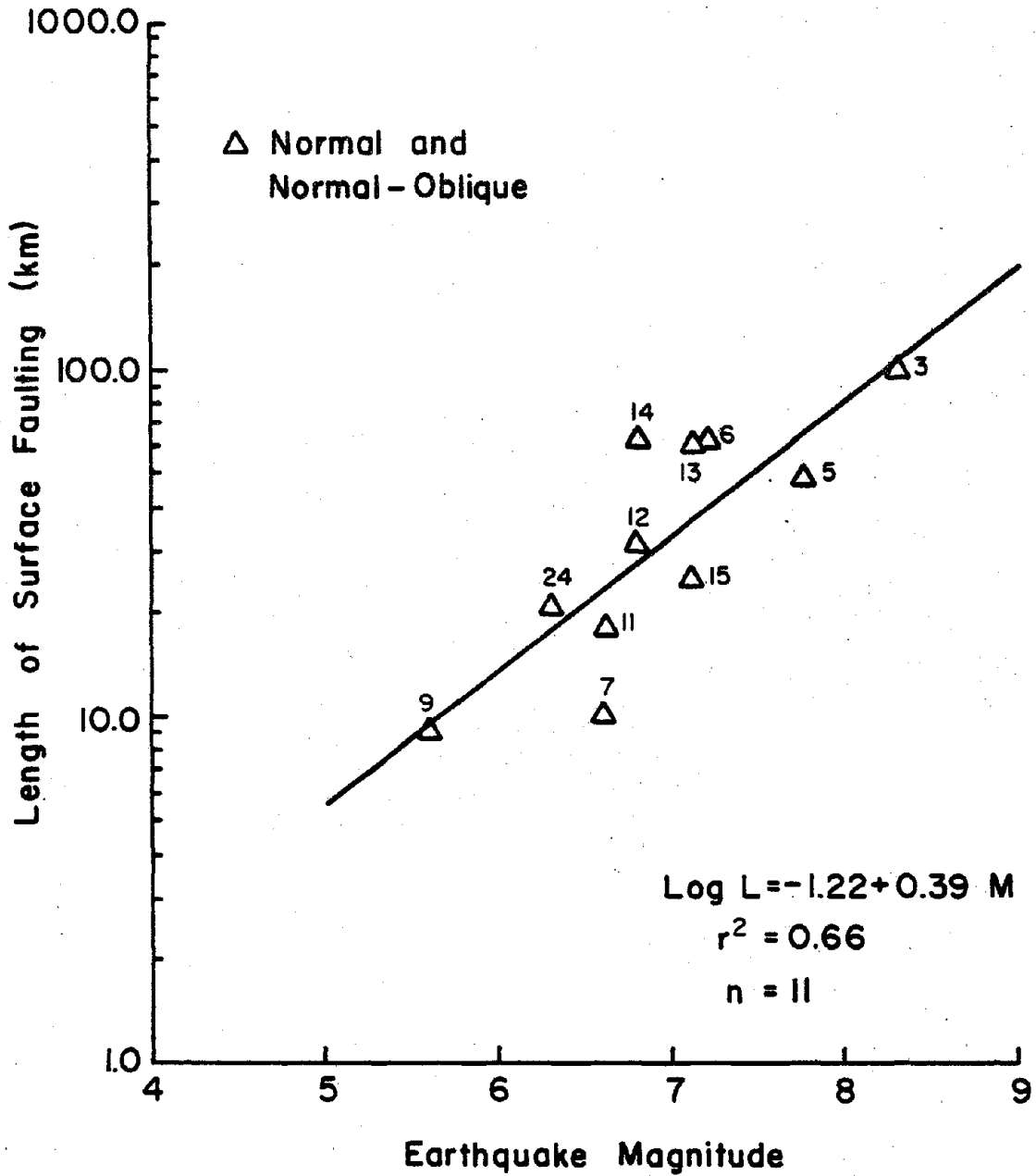


Figure 2.8. Plot of length vs. magnitude for normal and normal-oblique faults.

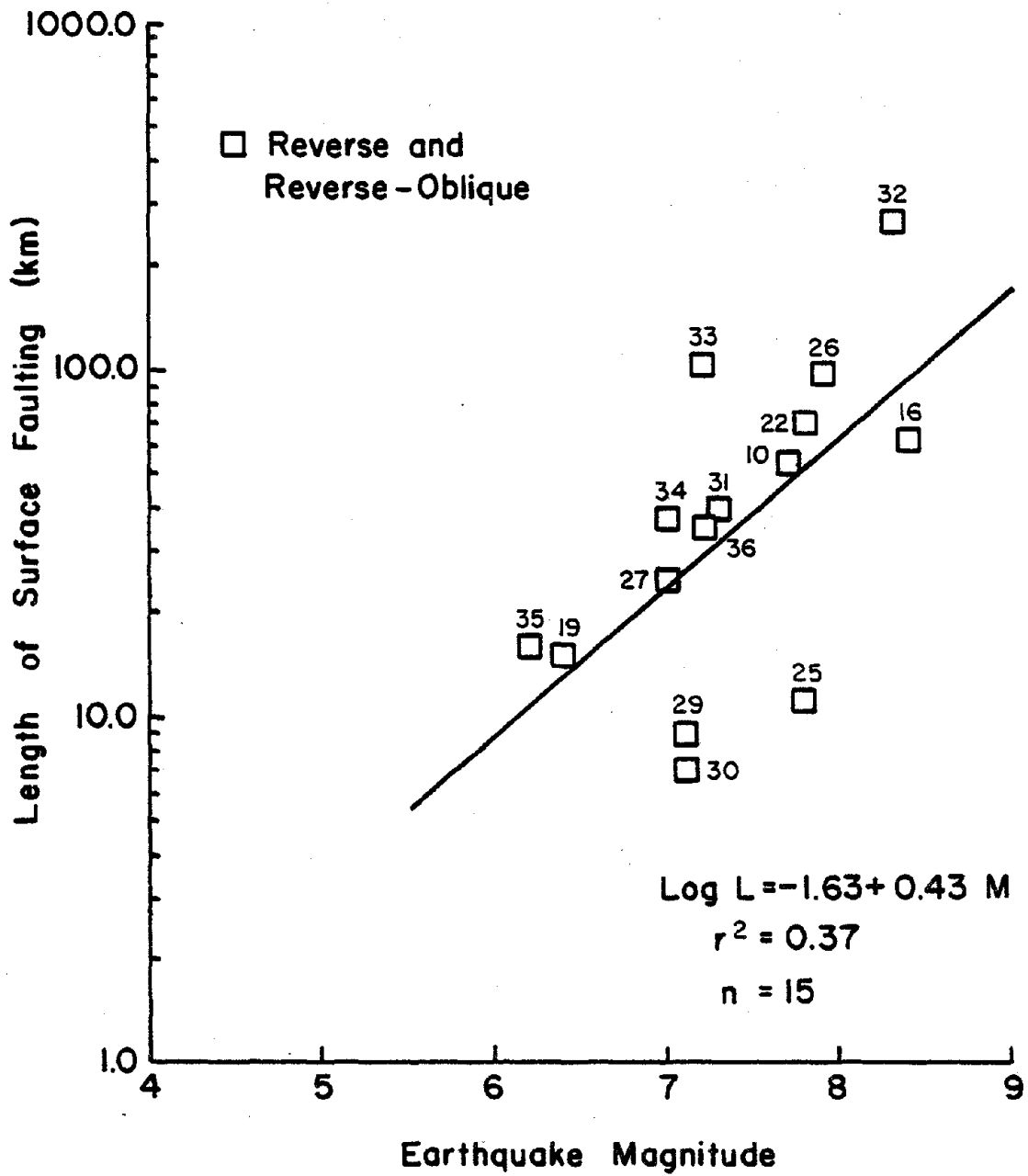


Figure 2.9. Plot of length vs. magnitude for reverse and reverse-oblique faults.

statistical significance pertains to strike-slip faulting. The coefficient of determination for this regression indicates that approximately 83% of the variation in the data is explained by the straight line plot. In contrast, the low coefficient of determination for reverse faulting indicates there is substantial variation between the data and the regression equation.

The strike-slip and normal faults are characterized by approximately equal lengths of faulting at magnitudes between 5 and 6. There is a substantial difference between them for magnitudes greater than 7, with strike-slip faults showing over three times the length of normal faults at a magnitude of 8.

Figures 2.10 and 2.11 compare the linear regression plots obtained in this study for U.S. events with those calculated from the surface faulting data compiled by Bonilla and Buchanan (1970) for North American strike-slip and normal faults, respectively. The linear regression equations associated with each data set are also shown in the figures. The agreement between the plots for strike-slip faults is good, even though there are considerable differences with respect to the faulting events used in the two correlations.

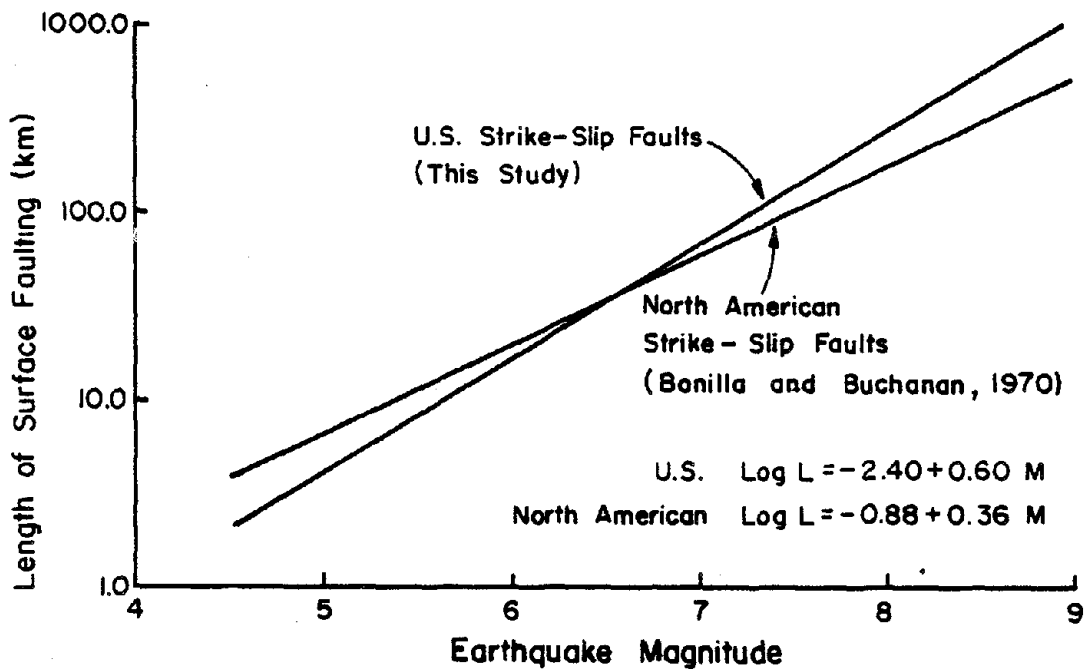


Figure 2.10. Plot of fault length vs. magnitude for strike-slip faults.

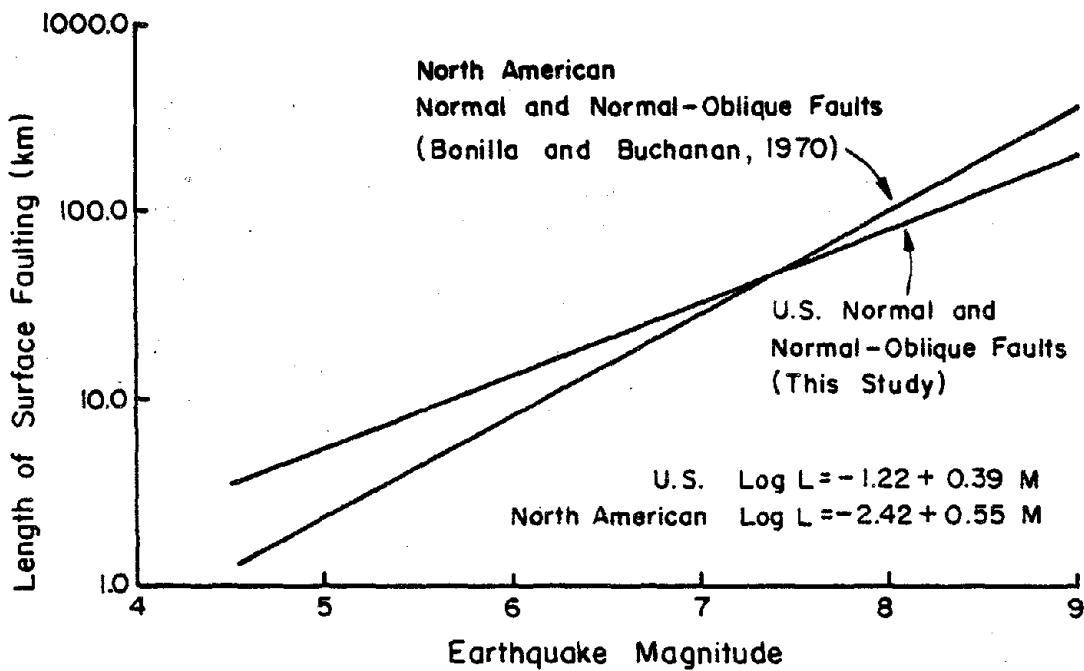


Figure 2.11. Plot of fault length vs. magnitude for normal and normal-oblique faults.

There is also good agreement between the plots for normal and normal-oblique faults, particularly for magnitudes between 7.0 and 8.0. The regression equation developed in this work for normal faults gives relatively large values of length for magnitudes less than 6.0, chiefly as a result of incorporating data from the 1980 Mammoth Lakes earthquake and not including data from the 1934 Excelsior Mountains earthquake.

#### 2.6.2 Correlation of Maximum Fault Displacement and Earthquake Magnitude

Linear regression analyses are commonly performed using the following expression for maximum fault displacement,  $D$ :

$$\text{Log } D = a + bM \quad (2.3)$$

where  $M$ ,  $a$ , and  $b$  are defined in the same manner as for Equation 2.2. Figures 2.12, 2.13, and 2.14 show the maximum fault displacement plotted against Richter magnitude on semi-log graphs for strike-slip, normal, and reverse faults, respectively. Events with oblique displacements are included in the plots for normal and reverse faults. The linear regression equation is shown in each figure in the form of Equation 2.3, and the straight line representing the equation is plotted

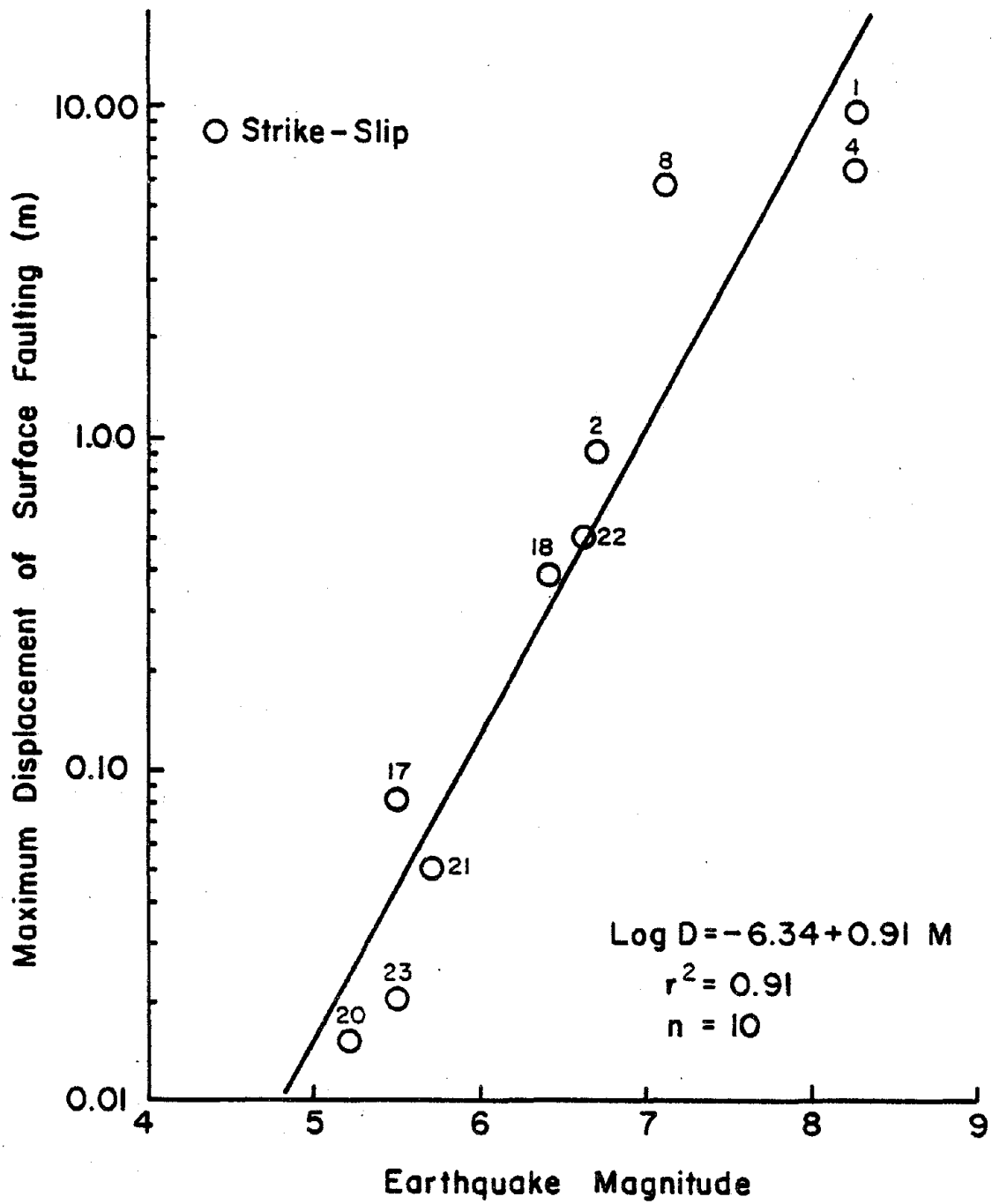


Figure 2.12. Plot of displacement vs. magnitude for strike-slip faults.



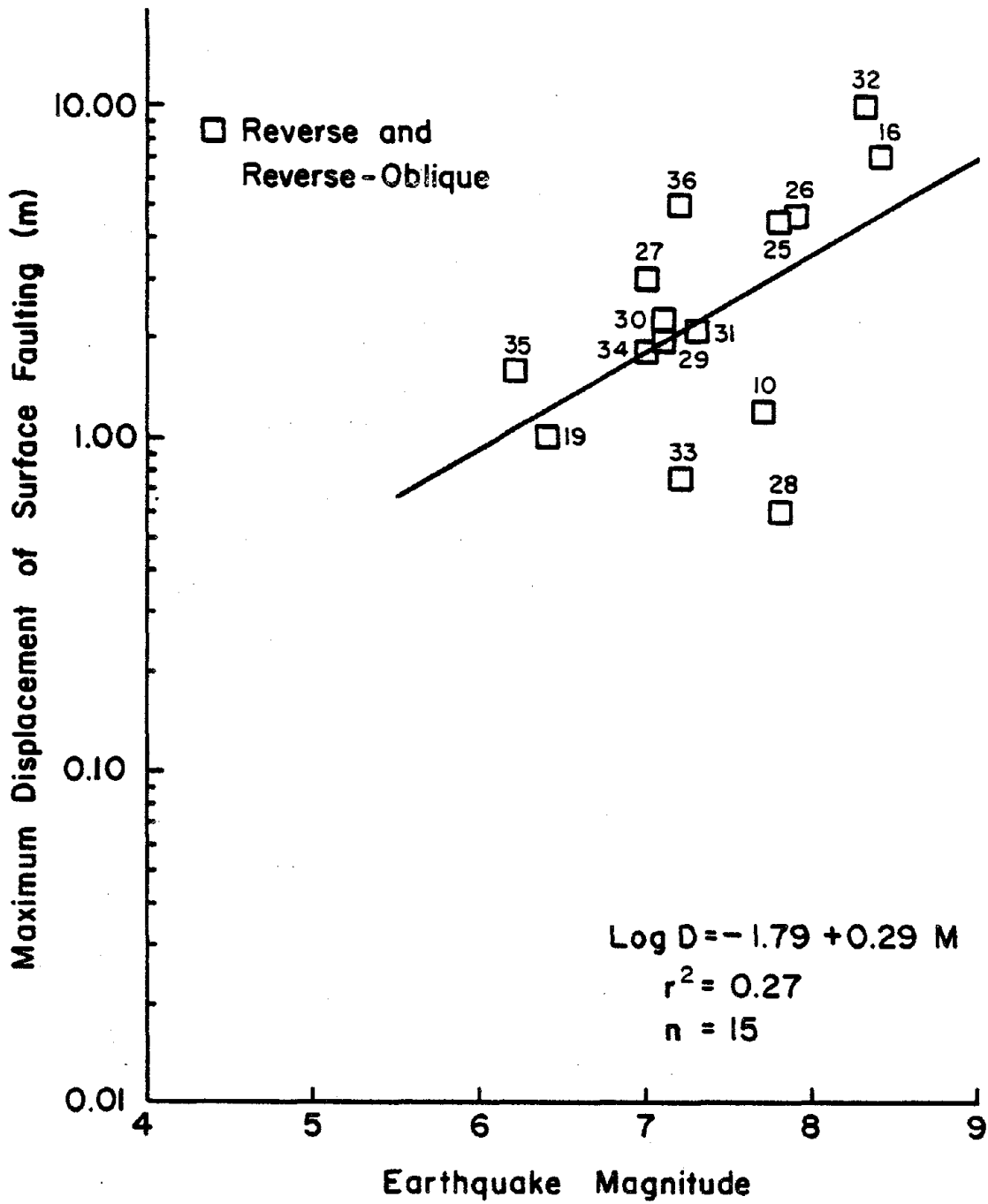


Figure 2.14. Plot of displacement vs. magnitude for reverse and reverse-oblique faults.

relative to the data points. The coefficient of determination,  $r^2$ , and the number of data points in each population set,  $n$ , are also shown in the figures. Standard statistical tests show that there is a statistically significant slope for each regression plot.

It should be emphasized that the linear regressions were developed for the most prominent components of movement for which there are consistent observations in the record of faulting events. For the strike-slip and normal faults, these components pertain to the maximum horizontal and vertical offsets, respectively. The maximum vertical offset is also used for the reverse faults, although substantial, and even predominant, amounts of heave and strike slip were observed during many of these events. For all fault types, sufficient information was lacking to develop correlations on the basis of maximum oblique movement.

The linear regression with the highest degree of statistical significance pertains to strike-slip faulting. The coefficient of determination of this regression indicates that approximately 91% of the variation in the data is explained by the straight line plot. In a manner similar to that for length of

faulting, substantial variation exists between the data and the regression line for reverse faults.

The strike-slip and normal faults are characterized by approximately equal amounts of maximum displacement for magnitudes between 7.0 and 8.0. There is a substantial difference between them for magnitudes less than 6.5. This discrepancy may be related to the fact that surface ruptures are amplified by gravity effects during normal faulting. At lower magnitudes, the gravity effects can contribute a significant part of the maximum fault offset.

Figure 2.15 and 2.16 compare the linear regression plots obtained in this study for U.S. events with those calculated from the surface faulting data compiled by Bonilla and Buchanan (1970) for North American strike-slip and normal faults, respectively. The linear regression equations associated with each data set are also shown in the figures. The agreement between the plots for both strike-slip and normal faults is good for magnitudes between 7.0 and 8.0. For magnitudes less than about 6.5, the displacements in this study are smaller. These differences are mainly the result of incorporating data on strike-slip faults from the 1975 Galway Lake, 1975 Oroville, and

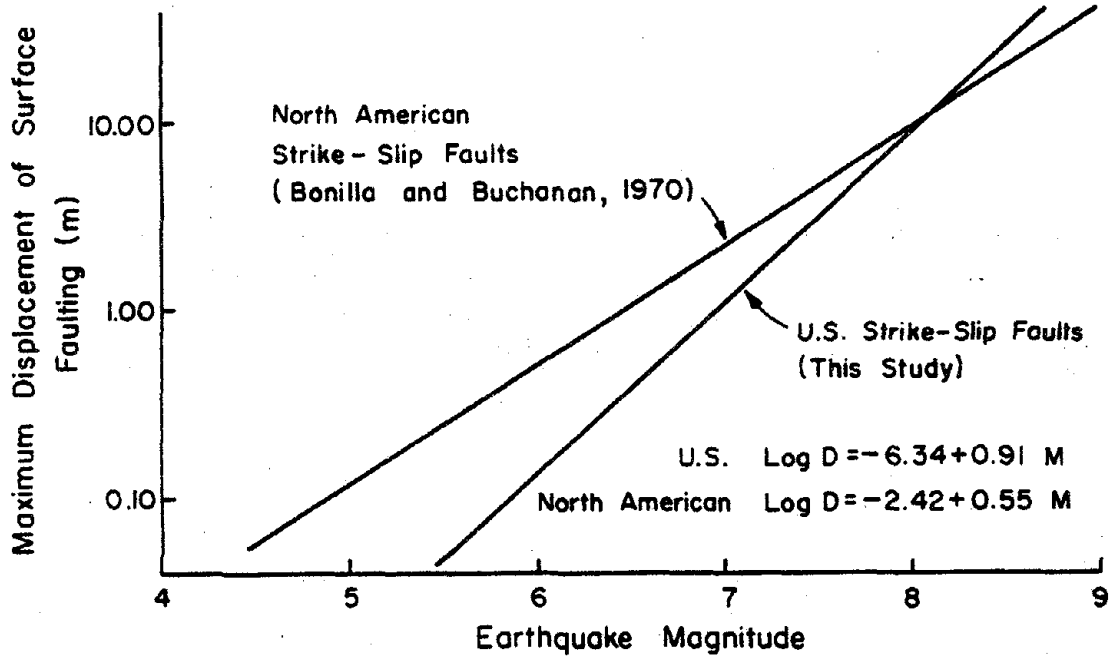


Figure 2.15. Plot of fault displacement vs. magnitude for strike-slip faults.

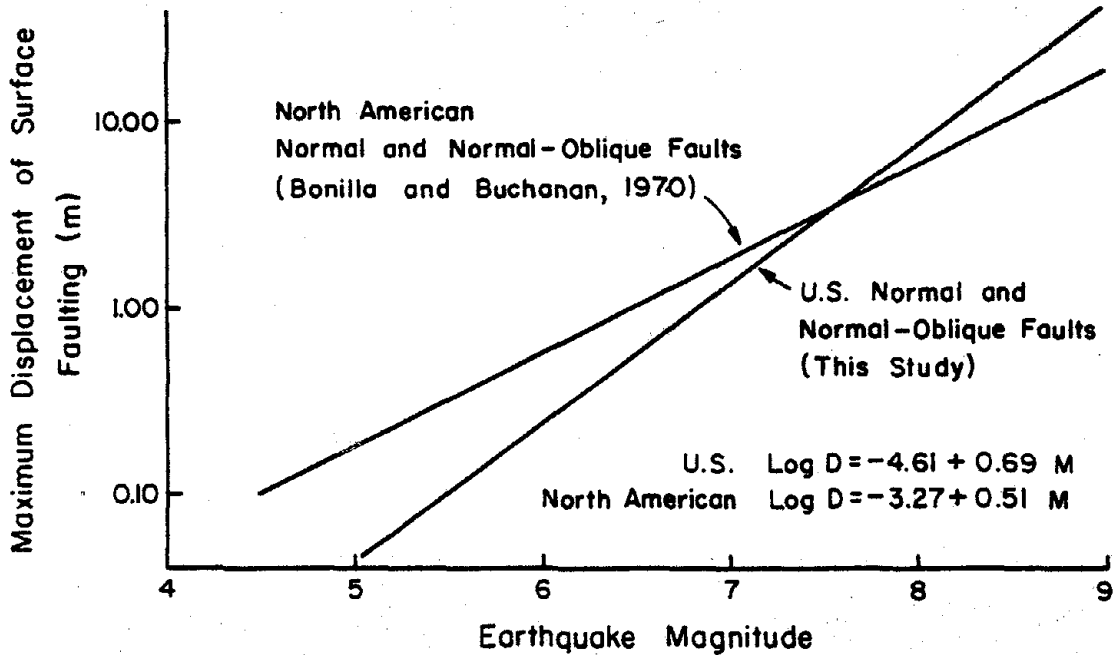


Figure 2.16. Plot of fault displacement vs. magnitude for normal and normal-oblique faults.

1980 Livermore Valley earthquakes. With respect to normal faults, the differences are partially caused by the selection of data in this study to include only vertical offsets.

### 2.6.3 Discussion of Fault Analyses

Table 2.2 summarizes the linear regression equations developed from the statistical analyses in this work. Equations are given for length of faulting and maximum fault displacement pertaining to strike-slip, normal, reverse, and all fault types. As indicated previously, the data for strike-slip faulting show the least amount of variation with respect to the linear regression equations.

Although the equations in Table 2.2 are helpful in visualizing trends and comparing different types of faulting, their use for predictive purposes is limited by at least two characteristics of the data set. First, there are relatively few data so that the population selection has a strong influence on the results of the regression analyses. In this work, the maximum displacement for the 1966 Imperial Valley earthquake was not included in the regression analyses because of uncertainty with regard to creep and afterslip. If this movement is analyzed with the other data, the re-

Table 2.2. Linear regressions for fault displacement data.

a. Length of faulting

Fault Type	Population n	Regression Equation (km)	Coefficient of Determination $r^2$
Strike-Slip	10	$\text{Log } L = -2.40 + 0.60 M$	0.83
Normal	11	$\text{Log } L = -1.22 + 0.39 M$	0.66
Reverse	15	$\text{Log } L = -1.63 + 0.43 M$	0.37
All	36	$\text{Log } L = -1.47 + 0.43 M$	0.54

b. Maximum fault displacement

Strike-Slip	10	$\text{Log } D = -6.34 + 0.91 M$	0.91
Normal	11	$\text{Log } D = -4.61 + 0.69 M$	0.68
Reverse	15	$\text{Log } D = -1.79 + 0.29 M$	0.27
All	36	$\text{Log } D = -4.88 + 0.71 M$	0.72

sulting regression equation gives nearly twice as much displacement for an earthquake of magnitude 5.5 than that given by the equation in Table 2.2. The second aspect of the data concerns the exponential relationships of length or displacement as a function of magnitude. By plotting the logarithm of length or displacement with respect to magnitude, even small departures from the regression lines will result in large variations of the arithmetic values.

Table 2.3 helps to illustrate this second point. Standard statistical techniques (e.g., Snedecor and Cochran, 1980) were used to develop predictive limits for the linear regression pertaining to strike slip displacements. Table 2.3 summarizes the results of these analyses. Maximum predicted displacements are listed for several different magnitudes of earthquake according to the probability,  $P$ , that the predicted value will be exceeded. The standard statistical methods assume that the displacement is log normally distributed about the predicted value of the regression equation. Accordingly, the predictive limits are calibrated with respect to exponential changes. Table 2.3 shows that the maximum predicted displacements change by roughly a factor of five as the probability,

Table 2.3. Summary of maximum predicted displacements for strike-slip faults.

Maximum Predicted Displacement, m

<u>Richter Magnitude</u>	<u>P=0.50<sup>a</sup></u>	<u>P=0.25</u>	<u>P=0.10</u>	<u>P=0.05</u>
6.0	0.13	0.23	0.40	0.58
6.5	0.36	0.64	1.12	1.62
7.0	1.04	1.82	3.23	4.68
7.5	2.95	5.24	9.33	13.80
8.0	8.31	15.49	28.18	42.65

---

<sup>a</sup>

Probability that predicted value will be exceeded.

P, decreases from 0.50 to 0.05.

The selection of earthquake events for regression analyses and the choice of appropriate measurements for each event entails a significant amount of judgment. As shown in Figures 2.10, 2.11, 2.15, and 2.16, the variations resulting from different interpretations of historic earthquake faulting are not large for earthquake magnitudes of 6.5 to 8.0. The variations associated with a given regression equation, however, lead to a substantial range of predicted displacements if standard statistical techniques are used.

It should be recognized that the maximum displacement may not represent the best choice of movement over the entire length of surface faulting. The maximum displacement provides an upper bound that may be appropriate only on a local basis. Furthermore, the displacement may be distributed over a fault rupture zone several meters to several tens of meters wide, rather than on a single rupture. Both the width of the main rupture zone and the distribution of displacement along the length of faulting are investigated with respect to strike-slip faults in Chapter 3. Information regarding these two factors is essential

for developing a rational method of predicting fault displacements.

## 2.7 SUMMARY

Fault displacements may occur in the form of coseismic slip, afterslip, and creep. Coseismic slip is the most damaging displacement for pipelines and other buried lifeline structures. There are three principal types of fault: strike-slip, normal, and reverse faults. Although the actual ground ruptures caused by an earthquake will involve complex distributions of movement, simplified models based on abrupt, planar displacement offer the most useful means of classifying faults with respect to their influence on pipelines. The aerial distribution of faulting can be visualized with the aid of a classification system (Bonilla, 1967), in which the surface ruptures are divided into three zones encompassing the main fault, branch faults, and secondary faults.

Information has been summarized pertaining to all historic, U.S. surface faulting events for which data on Richter magnitude, length of faulting, and maximum displacement are available. Linear regression analyses of the data according to fault type show statistically significant trends of increasing fault length

and maximum displacement with Richter magnitude. The highest degree of statistical significance is associated with strike-slip faults, whereas reverse faults show a relatively poor correlation between the linear regression equations and observed movements. Variations in the linear regression values resulting from different interpretations of historic faulting are not large for earthquake magnitudes of 6.5 to 8.0, but may be substantial for earthquake magnitudes less than 6.5.

## CHAPTER 3

### STRIKE-SLIP FAULTING

This chapter investigates historic strike-slip faulting in the U.S. Faults are related to the active global plate or subplate boundaries. Special geomorphic features are produced by repetitive surface fault movements. The nature of fault creep movements on several faults in California are discussed. The characteristics of fault rupture displacement from coseismic slip along the length and across the width of the main rupture zone is described, with special attention to the amount and distribution of fault displacement for siting of a pipeline/fault intersection.

#### 3.1 TECTONIC MECHANISM

Nearly all historic surface faulting occurs in the vicinity of major global plate boundaries or along tectonically conspicuous subplate boundaries. Two global belts of concentrated seismicity are prominent in the present distribution of earthquakes shown in Figure 3.1. These belts include the circum Pacific and the east-west seismic zone between Asia and the Mediterranean.

The key factor controlling fault movement is the

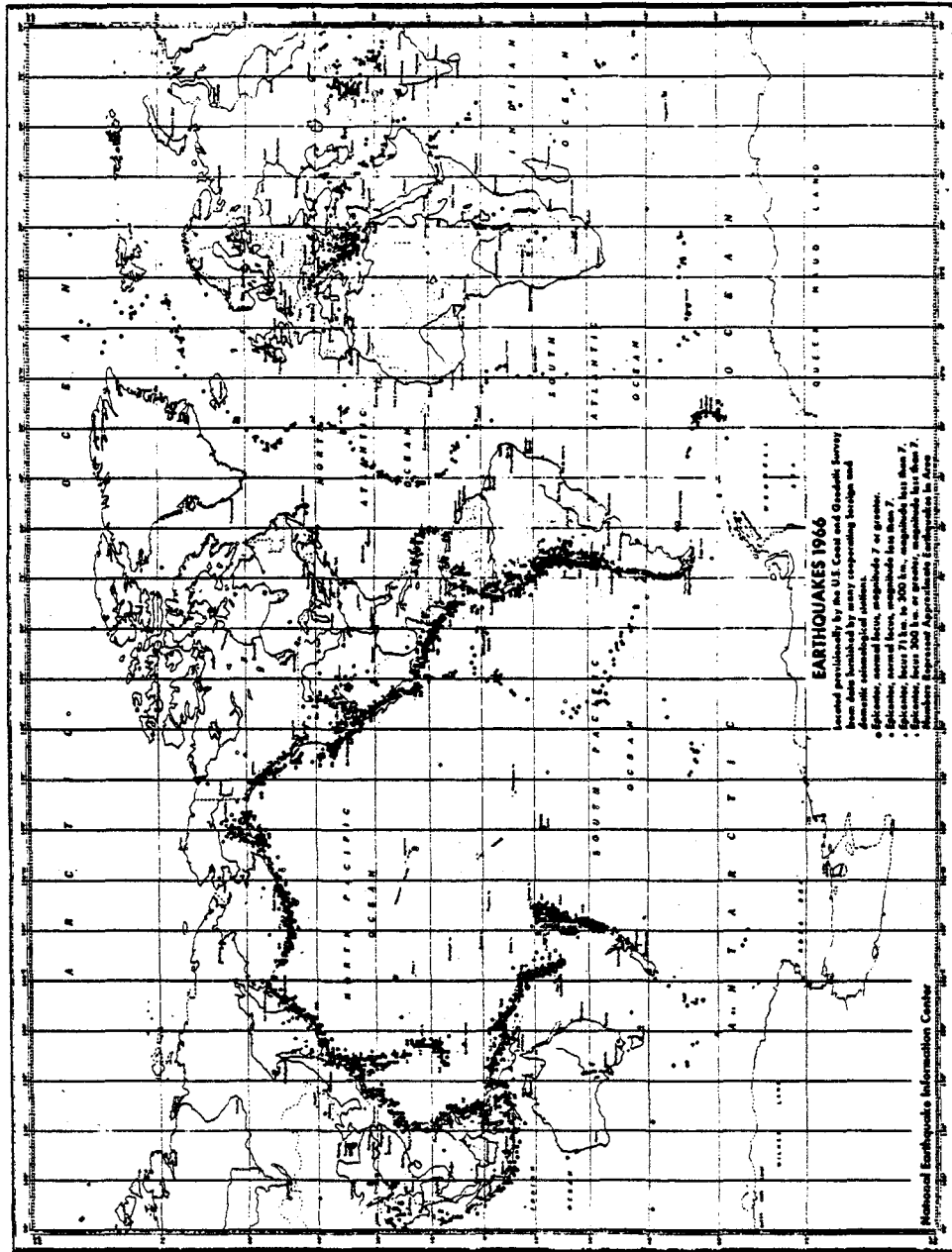


Figure 3.1. Map showing global seismicity for the year 1966 (after Bolt, 1970).

relationship of the fault to the regional tectonic stress. The stress will be relieved along the path of least resistance having a favorable orientation to the direction of stress. The expression of this stress relief, or strain, will be in the form of tectonic movement. Plate or subplate boundaries with high rates of regional deformation or strain, 20 mm/yr or greater, have the highest potential for seismic energy release and associated potential for surface faulting (Slemmons, 1977).

Active plate boundaries are identified on the basis of relative displacement, and include three types: separation, convergence, and parallel movement. The East Pacific Rise and Mid-Atlantic Ridge are examples of separating plate boundaries. Zones of coastal subduction are related to converging plates, with ocean trenches adjacent to island or mountain arc structures occurring at the Aleutian and Japanese arcs. Examples of parallel plate movement may be found along the western North American Continent, in New Zealand, and in northern Turkey. Major strike-slip faulting zones are formed by such subparallel movement of plate or subplate boundaries.

The major active strike-slip fault zones in the

U.S. occur along the boundary between the North American and Pacific plates and are located in California and Alaska. Strike-slip surface faulting in California has occurred along the San Andreas fault system including the San Andreas, Calaveras, and Hayward faults, and the San Jacinto and Imperial fault zones. Locations of historic surface rupture along these faults is shown in Figure 3.2. The arrow indicates the present movement of the Pacific plate relative to the North American plate. Right-lateral fault displacement is common to most active faulting in California, conforming to the influence of the relative right-lateral displacement between the plates. Significant exceptions occur in the vicinity of the Transverse Range where reverse faulting generally is accompanied by components of left-lateral slip.

Strike-slip surface faulting was observed on the Fairweather fault in 1958 (Tocher, 1960; Brogan, et al., 1975). This fault is located near the boundaries of the North American and Pacific plates. Figure 3.3 illustrates the major tectonic features along this plate boundary and shows the predominant direction of movement of the Pacific plate. Two distinct types of plate boundaries can be recognized in the figure. The

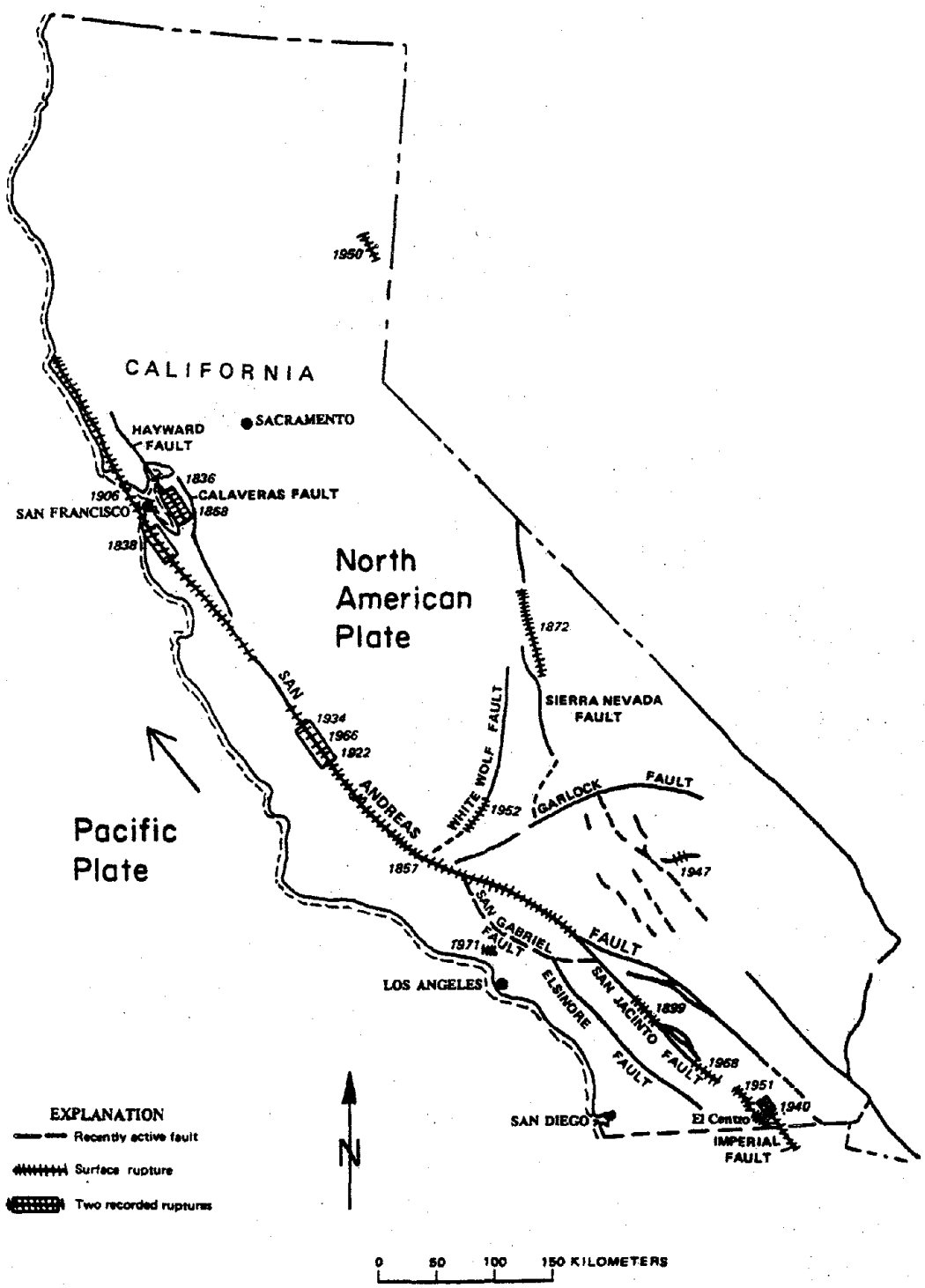


Figure 3.2. Major faults in California and locations of historic surface rupture (after Hays, 1980).

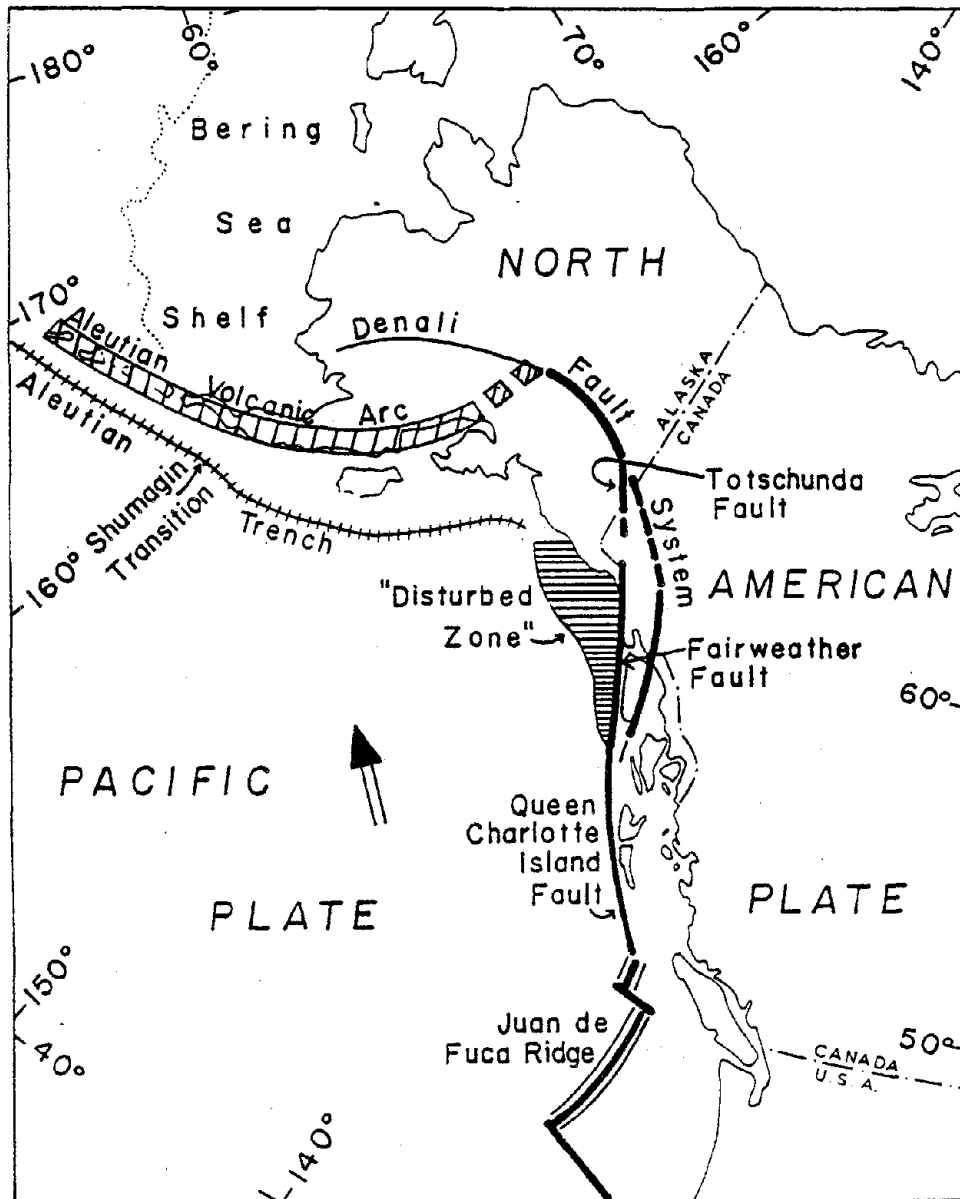


Figure 3.3. Sketch map of northwestern North America showing major tectonic features along Pacific-North American plate boundary (after Naugler and Wageman, 1973).

Aleutian trench is the location of a compression type boundary where the Pacific plate is subducted under the North American plate. Subparallel plate movement occurs along the southeastern Alaskan and western Canadian coast. This subparallel movement is reflected as right-lateral slip on the Fairweather fault.

Other major strike-slip fault systems are recognized in the circum Pacific belt by Richter (1958), Burk and Moores (1968), Dickinson and Grantz (1968), Hamilton and Myers (1968), Naugler and Wageman (1973), Brogan, et al. (1975), Slemmons (1977), and Hays (1980). Included among those referenced above is the Alpine fault system in New Zealand. Richter (1958) and Scholz (1973) drew attention to this system by noting that many of its characteristics are similar to the San Andreas fault system, including, size, type of offset, and association of secondary faults to the main fault. A major strike-slip fault outside of the Pacific is the Northern Anatolian fault system of Turkey. Wallace (1968a) and Ambraseys (1970) have noted the similarity between this and the San Andreas fault system. Features characteristic of large scale right-lateral, strike-slip faults are common to both.

### 3.2 GEOMORPHOLOGY

Repetitive fault displacements cause subtle but distinctive changes in the terrain, producing special geomorphic features. These features are prominent where active faults cross elongate geologic structures and drainage channels. The geomorphic features are distinguished as primary and secondary based on their relation to fault movements. Primary geomorphic features are directly related to fault displacements and may be caused by the offset of geologic structures, or by depression or compression along the fault trace. Secondary features are related to erosion, deposition, or ground water regimes that are altered because of the fault movements.

A fault scarp is a steep slope parallel to the plane of principal fault movement, and Slemmons (1977) describes it as one of the most common geomorphic features of strike-slip faults in California. It is formed as a direct result of offset, where the fault has bisected an area of topographic relief exposing a scarp or plane along which the displacement occurred. The offset of linears, such as drainage channels and ridges, produce an abrupt discontinuity at the plane of fault offset. Large offsets of drainage channels

are produced by repeated small shifts, with the channel reestablishing the continuity of its course during the intervening periods. Offset drainage channels have been detected along the San Andreas fault, and are described by Wallace (1968b) and Sieh (1978). A fault gap is formed by displacement which laterally offsets a ridge so that the two parts are no longer continuous. A saddle is a deep, short defile through a hill, ridge, or mountain where a notch resulting from displacement is produced at the fault intersection. Shutterridges are formed by lateral fault offset of ridge-and-canyon topography. The displaced part of a ridge shuts off the adjacent canyon. Closed depressions are created by the downward movement of large blocks between separate faults, or by the subsidence of small blocks between splays or strands of a given fault. An example of a large block depression is the Salton basin, California, which is described by Brown (1922) and Hamilton (1969). The Salton basin is bounded by the San Andreas fault to the east and the San Jacinto fault to the west, separated by 45 km. The Mesquite basin, California, described by Sharp, et al. (1982), is an example of an intermediate size depression. The Mesquite basin is bounded by the

Imperial fault to the west and the Brawley fault to the east, separated by 5 km. Smaller depressions are more common and, when filled with water, are termed sag ponds.

A fault-line scarp is a secondary feature created by erosion acting on rock units of different resistance juxtaposed by faulting. The relief of the fault-line scarp is due solely to erosion. Other fault-line features are similarly a product of erosion and include fault-line valleys, gaps, and saddles.

Select geomorphic features are illustrated in Figure 3.4. A summary of the geomorphic features associated with strike-slip faults is presented in Table 3.1. The geomorphic features listed in Table 3.1 are divided into two main sections, primary and secondary, with each main section subdivided into three subsections. The subsections for primary features are offset, depression, and compression, and for secondary features are erosion, deposition, and ground water barrier. Examples of each feature and associated references are listed in the table.

The identification of active faults can be made through knowledge and recognition of characteristic

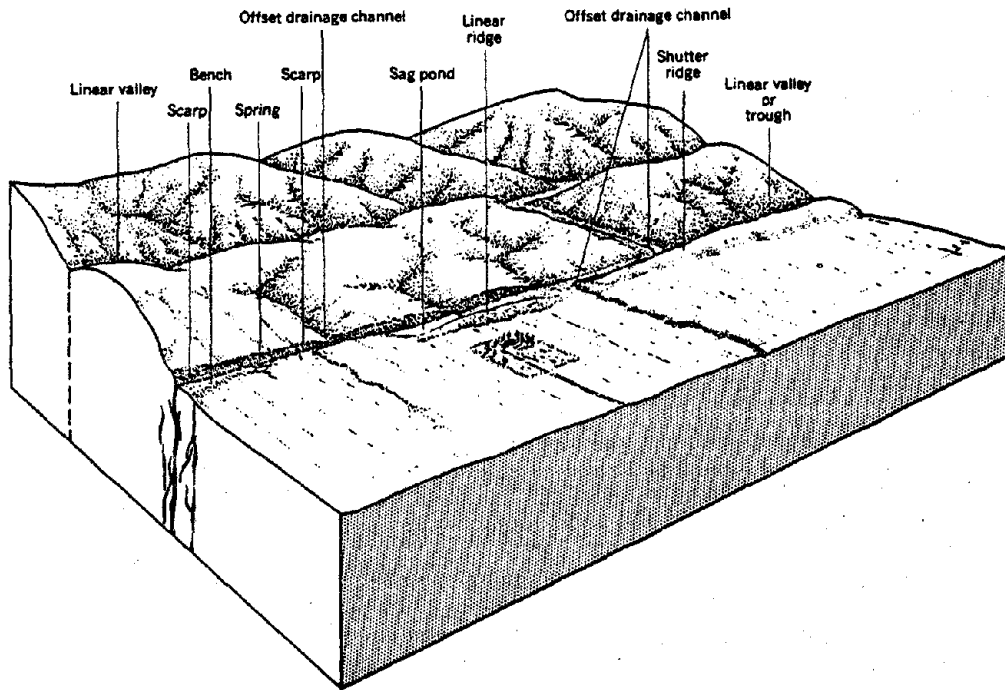


Figure 3.4. Geomorphic features developed along active strike-slip faults (after Wesson, et al., 1975).

Table 3.1. Summary of geomorphic features associated with strike-slip faults.

FEATURES	EXAMPLES	REFERENCES
<u>Primary Features</u>		
- Offset	fault scarp drainage channel  ridgeline gap saddle, notch shutterridge fissure (fault trace)	Sharp (1954); Slemmons (1977) Sharp (1954); Slemmons (1977); Wallace (1968) Slemmons (1977) Sharp (1954); Slemmons (1977) Sharp (1954); Slemmons (1977) Buwalda (1937) Slemmons (1977)
- Depression	linear valley, trough closed depression (sag pond when wet)	Sharp (1954); Slemmons (1977) Sharp (1954); Slemmons (1977)
- Compression	Pressure ridge mole track	Wallace (1949) Sharp (1954)
<u>Secondary Features</u>		
- Erosional	fault-line scarp fault-line valley, trough fault-line gap fault-line saddle, notch	Sharp (1954) Sharp (1954)  Sharp (1954) Sharp (1954)
- Depositional	ponded alluvium alluvial fan, apron	Slemmons (1977) Sharp (1954)
- Groundwater Barrier	elongated spring aligned springs	Slemmons (1977) Slemmons (1977)

geomorphic features. These features are often easier to detect from aerial views so that remote sensing can be a valuable means of locating active faults. The application of remote sensing for active fault identification is described by Babcock (1971), Krinitzsky (1974), Sherard, Cluff, and Allen (1974), NASA (1979), and Rowan and Wetlaufer (1981). The use of detailed field mapping, which may be required for detection of more subtle geomorphic features, is described by Taber (1923), Miller (1941), Wallace (1968), Krinitzsky (1974), Slemmons (1977), and Sieh (1978).

### 3.3 FAULT CREEP

Creep is the gradual, episodic movement of a fault without the associated occurrence of an earthquake. Nason, Philippsborn, and Yamashita (1974) have observed that creep movement generally occurs in cyclic episodes of short duration with little relative movement between episodes. Fault creep differs from fault slip during an earthquake because it occurs slowly. The discussion of creep will be confined mainly to faults on which movement results from tectonic activity. Nontectonic subsidence can be caused by the removal of fluids from the ground. For example, creep has been observed on the Buena Vista fault

in the Taft, California oil field (Koch, 1933; Wilt, 1958; and Howard, 1968), where creep apparently was caused by the pumping of petroleum and water.

Creep in the U.S. was first observed by Steinbrugge and Zacher (1960) on the San Andreas fault. Since then, creep has been observed on several other U. S. strike-slip faults. These include the Hayward, Calaveras, and Imperial faults. Creep observations are typically reported as a displacement per year. This rate often reflects an average developed from displacements measured over several years. Rates of creep up to 33.3 mm/yr have been observed by Burford and Harsh (1980) for a location on the San Andreas fault. The maximum rates of creep observed by Nason (1971a) for the Hayward and Calaveras faults are 7 and 15 mm/yr, respectively. The creep rate on the Imperial fault, determined by Cohn, et al. (1982), is 6 mm/yr.

The cumulative creep offset over time may be large, and the damage from creep to buried pipelines and other lifelines intersecting the fault may be significant in some instances. A discussion of buried pipeline response to fault creep is presented in Chapter 4.

Creep may occur intermittently with earthquake-induced faulting. For example, the San Andreas fault is creeping at San Juan Batista and Cholame, California, where coseismic slip occurred during the 1906 and 1857 earthquakes, respectively (Burford and Harsh, 1980). Similarly, the Hayward fault is creeping in a section on which coseismic slip occurred during the 1868 Hayward earthquake (Nason, 1971b).

Creep is generally confined to a narrow width of several meters (Nason, 1971b) on planes of the most recently active ruptures. Variations in the width over which creep displacements occur are to be expected for different faults, as are changes in the location of most intensive shearing within the width. The distribution of creep on the San Andreas fault is less than 70 m wide, with the most severe shear distortion within a 15-m-wide zone (Burford and Harsh, 1980). Observations of creep for portions of the San Andreas, Hayward, and Calaveras faults by Nason (1971b) have shown that widths are usually more than 1 m but less than 10 m, with 5 m common.

#### 3.4 DISTRIBUTION OF DISPLACEMENT

In the following, the distribution of displacement along the length of surface faulting is dis-

cussed. This is followed by a discussion of the distribution of displacement across the width of the main fault zone. Emphasis is placed on historic evidence of fault movements, and observed displacements are used to delineate patterns of surface faulting that are likely to occur during future earthquakes.

#### 3.4.1 Distribution of Displacement Along the Length of Surface Faulting

Information on the distribution of movement with respect to the length of surface faulting requires measurements at many locations. The fault movements should be relatively large so they can be distinguished clearly with respect to other ground movement features, and the locations of measurement should be spaced at reasonably small separations to obtain a good sense of the distribution pattern. There have been only a few earthquakes in the continental U.S. for which the records of surface faulting satisfy these criteria. The earthquakes include the 1857 Fort Tejon (Sieh, 1978), the 1906 San Francisco (Lawson, et al., 1908), the 1968 Borrego Mountain (Clark, 1972), and the 1979 Imperial Valley (Sharp, et al., 1982) earthquakes. The observations pertaining to the 1940

Imperial Valley earthquake are not of sufficient number and quality south of the U.S.-Mexico border to permit a detailed plotting of displacements along the entire fault length. Likewise, the records pertaining to the 1906 San Francisco earthquake do not cover the full rupture distance. The offshore displacements for the 1906 event between Point Arena and Shelter Cove represent a gap in the record of 115 km, and the displacements and length of faulting north of Shelter Cove are not known.

Figure 3.5 shows the observed displacements plotted as a function of the lengths of surface faulting for the 1857 Fort Tejon, the 1968 Borrego Mountain, and the 1979 Imperial Valley earthquakes. The observations for the 1979 Imperial Valley event were made four days after the earthquake so they do not include significant components of afterslip. The displacements have been expressed as fractions of maximum fault displacement, and the distances along the fault have been expressed as fractions of the full surface rupture length. In each case, the pattern of displacement is skewed. The points of maximum displacement are located between 0.13 and 0.38 of the total surface fault length, measured from the closest end of

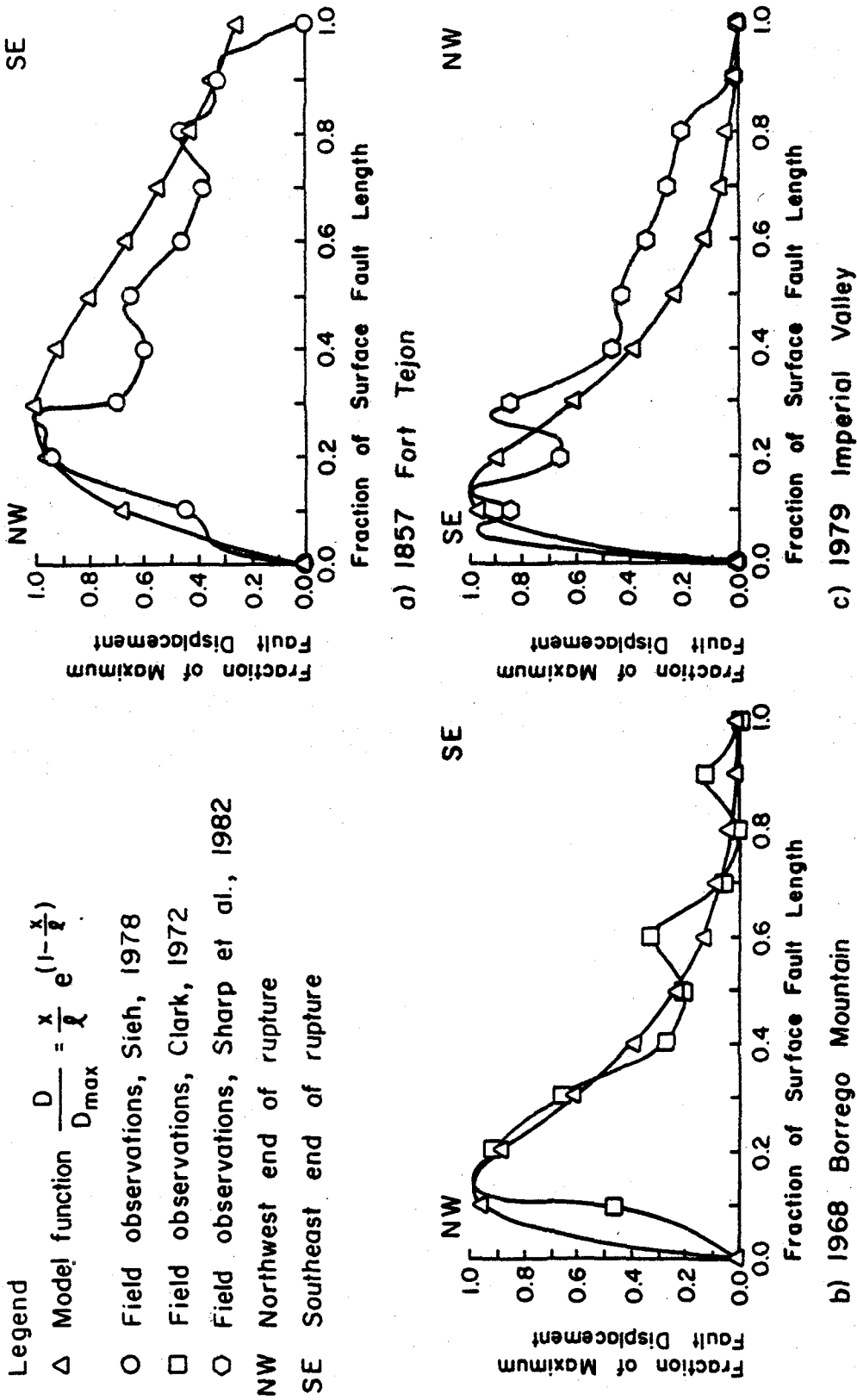


Figure 3.5. Plots of fractions of maximum fault displacement vs. fractions of surface fault length, comparing field observations with displacement model for the: a) 1857 Fort Tejon; b) 1968 Borrego Mountain; and c) 1979 Imperial Valley earthquakes.

faulting.

Because of the skewed nature of the distributed movements, it was felt that the displacement,  $D$ , could be expressed as a function of distance along the fault,  $x$ , by combining a linearly increasing function,  $Ax$ , with a decaying exponential function,  $e^{-Bx}$ , in which  $A$  and  $B$  are constants. The product of these functions is:

$$D = Axe^{-Bx} \quad (3.1)$$

If the distance is normalized with respect to the distance,  $\ell$ , at which the maximum displacement,  $D_{\max}$ , occurs, then it can be shown that:

$$D_{\max} = \frac{A}{B} e^{-1} \quad (3.2)$$

and

$$B = \frac{1}{\ell} \quad (3.3)$$

Combining Equations 3.1, 3.2, and 3.3, we obtain:

$$\frac{D}{D_{\max}} = \frac{x}{\ell} e^{(1 - \frac{x}{\ell})} \quad (3.4)$$

This function is plotted in Figure 3.5 with the observed distribution of displacement for the three surface faulting events.

Table 3.2 summarizes observations of displacements for the 1857 Fort Tejon, the 1906 San Francisco, the 1968 Borrego Mountain, and the 1979 Imperial Valley earthquakes. The table lists the length of surface faulting,  $L$ , the maximum displacement,  $D_{\max}$ , and the minimum distance along the length of surface faulting to the point of maximum displacement,  $\ell$ . The average fault displacements are listed on the basis of both the observed movements and the movements given by Equation 3.4. The observed average displacement,  $\bar{D}_E$ , was determined directly from the plot of the measured fault offsets. The model average displacement,  $\bar{D}_M$ , was calculated by integrating Equation 3.4 with respect to  $x$  to obtain the area under the function. This area then was divided by the surface faulting length,  $L$ , to obtain:

$$\bar{D}_M = \frac{\ell D_{\max}}{L} \left\{ e\ell - \left[ e^{(1 - \frac{L}{\ell})} \right] \ell \left( 1 + \frac{L}{\ell} \right) \right\} \quad (3.5)$$

The model average displacement is not given for the 1906 San Francisco earthquake because of the sub-

Table 3.2. Summary of observed displacements for four surface faulting events.

Event	Surface Faulting Length, L (km)	Maximum Displacement $D_{max}$ (m)	Minimum Distance Along Surface Fault To Point of Maximum Displacement, $z$ (km)	Average Observed Displacement, $\bar{D}_E$ (m)	Average Model Displacement, $\bar{D}_M$ (m)	References
1857 Fort Tejon	400.0	9.50	112.0	4.80	6.30	Steh, 1978
1906 San Francisco	435.0+	6.40	165.3	2.54	c	Lawson, et al., 1908
1968 Borrego Mountain	33.0	0.38	4.2	0.12	0.13	Allen, et al., 1968 Clark, 1972
1979 Imperial Valley	30.5	0.60	4.0	0.28	0.21	Sharp, et al., 1982

a - Determined from the plots of observed displacement vs. faulting length.

b - Calculated on the basis of Equation 3.5.

c - Not modeled because of uncertainties in the rupture length and displacements.

stantial gaps in the record of displacement associated with subaqueous locations of the San Andreas fault. Richter (1958) points out that there is a distinct possibility that faulting continued for a significant distance offshore of the northern terminus of the fault observations. Accordingly, both the length of faulting and the minimum distance to the location of maximum surface displacement are not known with sufficient accuracy for application in the model function. The distances and displacements given for the 1906 San Francisco earthquake are based on the mapped lengths of terrestrial faulting.

Table 3.3 summarizes fault movements, expressed as fractions of the maximum displacement, with respect to distance along the fault, expressed as a fraction of the total length of faulting. The fractions of the maximum displacement represent the largest displacements occurring along 0.95, 0.90, 0.75, and 0.50 of the total fault length. This table may be regarded as a vehicle for evaluating movement on a probabilistic basis. Each fractional displacement is, in effect, the probability that movement generated along the length of faulting will be less than or equal to the fraction of the maximum displacement associated with

Table 3.3. Fractions of maximum fault displacement associated with various fractions of surface fault length.

Fraction of Fault Length	Fraction of Maximum Displacement							
	1857 Fort Tejon Earthquake		1906 San Francisco Earthquake		1968 Borrego Mountain Earthquake		1979 Imperial Valley Earthquake	
	Observed	Estimated	Observed	Estimated	Observed	Estimated	Observed	Estimated
0.50	0.47	0.68	0.56	0.24	0.21	0.41	0.21	0.21
0.75	0.66	0.90	0.68	0.49	0.62	0.68	0.62	0.62
0.90	0.92	0.98	0.74	0.87	0.94	0.88	0.94	0.94
0.95	0.96	0.99	0.76	0.95	0.98	0.95	0.98	0.98

Observed - Displacement fractions derived from field observations

Estimated - Displacement fractions derived from model function

it in the table.

The fractions of maximum displacement listed in the table were determined from the field observations associated with given earthquakes and from the integration of Equation 3.4. The model displacements associated with the 1906 San Francisco earthquake are not listed for reasons previously discussed in conjunction with Table 3.2. The displacements estimated with the aid of Equation 3.4 generally show good agreement with those derived from the field observations. The model function generally gives conservative estimates for fractional fault lengths exceeding 0.75.

In summary, the observed displacements for the strike-slip faulting events studied are skewed with respect to length of surface faulting. They have maximum displacements near one end of the surface faulting lengths. The model function proposed by Equation 3.4 describes the trend of the displacement when compared with measurements for the 1857 Fort Tejon, the 1968 Borrego Mountain, and the 1979 Imperial Valley earthquakes.

#### 3.4.2 Distribution of Displacement Across the Width of Surface Faulting

Strike-slip fault rupture seldom occurs as a sin-

gle fracture, but often occurs as a succession of overlapping en echelon fractures. Large lengths of continuous ruptures step over to the next overlapping length of rupture. Distances up to several kilometers between these continuous ruptures may contribute to an apparently large fault zone width, although most of the displacement is concentrated within narrow zones associated with the individual rupture lengths. The individual ruptures may be composed of a continuous set of small scale, en echelon fractures having a stepover distance of several millimeters to meters, or may be composed of one or more abrupt planes of displacement. Descriptions of the formation and occurrence of en echelon fracture patterns are given by Tchalenko (1970), Slemmons (1977), Bornyakov (1980), and Segal and Pollard (1980). Several faulting events have shown prominent en echelon fracturing, including the 1906 San Francisco (Lawson, et al., 1908), the 1966 Parkfield-Cholame (Brown and Vedder, 1968), the 1968 Borrego Mountain (Clark, 1972), the 1975 Galway Lake (Beeby and Hill, 1975), the 1975 Oroville (Hart and Rapp, 1975), and the 1979 Imperial Valley (Sharp, et al., 1982) earthquakes. The narrow belt of en echelon fractures and abrupt planar offsets represents

the main fault zone, designated as Zone I in Figure 2.4. The main fault zones of historic strike-slip faulting in the U.S. generally have been less than 50 m wide (Bonilla, 1970).

Taylor and Cluff (1977) and Taylor (1982) present a general view of the deformation associated with the main zone of surface faulting. Figure 3.6 shows that the surface deformation can be visualized in terms of slip, which includes abrupt offsets, and distortion. The total offset associated with both slip and distortion is referred to as shift. This latter component is often related to the maximum displacement at a given location along the fault.

Slip, or abrupt offset, represents the most severe condition of deformation. Accordingly, it is useful to know how much of the total shift will be contributed by abrupt movement. The distortion is helpful in defining the distance through which significant deformations can occur. It can be used to estimate the distance either side of the fault centerline within which special trenching or backfill procedures should be used for pipelines at fault crossings.

The historic evidence concerning fault movement

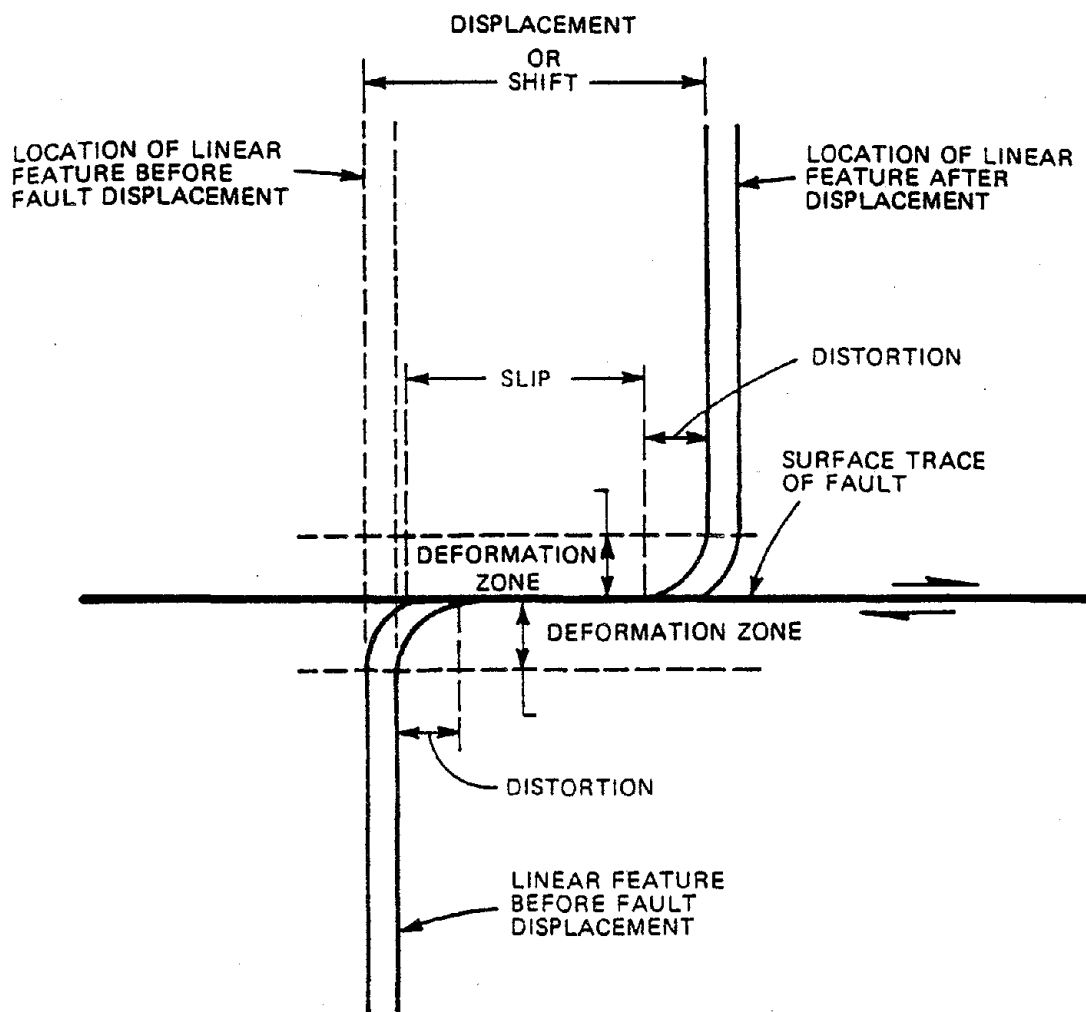


Figure 3.6. Relation of slip, shift, and distortion (after Taylor, 1982).

indicates that displacements are often concentrated within a narrow zone. For example, the main zone of surface rupture on the San Andreas fault from the 1906 San Francisco earthquake is described by Lawson, et al. (1908) as typically occurring across a width of 1 to 15 m. Sharp, et al. (1982) reports that much of the 1979 Imperial Valley main rupture zone occurred as a mole track with widths commonly less than 1 or 2 m. The combined widths of the main and branch ruptures associated with faulting during the 1968 Borrego Mountain earthquake were less than 50 m along 64% of the length of surface faulting (Clark, 1972). A similar trend in the width of rupture zone is noted along the Cleveland Hill fault for the 1975 Oroville earthquake. The main rupture zone reported by Hart and Rapp (1975) was generally less than 3 m wide, with widths less than 1 m along 60% of the faulting length.

Figure 3.7 shows the fraction of surface rupture length plotted against the width of main and branch ruptures for the 1968 Borrego Mountain earthquake. Clark (1972) reports that, where the zone was wider than 50 m, most of the displacement took place in a narrow belt of fractures ranging in width from less

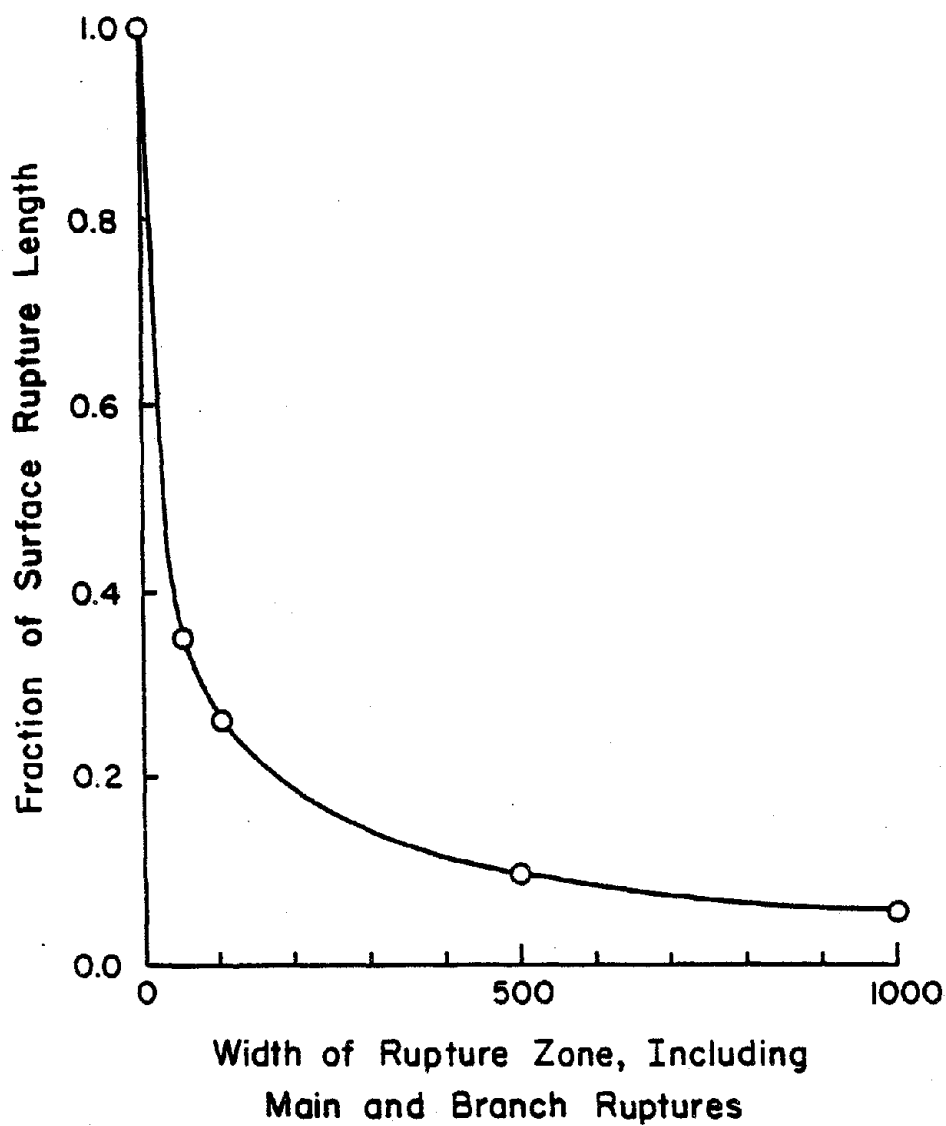


Figure 3.7. Fractions of surface rupture length vs. width of main and branch ruptures for the 1968 Borrego Mountain earthquake rupture (based on data reported by Clark, 1972).

than 1 m to 20 m. The maximum displacement of 380 mm was distributed across 6 to 10 m.

Lawson, et al. (1908) have made detailed measurements after the 1906 San Francisco earthquake of the distribution of displacement along structures intersected by the San Andreas fault. Many of these measurements are associated with wooden fences, for which the fence posts provide a relatively closely spaced set of observation points. In this study, the offset measurements at four fences were selected because they provide well marked and closely spaced points of measurement. Figure 3.8 summarizes the results of these measurements. The strike slip displacement is expressed as a fraction of the maximum offset and plotted as a function of the width of the deformation zone. The deformation zone width varies between 50 and 200 m. Abrupt displacements occur across very narrow widths of approximately 5 m or less. Abrupt displacement accounts for 40% to 90% of the maximum displacement across the zone. Three of the four distributions show that over 90% of the total displacement occurred within a width of 50 m.

Three buried gas pipelines, with internal diameters of 100, 200, and 250 mm, were intersected by

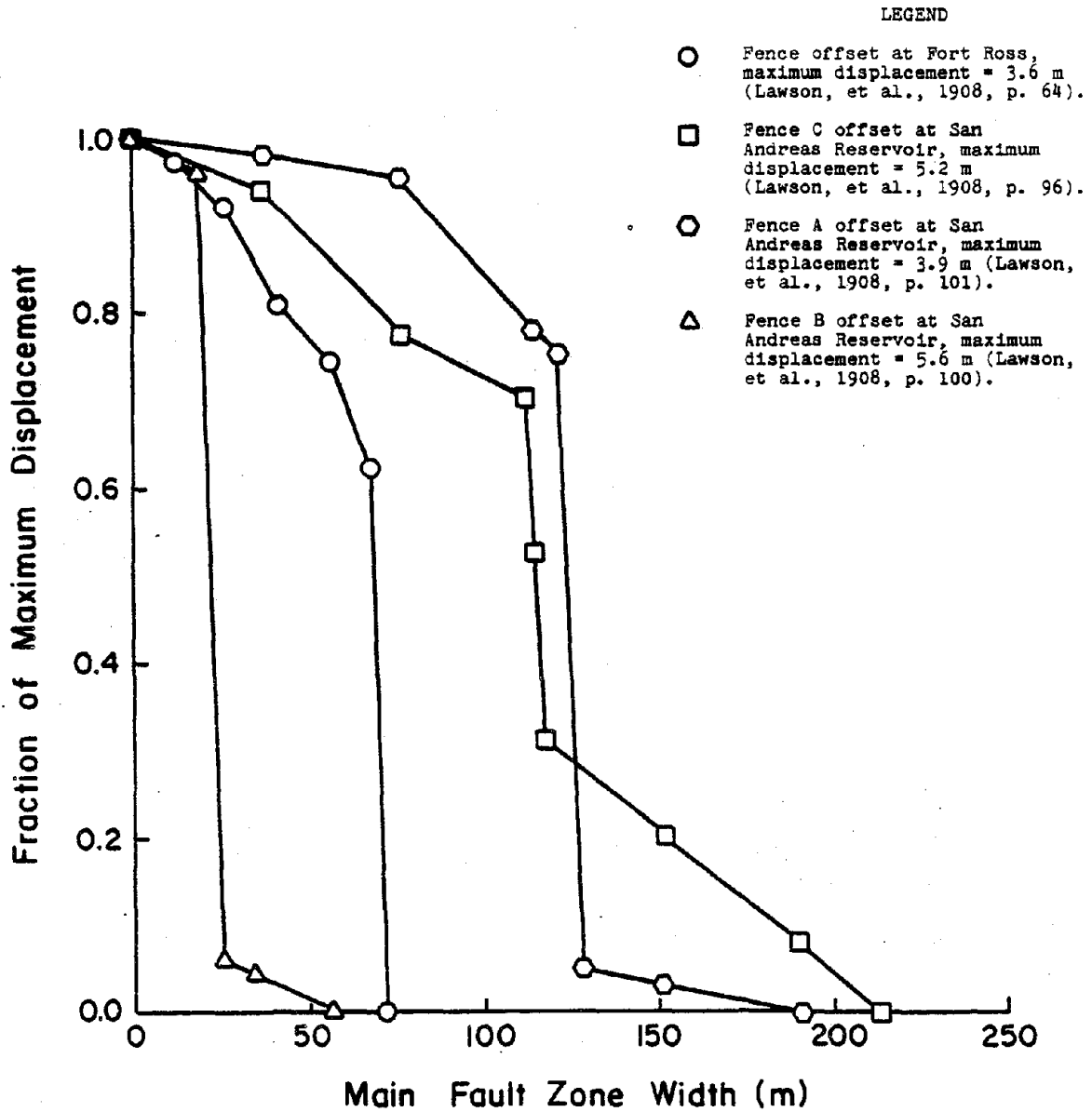


Figure 3.8. Distribution of displacement across the San Andreas Fault, determined from fence offsets, after the 1906 San Francisco earthquake.

strike-slip faulting during the 1979 Imperial Valley earthquake. Records of the observed pipeline deformations were taken during field inspection after the earthquake (McNorgan, 1982). Only the 100-mm-diameter pipeline was oriented such that substantial tension was imposed in the line by fault offset. Studies of pipeline-soil interaction by Harris and O'Rourke (1983) have shown that 100-mm-diameter pipelines are sufficiently flexible to deform in compliance with the pattern of soil movements. Accordingly, the 100-mm-diameter pipeline can be used to estimate the width of the main fault zone.

A 10-m-length of the 100-mm-diameter pipeline was excavated in the vicinity of the observed surface fault rupture. The pipe had a wall thickness of 6 mm, and was acetylene butt-welded. It was buried at a depth of 1 m in sandy backfill. The pipeline intersected the fault trace at approximately 55 degrees as shown in Figure 3.9. Although the pipe was not ruptured, an S-shaped curve was observed along the pipeline, caused by fault offset. McNorgan (1982) measured pipeline offsets perpendicular to the straight segments of the pipeline at distances parallel to the axis of the pipeline. The actual distribution of dis-

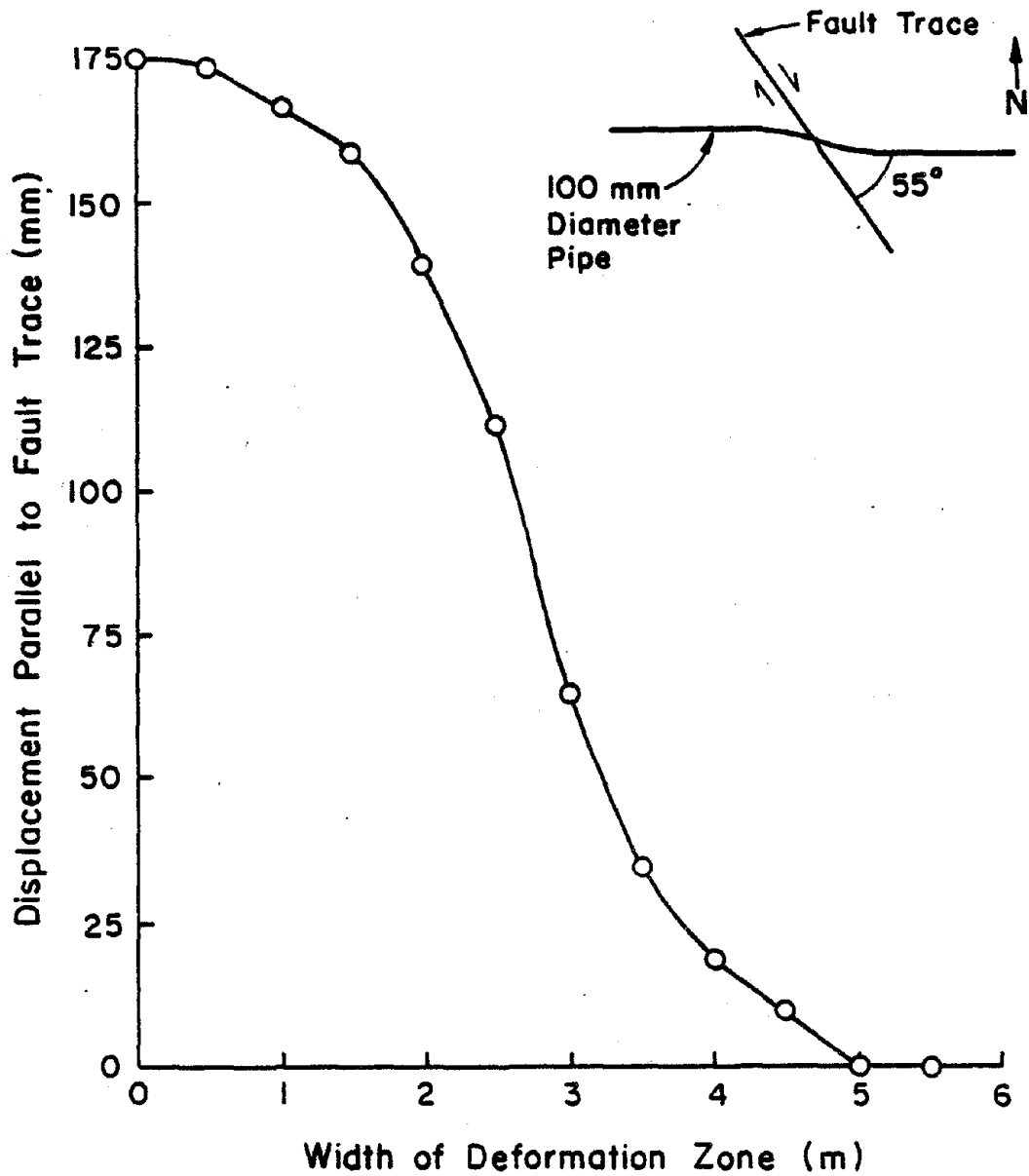


Figure 3.9. Plot showing distribution of fault displacement based on pipeline offset measurements by McNorgan (1982) for the 1979 Imperial Valley strike slip displacement.

placement perpendicular to the fault is not represented by these pipeline measurements, because the pipeline crossed the fault at an angle. Therefore, the pipeline offsets have been converted to reflect the relative displacement of a line perpendicular to the fault trace. The plot shown in Figure 3.9 shows that a displacement of 174 mm was distributed across a zone 4.5 m wide.

The observations summarized in this work for the 1906 San Francisco, 1968 Borrego Mountain, and 1979 Imperial Valley earthquakes indicate that a substantial part of the total fault offset is often concentrated at a single planar rupture or zone of closely spaced planar ruptures. These observations suggest that the best way to model fault offset is as a planar displacement. This modeling assumption will generally provide a moderate degree of conservatism.

### 3.5 LOCATION OF FAULT MOVEMENT

A major problem associated with building a pipeline at a fault crossing concerns the location of the main ruptures likely to develop during an earthquake. Cluff (1968) indicates that the most recently active fault trace would be the most likely site of future movements. Observations of fault rupture along the

San Andreas (Burford and Harsh, 1980) and Imperial (Cohn, et al., 1982) faults indicate that zones of creep are likely to be the locations of future coseismic movement.

Geologic surface mapping, geophysical exploration, historic accounts of faulting, and remote sensing can provide information regarding the location of the most recently active ruptures. Trenching perpendicular to the fault trace can provide perhaps the most positive and detailed evidence for assessing fault activity and precisely locating rupture planes. Taylor and Cluff (1973) discuss the procedures for conducting a trench exploration program, and point out features exposed in the trench that are relevant for assessing fault activity.

Five trenches excavated in a study by Taylor and Cluff (1973) along 245 m of the Hayward fault were used to locate the active trace and determine its width. The width was found to vary from 3 to 24 m, but the previous movements were concentrated on isolated planes a few centimeters in width and zones of concentrated planes having widths up to 3 m. A similar study by Woodward-Clyde Consultants (1978) on a 1.1-km-long section of the Hayward fault near the

Fairmont Hospital and Juvenile Hall in San Leandro has found the width of the active trace to vary from 0.3 to 13 m, with concentrated movements similar to those found by Taylor and Cluff. Taylor, Cummings, and Ridley (1980) have located a discontinuous set of en echelon fractures, associated with the 1906 earthquake, from the excavation of six trenches on the San Andreas fault in the Portola Valley west of San Jose. The widths of the fractures were from 2 to 7 m with isolated planes a few centimeters wide and zones of concentrated planes up to 4 m wide. The stepover distance between en echelon fractures was 100 m.

Information from conditions encountered during excavation of pipeline trenches could be useful in the location and assessment of fault activity, and for confirmation of design assumptions. Effective field engineering during pipeline excavation can provide feedback useful for determining whether conditions are consistent with design assumptions, and allowing design changes reflecting the differences in field conditions with those on which the design was based. Examples of design changes at the location of a fault crossing include alteration of backfill material and compaction, and application of coatings aimed at reducing the pipe/

soil friction to minimize pipe stress from fault offset. Other design measures benefiting from trench exploration feedback could involve installation of a more flexible pipe, change of the pipeline/fault angle of intersection, and provision for cut-off valves on opposite sides of the fault.

### 3.6 SUMMARY

Strike-slip faults are associated with active global plate or subplate boundaries. Repetitive surface faulting can be recognized by special geomorphic features. The most prominent geomorphic features are linear valleys, scarps, and offset drainage channels and ridges. Creep is the gradual, episodic movement of a fault without the associated occurrence of an earthquake. Although magnitudes of creep offsets over a period of years may be similar to a coseismic slip offset, the damage from creep movements is expected to be significantly less. Rates of creep up to 33.3 mm/yr have been observed at a location on the San Andreas fault. Most creep movements are distributed within a zone less than 15 m wide.

The measured displacements along strike-slip faults have shown a skewed distribution with respect to the length of rupture. The pattern of movement can

be represented by an expression that combines both linear and exponentially decaying functions of the fault distance. This model tends to give conservative estimates of displacement for fractional fault lengths exceeding 0.75. Field measurements of displacement associated with the 1857 Fort Tejon, 1906 San Francisco, 1968 Borrego Mountain, and the 1979 Imperial Valley earthquakes indicate that the average displacement along the fault is between 32 and 50% of the maximum fault displacement. Most fault displacements are concentrated as abrupt movements in zones less than 15 m wide. A zone of distortion less than 50 m wide generally accompanies abrupt displacement.

## CHAPTER 4

### BURIED PIPELINE RESPONSE TO CREEP

This chapter describes the measurements of distributed creep movements across the Hayward and San Andreas faults, and the long-term performance of buried pipelines crossing the Hayward fault. Repair records associated with several water distribution systems are summarized. A mathematical function, representing the pattern of displacements across zones of creep, is fitted to the data. A limit on the maximum fault creep offset that can be tolerated by buried, flexible mains is derived. Recurrence intervals for pipeline damage are estimated from the limit.

#### 4.1 INTRODUCTION

Displacement along the Hayward fault occurs as gradual to episodic right-lateral slips, which accumulate over a period of years to cause substantial offsets across streets, railroads, tunnels, and pipelines that intersect the fault. Rates of creep vary along the length of the fault, and with time. The effects of creep on pipelines intersecting the Calaveras fault in the City of Hollister, California, have been studied by O'Rourke and Trautmann (1980b). Bending was

HAYWARD FAULT CREEP OBSERVATIONS

NUMBER	LOCATION	RELATIVE DISPLACEMENT	MEASUREMENT OF	REFERENCE
1	Culvert, Berkeley Memorial Stadium	109 mm over 42 yrs.	Culvert offset	Radbruch & Lennert, 1966, p. 303
2	Claremont Water Tunnel	168 mm over 35 yrs.	Tunnel offset	Brown, Brekke & Korbin, 1981, p. 24
3	BART C2 Tunnel	43 mm over 11 yrs.	Tunnel offset	Brown, Brekke & Korbin, 1981, p. 80
4	BART C1 Tunnel Rose St., Hayward	32 mm over 11 yrs. 200 mm over 37 yrs.	Tunnel offset Curb offset	Nason, 1971a, p. 121
5	Sunset Blvd., Hayward Simon St., Hayward	240 mm over 37 yrs. 180 mm over 37 yrs.	Curb offset Curb offset	Nason, 1971a, p. 123 Nason, 1971a, p. 123
6	B St., Hayward C St., Hayward D St., Hayward	470 mm over 55 yrs. 300 mm over 54 yrs. 300 mm over 45 yrs.	Blidewalk offset Curb offset Curb offset	Nason, 1971a, p. 121 Nason, 1971a, p. 123 Nason, 1971a, p. 123
7	Western Pacific RR track W# 4, Miles Southern Pacific RR track SP 2, Miles	196 mm over 12 yrs. 152 mm over 56 yrs.	Track offset Track offset	Bontila, 1966, p. 283
8	Hetch Hetchy Aqueduct Line 2, Irvington Hetch Hetchy Aqueduct Line 1, Irvington	254 mm over 40 yrs. 254 mm over 60 yrs.	Pipe offset Pipe offset	Cluff & Steinbrugge, 1966, p. 275
8	Fence, Irvington	152 mm over 25 yrs.	Fence post offset	Cluff & Steinbrugge, 1966, p. 264

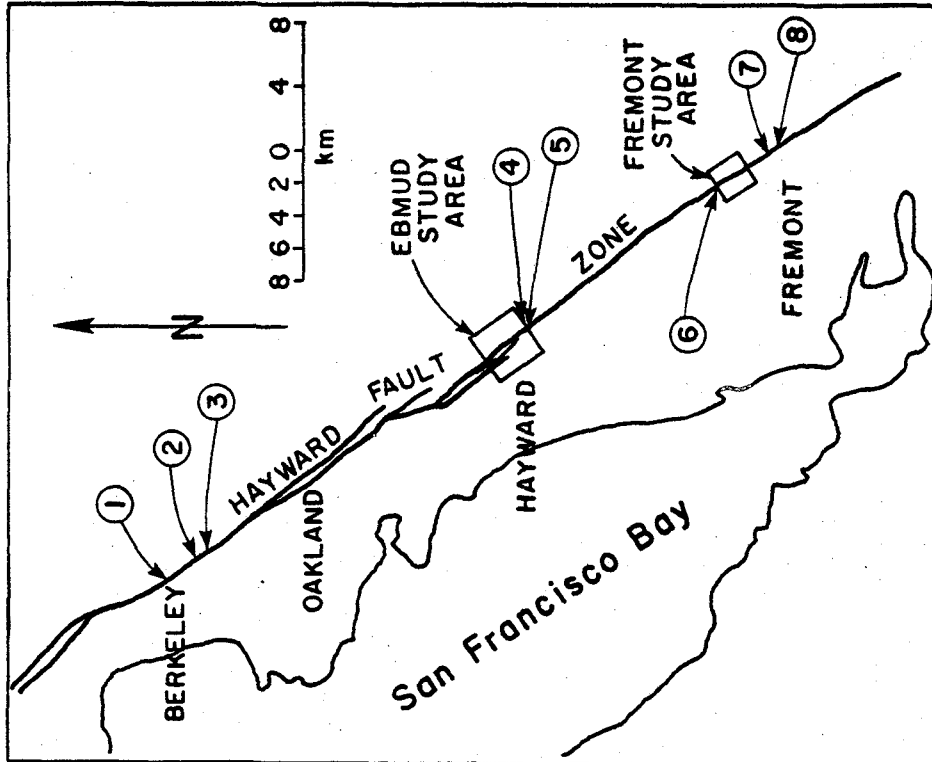


Figure 4.1. Locations of creep observations along the Hayward fault.

observed on several gas pipelines, and at one location the pipe was cut to relieve the stress induced by creep. Joint rotation of bell-and-spigot couplings of cast iron water pipelines were observed.

Figure 4.1 summarizes the observation locations and offsets reported by several investigators along the Hayward fault from Berkeley to Fremont, California. Eight locations of creep are shown in the figure and a summary of the observations are listed in the accompanying table. Observations, designated by numbers through 3, are for displaced underground water and transit tunnels (Radbruch and Lennert, 1966; Brown, Brekke, and Korbin, 1981). Observations, designated by numbers 4 and 5, are for displaced curbs and sidewalks (Nason, 1971a), and are within the East Bay Municipal Utility District (EBMUD) study area shown in the figure. Observation 6 is for displaced railroad tracks discussed by Bonilla (1966), and observations 7 and 8 are for pipeline and fence post offsets, respectively, measured by Cluff and Steinbrugge (1966). With the exception of the Western Pacific track offset in Niles, California, the average rate of creep for the observations summarized in the figure is approximately 5 mm/yr.

#### 4.2 PIPELINE REPAIR

A substantial portion of the water service in the eastern San Francisco Bay area is provided by three organizations: the East Bay Municipal Utility District, the City of Hayward Water Department, and the Alameda County Water District. Each of these organizations provided information for this study.

A study site in the EBMUD distribution system was selected to include a relatively large, representative sample of pipelines in an area where ground movement influences are associated chiefly with creep along the Hayward fault. The study site, which is shown in Figure 4.1, is bounded on the north by the Fairmont Hospital and on the south by Grove St. at the border of the City of Hayward. It is intersected by nearly 5 km of the Hayward fault trace. It covers an area of 6.0 km<sup>2</sup> and includes approximately 76 linear km of buried pipelines of which 57, 25, and 18% of the total are composed of cast iron, steel, and asbestos cement, respectively.

Pipeline repairs were identified from EBMUD utility repair record maps and leak repair reports for the time period of 1961 to 1981. Information concerning the repairs was summarized to include the age and type

of pipe repaired, date and nature of the repair, and condition of the pipe at the time of repair. The location of the repair relative to the centerline of the Hayward fault zone was noted.

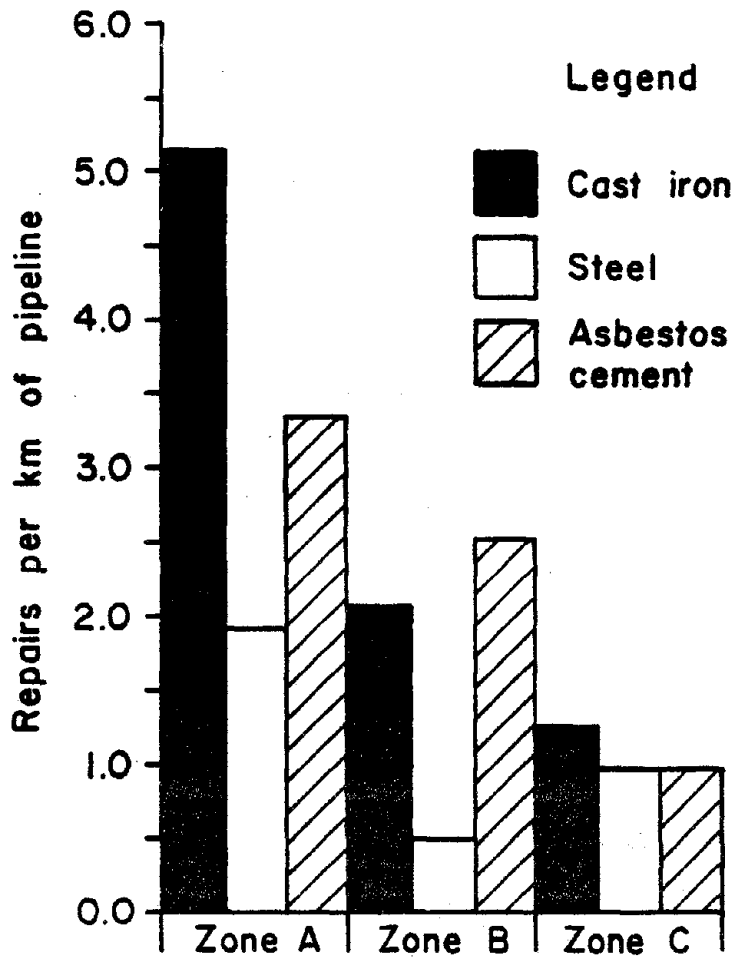
The centerline of the fault zone was taken as the main fault trace shown on the Special Study Zones Map, Hayward Quadrangle (California Division of Mines and Geology, 1982). Where possible, the fault trace location was verified with fault locations delineated in the vicinity of the study site by other investigators (Nason, 1971a; Woodward-Clyde Consultants, 1978).

Three zones adjacent to the fault trace were established: Zone A, within 60 m either side of the fault trace; Zone B, outside the 60 m zone but within the boundaries of the special studies zone as defined by the Alquist-Priolo Special Studies Zones Act (Hart, 1980); and Zone C, beyond the Alquist-Priolo Zone. The Alquist-Priolo Zone is delineated by the State Geologist to regulate development near traces of potentially hazardous faults. At the study site, the width of the Alquist-Priolo Zone is approximately 300 m. Because of active branches or splays of the fault, the width of the Alquist-Priolo Zone often is not symmetric with respect to the main fault trace.

Figure 4.2 shows the frequency of pipeline repairs per kilometer of line at the study site. The repair frequency is plotted for each type of pipe composition according to zone. The repairs from which the figure was developed do not include repairs to gate valves or cast iron pipelines with leadite-caulked joints. In the latter case, leadite has been observed to swell in response to decomposition of its sulphide constituents and causes damage unrelated to ground movements.

The frequency of repair is more than three times greater for cast iron and asbestos cement pipe within the zone nearest the fault trace as opposed to the areas outside the Alquist-Priolo Zone. The steel pipelines, which can accommodate significant differential movement by virtue of their ductility, do not show appreciable differences in repair frequency among the three zones, although an increase in repair frequency does occur near the main fault trace.

Although the repair records indicate that differential ground movements were associated with much of the pipeline damage, many of the records show that corrosion also contributed to damage. The soils in the study site are principally adobe soils with a high



**Zone A: 60m distance from fault trace**

**Zone B: Outside 60m distance from fault trace  
but within the Alquist-Priolo zone**

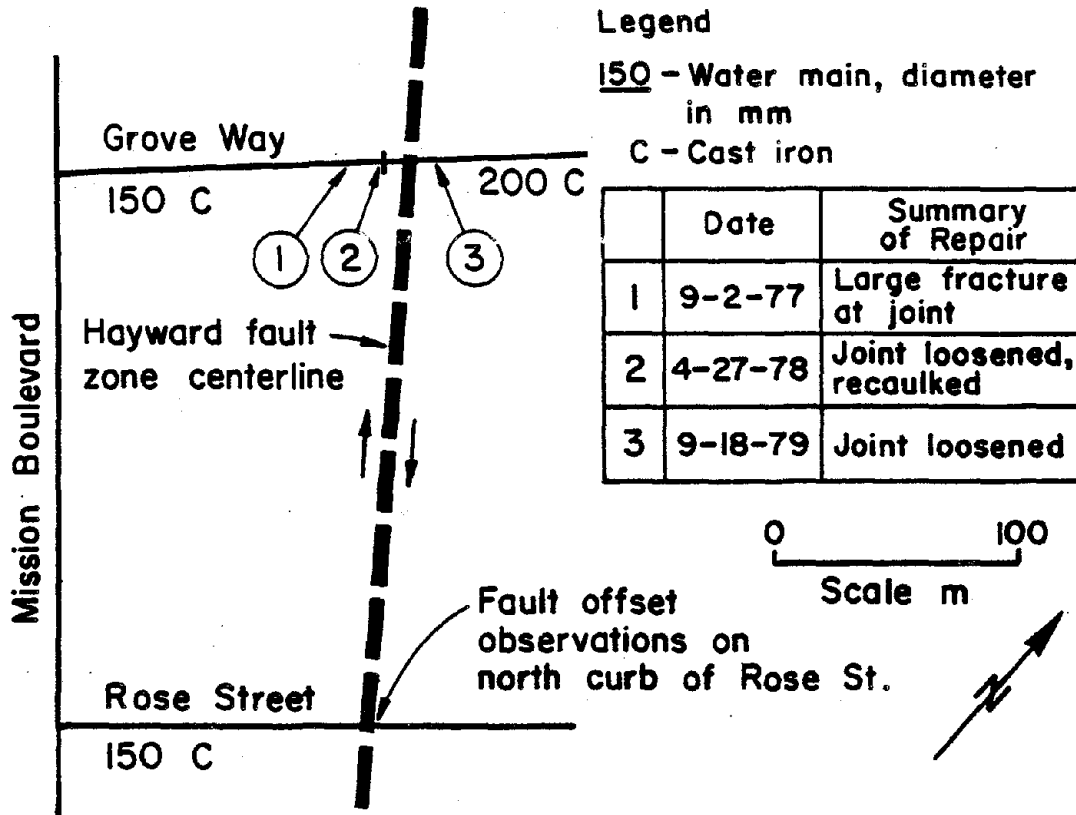
**Zone C: Outside the Alquist-Priolo zone**

Figure 4.2. Repair frequency for 1961 - 1981 time interval, for the EBMUD study area.

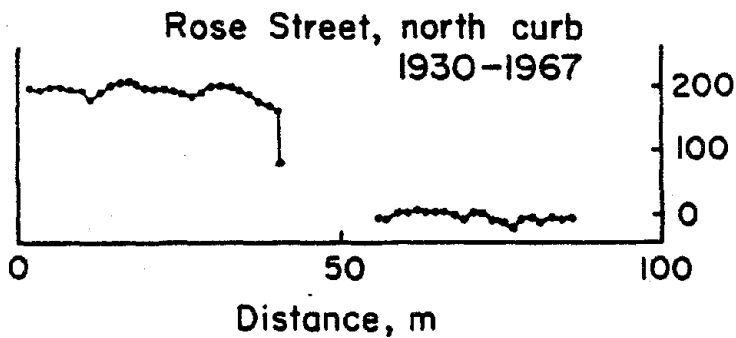
clay content. Soils of this type frequently are associated with corrosive environments.

Pipeline response to differential movement depends on its composition, age, state of repair, and method of installation. In particular, the performance of a cast iron pipeline is affected by lead-caulked joints, which may be responsible for differences in behavior among mains of the same age subjected to similar patterns of movement. This is illustrated in Figure 4.3, which shows the fault centerline intersecting Grove Way and Rose St. near the boundary of the City of Hayward, California. Observations by Nason (1971a) on Rose St. indicate a relative displacement of 200 mm over 37 years. Damage to the cast iron pipelines on Grove Way occurred at lead-caulked joints. The 150 mm and 200-mm-diameter lines were installed in 1934 and 1955, respectively. Joint repairs were made on three occasions from 1977 to 1979. In contrast, no repairs were recorded for the 150 mm diameter pipeline on Rose St., even though it is similar in composition to those on Grove Way and was installed in 1936.

Figure 4.4 shows a typical portion of the EBMUD study site. The internal diameters of all pipelines



a) Plan view, Hayward fault in Hayward, CA.



b) Curb offset (after Nason, 1971)

Figure 4.3. Creep displacement and pipeline damage on the Hayward Fault.

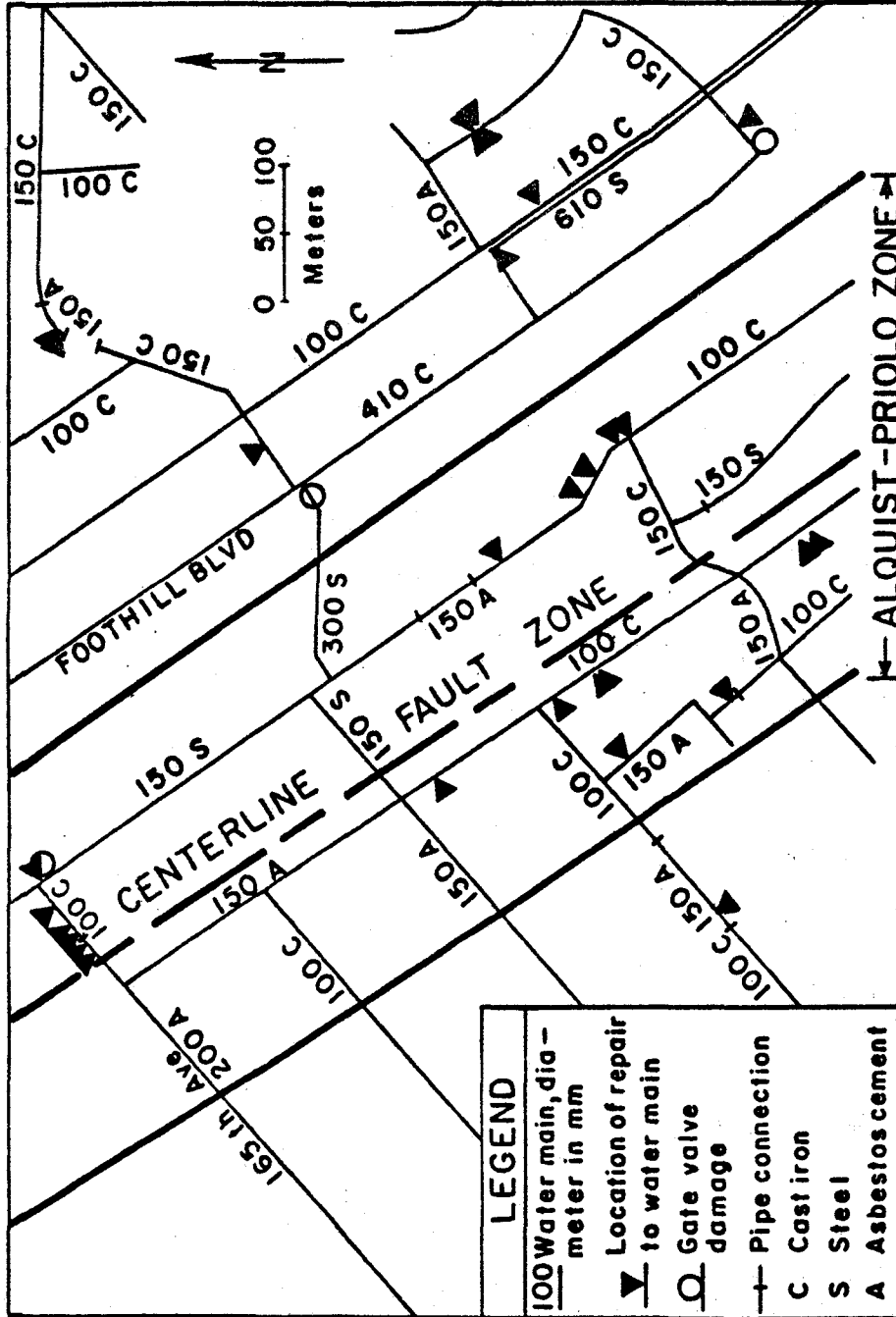


Figure 4.4. Pipeline repair locations for a typical section of the EBMUD water distribution system study area along the Hayward Fault.

are shown in millimeters, and locations of repair are indicated for a 20 year interval. The increased frequency of pipeline repairs can be seen near the fault zone centerline.

Pipeline repairs were reviewed for the distribution system operated by the Alameda County Water District in Fremont, California. The study area for pipeline repairs is bounded on the north by the Alameda County Flood Control Channel and on the south by Warren Avenue. In particular, the repair records for asbestos-cement pipelines were examined for the time interval from 1970 to 1981. Of the 13 pipelines installed across the Hayward fault between 11 and 25 years ago, four have broken at fault crossings during the 11 year period for which repair records were kept.

The City of Hayward Water Department also was contacted regarding pipeline repairs in the vicinity of the Hayward fault trace, but detailed records of repair were not studied. Although some joint rotations have been noticed in cast iron mains near the fault trace, the number of pipeline repairs in Hayward are reported to be very small at fault crossings.

#### 4.3 MODELING OF PIPELINE RESPONSE TO CREEP

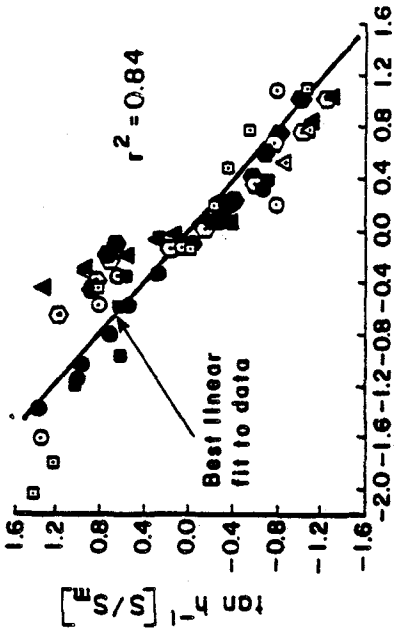
Pipelines 150 mm or less in internal diameter

generally are flexible with respect to the soil in which they are embedded. Because the pipelines tend to move as the ground moves, a mathematical function describing the pattern of ground movements can be used to estimate pipeline distortion.

Measurements of distributed movements within zones of fault creep for the Hayward fault were made from offset curbs and sidewalks by Nason (1971a), and from alignment arrays and pavement offsets for the San Andreas fault by Burford and Harsh (1980). These measurements were plotted and analyzed using the coordinate system shown in Figure 4.5a. The survey locations associated with these data are listed in Figure 4.5b.

For each data set, the centerline of the fault zone was located at a point corresponding to half the maximum offset across the fault. An effective fault width,  $2W_{90}$ , was defined as the horizontal distance separating the points corresponding to 90% of the maximum fault offset. This definition was adopted to provide a consistent basis for normalizing the data from different locations.

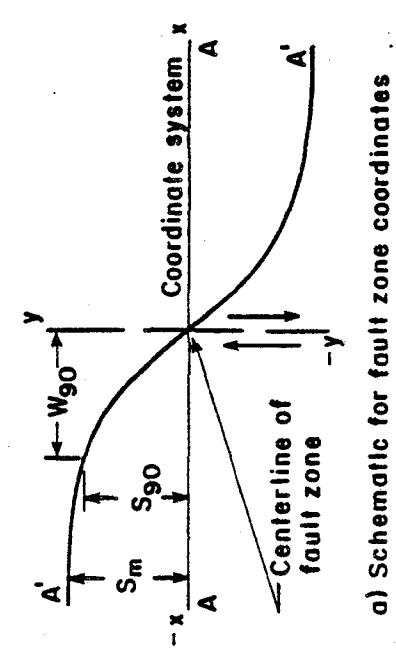
Initially, the data were shifted so that the center of the fault zone coincided with the origin.



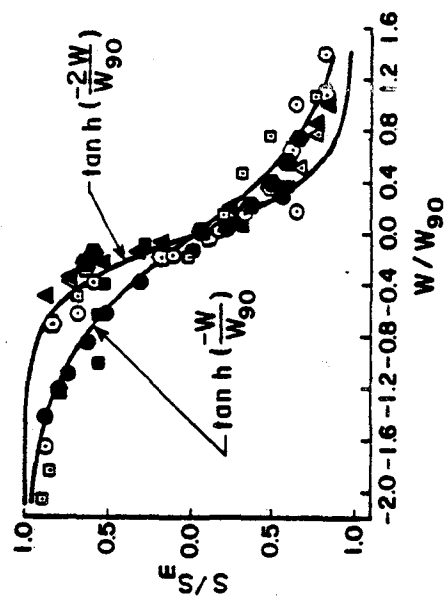
c) Plot of transformed data

Symbol	Location/Reference
●	Sunset St., curb, City of Hayward (Nason, 1971a, p. 119)
○	Simon St., curb, City of Hayward (Nason, 1971a, p. 119)
▲	B St., sidewalk, City of Hayward (Nason, 1971a, p. 121)
△	B St., curb, City of Hayward (Nason, 1971a, p. 121)
■	D St., curb, west fault trace, City of Hayward (Nason, 1971a, p. 123)
□	D St., curb, east fault trace, City of Hayward (Nason, 1971a, p. 123)
◆	San Juan alignment array, San Andreas fault zone (Burford and Harsh, 1980, p. 1247)
◇	San Juan Bautista - Hollister Highway, San Andreas fault zone (Burford and Harsh, 1980, p. 1246)

b) List of symbols for observation points



a) Schematic for fault zone coordinates and dimensions



d) Ground displacement vs. distance from fault

Figure 4.5. Analysis of displacements within zones of fault creep.

Next, the data were normalized by dividing the fault offset values,  $S$ , by the half maximum offset,  $S_m$ , and by dividing the distance from the fault centerline,  $W$ , by half the effective fault zone width,  $W_{90}$ .

The normalized data were fitted with a hyperbolic tangent function of the form:

$$\frac{S}{S_m} = \tanh \left[ \frac{CW}{W_{90}} \right] \quad (4.1)$$

where  $C$  is a constant. By taking the inverse hyperbolic tangent of both sides of Equation 4.1, one obtains:

$$\tanh^{-1} \left[ \frac{S}{S_m} \right] = \frac{CW}{W_{90}} \quad (4.2)$$

By plotting  $\tanh^{-1} [S/S_m]$  vs.  $W/W_{90}$ , a straight line is obtained which passes through the origin with slope  $C$ . Standard linear regression (Snedecor and Cochran, 1980) indicates that  $C = -1.0$ , with a 95% confidence interval of plus or minus 0.1. The coefficient of determination,  $r^2$ , is 0.84, which indicates a good fit to the data.

Figure 4.5c shows the transformed data plotted with the best fit straight line, and Figure 4.3d shows

the actual dimensionless data plotted with two hyperbolic tangent functions. The function using  $C = -1.0$  corresponds to the average pattern of displacement for the fault data, and the function using  $C = -2.0$  corresponds to an approximate upper limit of the deformation from fault creep for the same data.

The maximum tensile strain,  $\epsilon_m$ , imposed on a pipeline subjected to bending is given by

$$\epsilon_m = \frac{K_m d}{2} \quad (4.3)$$

where  $K_m$  is the maximum curvature imposed on the pipeline by differential soil displacement and  $d$  is the outside diameter of the pipe.

The maximum curvature imposed on a relatively flexible pipeline within the fault zone can be derived by differentiating Equation 4.1 as:

$$K_m = \frac{0.77S_m C^2}{(W_{90})^2} \quad (4.4)$$

The maximum tolerable fault offset for a pipeline crossing a strike-slip fault at a right angle is found by combining Equations 4.3 and 4.4:

$$2S_m = \frac{5.2\epsilon_m (W_{90})^2}{C^2 d} \quad (4.5)$$

in which  $2S_m$  is the offset across the entire fault zone. It should be emphasized that pipelines oriented at an oblique angle with respect to the fault are vulnerable to axial strains that can lead to pull-out or compression at couplings. Modifications to account for the consequences of displacement at oblique fault crossings have been described by O'Rourke and Trautmann (1981).

Equation 4.5 can be used to estimate recurrence intervals for pipeline damage. As an example, consider a 150-mm-diameter cast iron pipe with a maximum permissible strain of 0.001 and an outside diameter of 175 mm crossing a fault zone of effective width,  $2W_{90}$ , of 7 m. According to Equation 4.5, using a mean value for  $C$  of -1.0, the maximum tolerable offset would be 364 mm. Assuming an average fault creep rate of 5 mm/yr, the recurrence interval for damage to a pipeline with zero initial strain would average 73 years. If, however, the curvature of the distributed movement within the fault zone approached the upper limit, such that a value of -2.0 were appropriate for  $C$ , the recurrence interval for damage would decrease to only 18 years.

It is clear from Equation 4.5 that the maximum

tolerable fault offset is very sensitive to the parameter C and the width of the fault zone. The wider the zone of creep movement, the more distributed the pipeline strain due to curvature will be. A corresponding increase in the maximum tolerable fault offset is obtained for a wider zone of creep.

Fault creep offset will gradually increase the strain in an intersecting buried pipeline. In contrast, earthquake rupture offset occurs within a few seconds causing a rapid strain increase. Accordingly, fault movements during earthquakes may cause significantly greater damage to buried mains than that associated with creep, even though the maximum fault offset is identical for the two cases.

#### 4.4 SUMMARY

Repair records for the EBMUD water distribution system indicate that the frequency of repair for cast iron and asbestos cement pipe within 60 m of the centerline of the Hayward fault zone is from three to four times higher than that for the same types of pipe beyond a distance of roughly 150 m from the fault zone centerline. A similar review of repair records for the distribution system operated by the Alameda County Water District shows that several asbestos cement

pipelines, which cross the fault and are over 10 years old, have been damaged. Because the Hayward fault intersects a relatively small portion of the East San Francisco Bay distribution systems, the increased frequency of repair does not represent a significant maintenance problem. Although the likelihood of pipeline damage increases at fault crossings, the actual number of repairs caused by fault creep is a relatively low number when considered on an annual basis. Repair records indicate that cast iron pipelines are damaged by both excessive joint rotation and bending strains in zones of creep along the fault trace.

A hyperbolic tangent function is found to provide a good representation of the pattern of displacement at zones of fault creep. Using the hyperbolic function, a theoretical limit is derived for the maximum offset that can be tolerated by buried, flexible mains. The maximum tolerable offset is proportional to the square of the fault zone width.

## CHAPTER 5

### BURIED PIPELINE RESPONSE TO FAULTING DURING THE 1971 SAN FERNANDO EARTHQUAKE

This chapter focuses on the effects of surface faulting on gas distribution and transmission pipelines during the 1971 San Fernando earthquake. The chapter begins by identifying the zones of surface faulting and the nature of the displacement in these zones. Pipeline damage is evaluated as a function of both the distance from the fault trace and the orientation of the pipelines relative to the fault. Damage to high pressure transmission pipelines intersected by the fault rupture and the association of explosion craters with the type of ground movement and pipe damage are evaluated. A detailed investigation is made at two locations to study the effects of surface faulting on distribution mains. A model is presented for siting a pipeline in an area of potential reverse and strike slip displacement.

#### 5.1 INTRODUCTION

The San Fernando earthquake of February 9, 1971 has been assigned a local Richter magnitude of 6.4 (Allen, Hanks, and Whitcomb, 1975). The fault break

that caused the earthquake originated on the San Fernando fault at a hypocenter about 8 km deep, approximately 13 km north-northeast of the City of San Fernando. Tectonic surface faulting extended 15 km along the front of the San Gabriel Mountains from the Lower San Fernando Lake area eastward across the Sylmar and San Fernando communities to the Big Tujunga Canyon. The San Fernando fault plane dips northward at an average angle of 55 degrees (U.S. Geological Survey Staff, 1971). Left-reverse-oblique fault movement along this plane produced a 2 m uplift of an 800 km<sup>2</sup> block of the San Gabriel Mountains and a shortening of 2 m as the block moved south (Oakeshott, 1973). A significant left lateral displacement component of nearly 2 m accompanied the reverse displacement. The left-lateral strike slip movement was of the opposite sense compared to the predominant right-lateral movement in California.

A significant part of the surface faulting occurred in culturally well-developed, urban and suburban communities. Although only one-half of one percent of the area affected by strong ground shaking was influenced by surface faulting (Housner and Jennings, 1972), the principal cause of utility damage has been

ascribed to permanent ground movements (Moran and Duke, 1971). Over 2,400 breaks in water, natural gas, and sewer pipelines have been reported in the area of fault displacements (Steinbrugge, et al., 1971).

The disruption of utility services during the earthquake raises significant questions with regard to the seismic performance of lifeline systems in zones of surface faulting. These questions pertain to the response of individual pipelines as well as their system-wide performance, and require an investigation of: 1) how pipeline damage was distributed with respect to the location of fault movement; 2) what orientations, soil conditions, and mechanical features have the most significant impact on performance; and 3) what measures can be taken to mitigate damage during future earthquakes. To answer these questions, this chapter concentrates on the field observations and repair records associated with the natural gas distribution and transmission system in the zones of largest ground deformation along the San Fernando fault. The patterns of repair and pipeline replacement are analyzed. Factors affecting seismic performance are investigated, including pipeline orientation and weld charac-

teristics. Specific instances of pipeline distortion are reviewed relative to the ground movement patterns, and a model for estimating the longitudinal distortion of pipelines subjected to reverse and strike-slip faulting is developed.

## 5.2 PATTERN OF SURFACE FAULTING AND PIPELINE DAMAGE

Three principal zones of surface faulting have been identified along the San Fernando fault (U.S. Geological Survey Staff, 1971), and at least two other zones of fault-related movements have been reported in a subsequent study (Weber, 1975). Figure 5.1 shows a plan view of the Mission Wells and Sylmar segments of the San Fernando fault as well as a zone of prominent ground ruptures and street cracks, referred to by Eguchi, et al. (1981) as the Harding School fault area. Each zone of prominent ground movement is bounded in the figure by a solid line.

The Mission Wells segment trends east-northeast and shows both left-lateral and reverse displacement. Where it crosses Osceola Street, in the middle of the segment, the fault dips 60 degrees north with the northern block uplifted 250 mm, thrusting 200 mm to the south, and left-laterally displaced 30 mm (U.S. Geological Survey Staff, 1971 and Weber, 1975). The

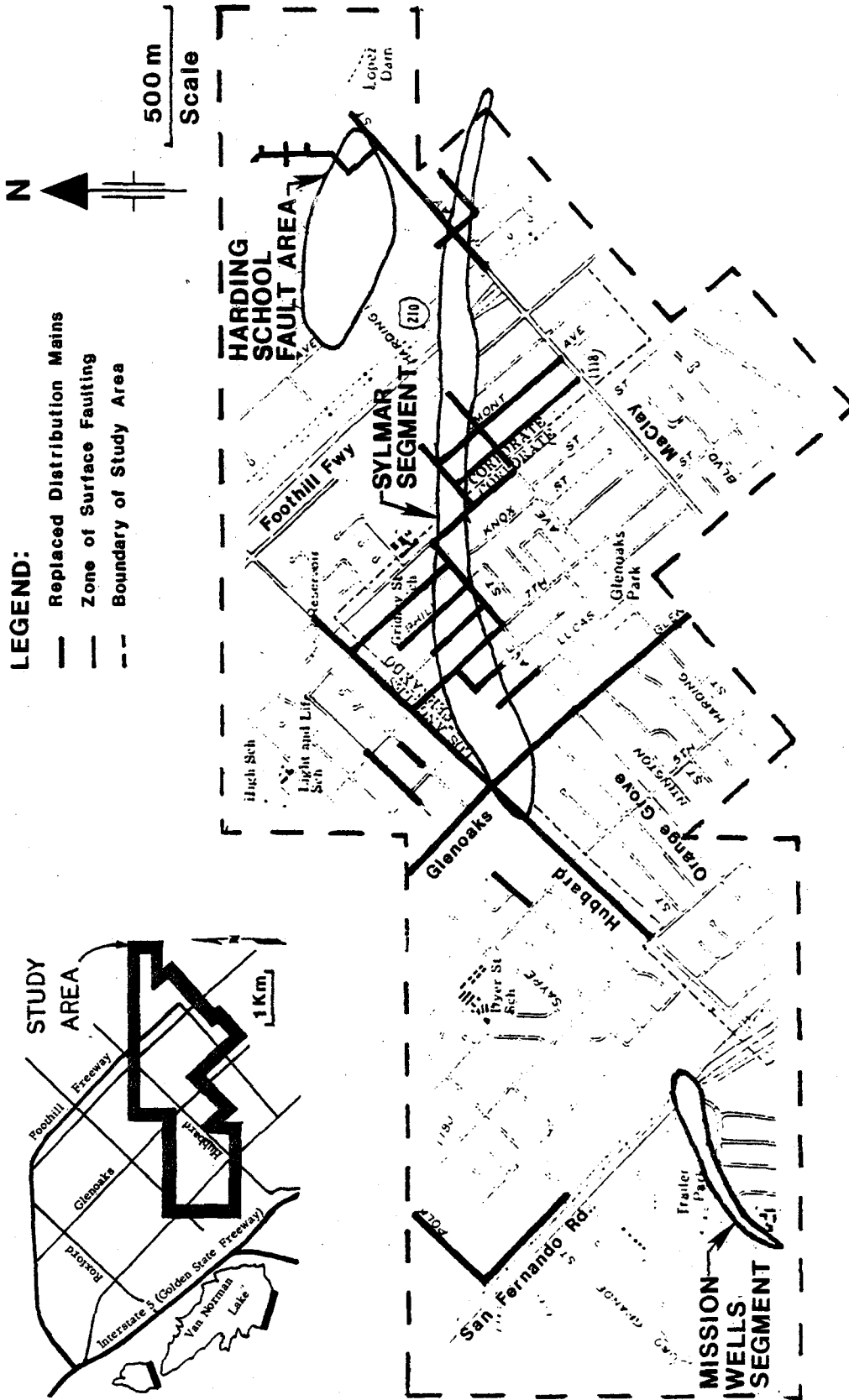


Figure 5.1. Plan view of surface faulting and replaced gas distribution pipelines.

segment had a length of nearly 1 km.

The 3-km-long Sylmar segment trends east-west across a densely populated area. The width of the zone of surface ruptures varied from 30 to 200 m. In the central part of the segment, displacements across the entire fault zone were composed of 1.9 m of left-lateral slip, 1.4 m of vertical offset, and 0.6 m of thrust (U.S. Geological Survey Staff, 1971). The largest individual ground ruptures showed displacements approximately one-half of the maximum displacements across the entire width of the zone. Most of the left-lateral slip and thrust was concentrated along the southern 25 to 80-m-wide section of the fault zone. North of this section, vertical offsets and extension fractures were the predominant forms of ground rupture (U.S. Geological Survey Staff, 1971).

The Harding School fault area is located between 0.2 and 1.0 km north of the eastern part of the Sylmar segment. This zone contained surface breaks that were offset vertically and downward to the north with right-lateral displacements. The maximum displacements were relatively small, varying from 10 to 50 mm. Weber (1975) suggests that these displacements reflect a tension release across bedding planes in the

underlying bedrock.

The study area for pipeline damage is shown as an inset in Figure 5.1 and is bounded by a dashed line in the main part of the figure. Within the study area, gas distribution pipelines were buried along rights-of-way that followed existing streets. The distribution mains were composed principally of 12-m-long segments of 25 to 200-mm-internal diameter steel pipe, connected at oxy-acetylene welded joints. Gas pressure in the pipelines at the time of the earthquake was approximately 0.24 MPa. The pipelines were buried at a nominal depth of 0.9 m, measured from the street surface to the top of the pipe. The soils in the Sylmar segment are mostly silty sands and gravels. A groundwater barrier exists across the Sylmar segment, with the water table measured at depths well below the pipelines of 20 and 40 m on the north and south sides, respectively, of the barrier (Oliver, et al., 1975).

Records of pipeline repair and replacement in the study area were provided through the courtesy of the Southern California Gas Company, and the repair records were checked and supplemented by information reported by the Southern California Gas Company (1973). Within the study area, a total of 112 repairs

was recorded.

Pipeline segments from 100 m to 2 km in length were replaced within several months after the earthquake. The replaced pipelines are shown in Figure 5.1. At locations where two or more pipelines were adjacent to each other under the same street, only the replaced pipeline is indicated. Sixteen percent of the total length of all distribution lines in the study area was replaced. There was a high concentration of replacements within and adjacent to the Sylmar segment, with replacements made for 67% of the total length of all lines within the segment. The number of replacements was influenced by the orientation of pipelines relative to the trace of the fault. Sixty-two percent of the total length of northwest oriented pipelines within the Sylmar segment was replaced, whereas 79% of the total length of northeast oriented pipelines was replaced.

Figure 5.2 shows a plan view of the Sylmar segment and Harding School fault area, on which the location of individual pipeline repairs are plotted. The types of repairs were determined from gas leak repair sheets provided by the Southern California Gas Company. The causes of repair were typically noted as

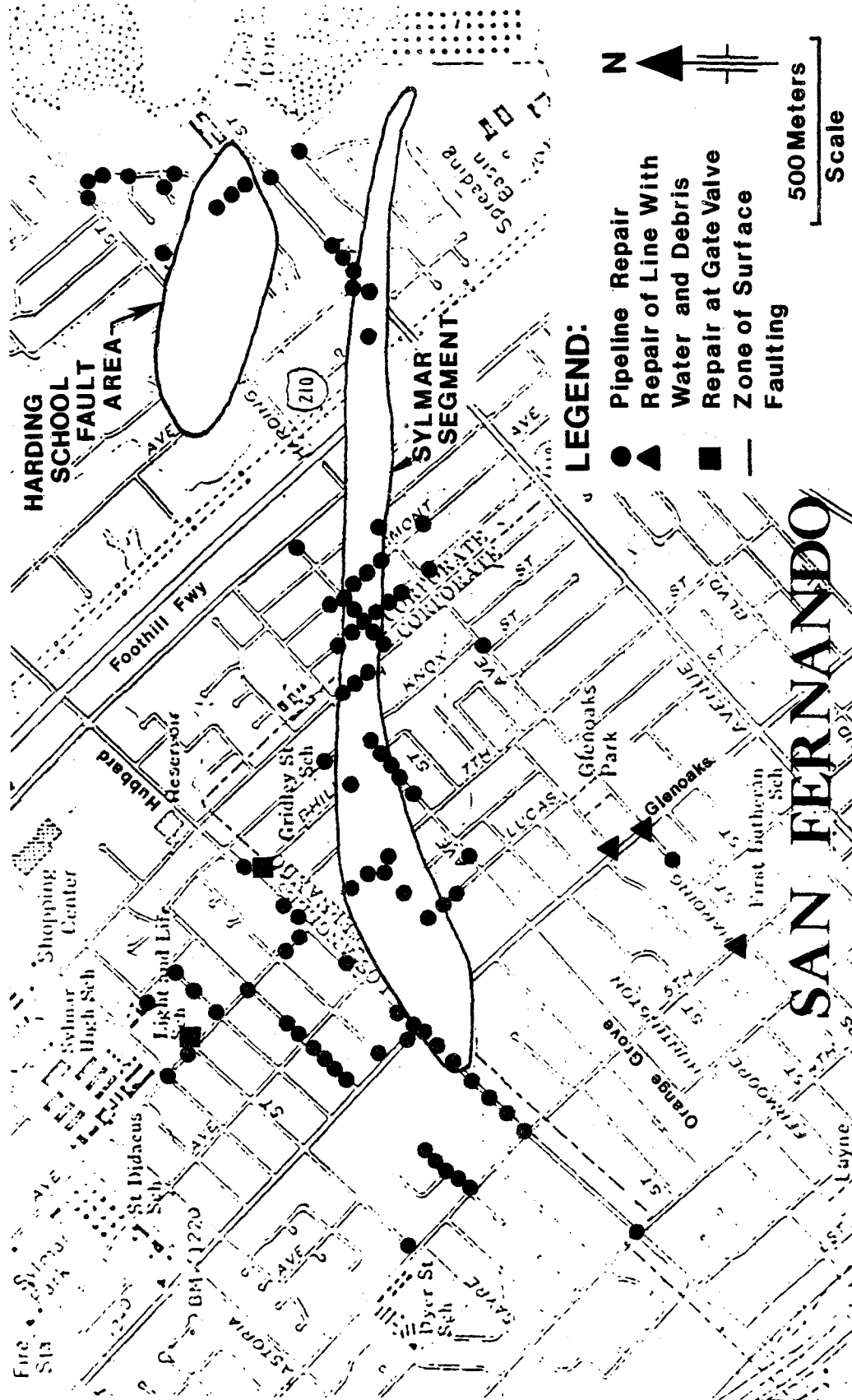


Figure 5.2. Plan view of repairs to gas distribution pipelines.

breaks in the pipe and damage at welded joints.

Water from broken water distribution lines washed soil and debris into ruptured gas pipelines so that repairs were occasionally performed to remove blockages at a relatively long distance from the locations of most severe deformation. Three locations associated with repair of gas pipelines clogged with soil and debris are shown in Figure 5.2. All are located several hundred meters downgrade from areas of concentrated gas pipeline damage.

Gate valves were also damaged by the earthquake, and two locations of valve repair are shown north of the fault zone in Figure 5.2. Gate valves made of cast iron generally showed a significantly higher incidence of damage than those composed of steel or brass (LePire, 1982).

### 5.3 PIPELINE REPAIRS RELATIVE TO THE FAULT ZONE CENTERLINE

The pattern of pipeline repair along the Sylmar segment was analyzed as a function of distance from the fault zone centerline. The centerline of the fault was taken at the middle of the zone showing the most severe surface displacements near the southern boundary of the segment. The analysis did not include

the eastern end of the Sylmar segment because the permanent movements in the Harding School fault area would have biased the data at this location. Fifty-one records of repair were used in the analysis.

Figure 5.3 shows the number of repairs per kilometer of pipeline plotted as a function of distance from the center of predominant fault movement. The repairs were determined for 50-m-wide intervals. The upper part of the figure shows the number of repairs on the upthrown and downthrown sides of the fault normalized with respect to the total pipe length in each 50-m-wide interval on the upthrown and downthrown sides, respectively. In a similar manner, the lower part of the figure shows the number of repairs on the northeast and northwest oriented pipelines normalized with respect to the total pipe length in each 50-m-wide interval for each group of northeast and northwest oriented pipelines, respectively.

The relatively high number of repairs within 100 m of the fault centerline is related directly to the permanent fault movements. It is of interest to note that the number of repairs per kilometer within or near the fault zone is comparable to the number of repairs at the same locations for water distribution

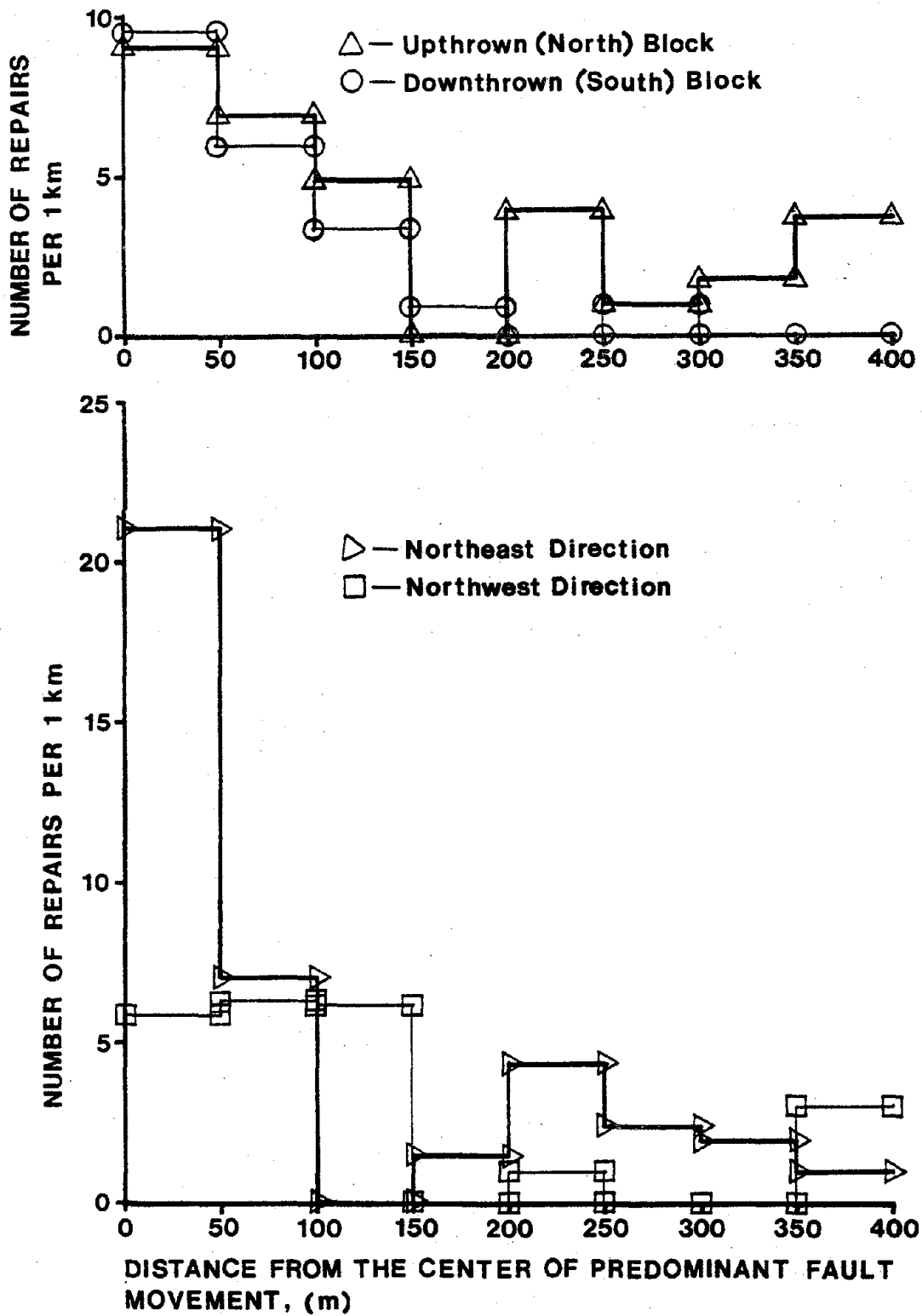


Figure 5.3. Plot showing number of pipeline repairs as a function of distance from the fault zone.

pipelines reported by Eguchi, et al. (1981), even though the latter were composed of cast iron. At a distance greater than 200 m there is a significant difference in the level of damage, with the greater number of repairs per kilometer on the upthrown block. Nason (1973) has pointed out that the high incidence of "shattered earth" observed north of the San Fernando fault implies a significantly higher level of seismic intensity on the upthrown as opposed to the downthrown side of the fault. This concentration of damage from seismic shaking may have been related to the special characteristics of elastic strain release and the multiple reflection of seismic waves above the fault plane, as discussed by Nason.

The effect of pipeline orientation relative to the fault had a significant effect on damage. Pipelines oriented in the northeast direction were subject to compressive strains from both the thrust and left-lateral strike slip components of the fault movement. The number of repairs per kilometer of pipeline at or near the fault centerline was nearly four times higher for the northeast compared to the northwest oriented pipelines.

#### 5.4 PERFORMANCE OF GAS TRANSMISSION PIPELINES

Four natural gas transmission pipelines were located at or near the zones of surface faulting. The lines were composed of welded steel pipe lengths and were buried in silty sand and gravel at depths of 1.2 to 1.8 m from the ground surface to the top of pipe. Table 5.1 lists the internal diameter, type of welds, date of installation, and nominal operating pressure for each pipeline.

Figure 5.4 shows a plan view of the San Fernando area, on which are superimposed the transmission pipelines and outlines of the Mission Wells and Sylmar segments of the San Fernando fault. The approximate locations of pipeline damage as well as the locations of explosion craters are indicated. The explosion craters were typically 3 m to 5 m in diameter and were formed by the sudden release of high pressure gas. Their round shapes and associated debris patterns made them relatively easy to identify on aerial photographs. The 1:2,400 scale aerial photographs used to locate the explosion craters were taken on February 12, 1971. When possible, the air photo interpretation was checked by reference to ground level photographs and by discussion with utility personnel. Because the

Table 5.1 Summary of information for gas transmission pipelines.

Line	Internal Diameter (mm)	Type of Weld	Approximate Date of Installation	Nominal Operating Pressure (MPa)
85	660	Initially oxy-acetylene welded, but rewelded in 1932 with electric arc techniques	1930	2.10
102.9	310	Oxy-acetylene	1927	1.04
115	410	Oxy-acetylene	1930	1.40
1001	310	Oxy-acetylene	1926	1.40

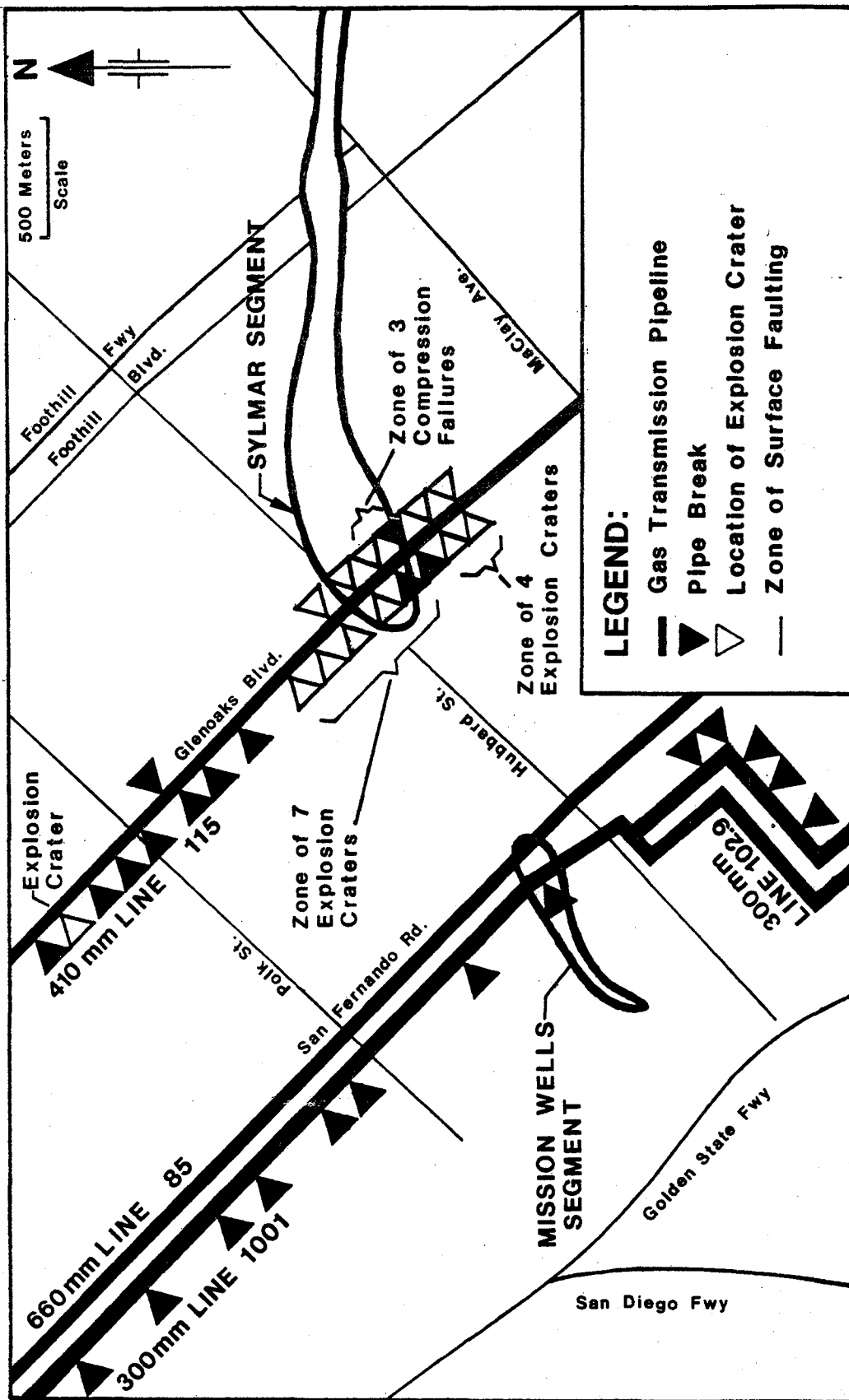


Figure 5.4. Plan view of breaks and explosion craters for gas transmission pipelines.

air photo interpretation was confined to a limited area within and adjacent to the Sylmar segment, it is possible that additional explosion craters were located at points other than those designated in Figure 5.4. The crater near the northern end of Line 115 was identified on the basis of discussions with field personnel of the Southern California Gas Company (Buchanan, 1982).

The presence of explosion craters implies that damage to Line 115 occurred rapidly, before escaping gas at a given rupture could diminish pressures at other break locations. Most of the explosion craters were associated with tensile failures at welded joints, and one crater was located at a point of severe compressive wrinkling of the pipeline at the southern edge of the fault. Explosion craters at the fault edge and at substantial distances from the zone of faulting suggest that damage north of the fault occurred within a very short time of the damage from permanent ground movements at the fault. There were some fires caused by escaping gas, one of which was reported by Steinbrugge, et al. (1971) at the location of the southern-most crater on Line 115.

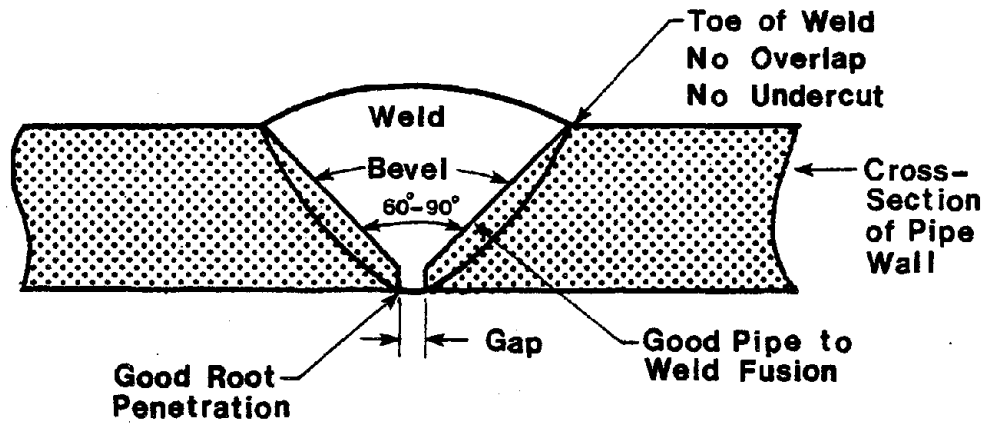
There was no damage to Line 85 in the area shown

by Figure 5.4, even though the pipeline crosses the Mission Wells segment. Line 85 had originally been constructed with oxy-acetylene welds, but was later repaired and rewelded using electric arc techniques.

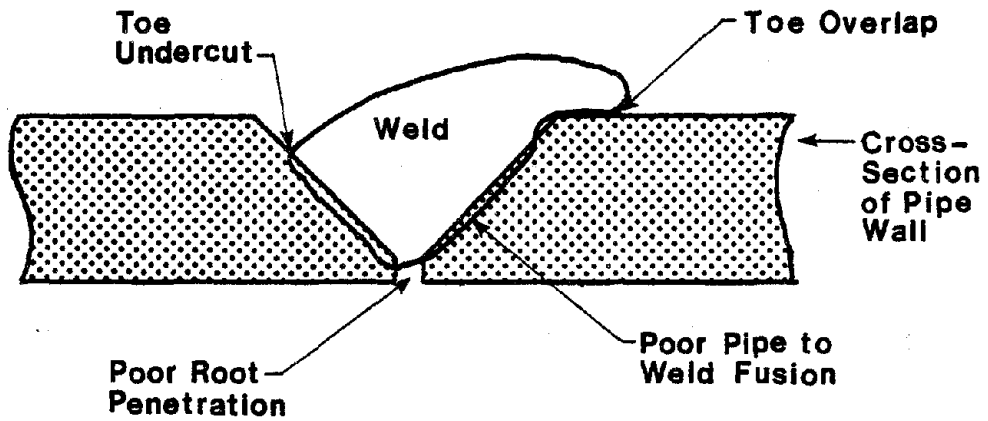
Damage to welded, steel pipelines has been reported during the 1952 Kern County earthquakes (Lind, 1954 and Newby, 1954), when lines with oxy-acetylene welds required a greater number of repairs than those with electric arc welds. The apparently higher incidence of earthquake damage for oxy-acetylene welds may be related to weld quality. Figure 5.5 shows a cross-sectional view of a pipeline weld. The figure illustrates some of the features of a proper weld, which are compared with an improper weld. A proper weld requires good fusion between the weld and pipe wall in the root and bevel areas. An improper weld may be caused by poor root penetration, undercutting and overlapping at the toe, and a lack of good fusion between the pipe and the weld. During the repair of Line 115, toe undercutting was observed at several of the welded joints.

#### 5.5 DETAILED OBSERVATION OF PIPELINE AND GROUND DEFORMATION

Figure 5.6 shows a plan view of the eastern end



a) Proper weld



b) Improper weld

Figure 5.5. Cross-sectional view of pipeline welds.

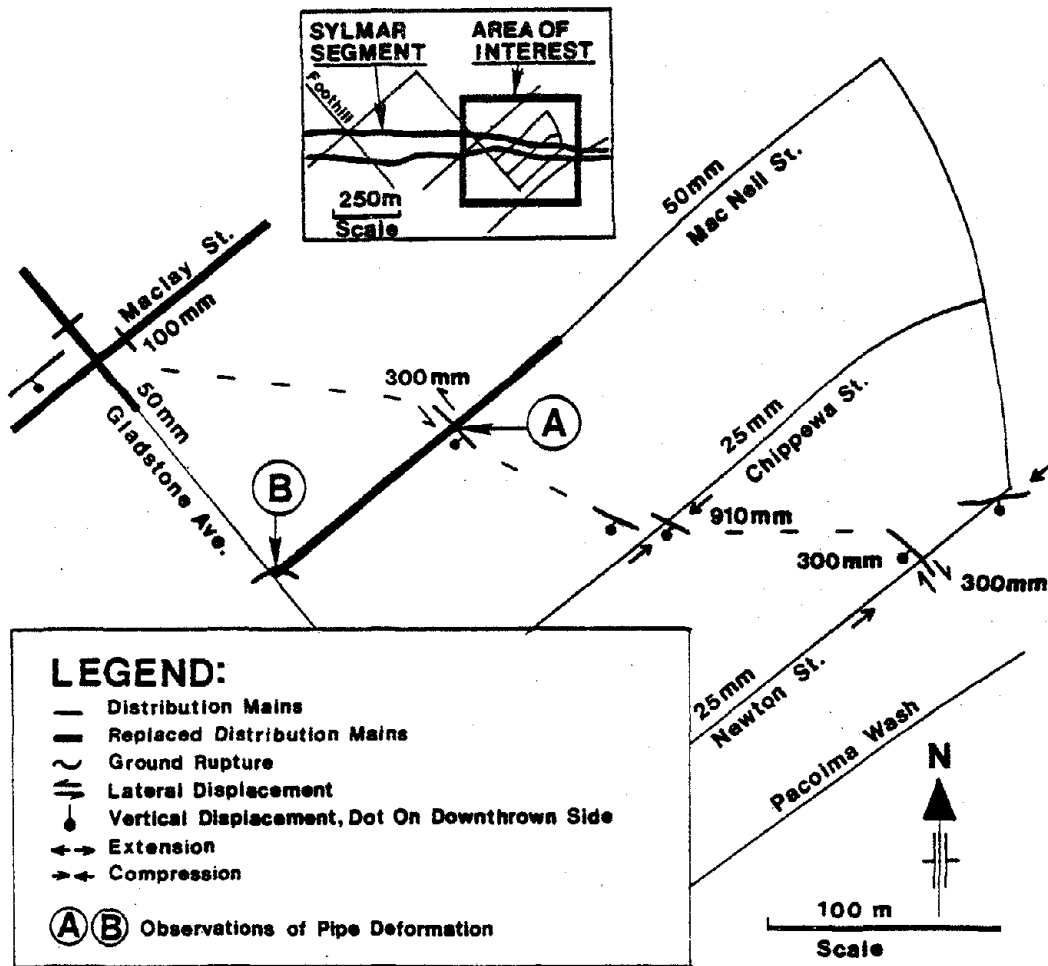


Figure 5.6. Plan view of ground ruptures and pipeline damage in the eastern Sylmar segment.

of the Sylmar segment. The inset in the figure indicates the location of this area with respect to the main portion of the fault zone. Ground ruptures and surface displacements are shown relative to sections of replaced distribution pipelines. The displacements are those reported by Kamb, et al. (1971) and U.S. Geological Survey Staff (1971). In this area, the compressive displacement parallel to the northeast oriented pipelines was approximately 900 mm, and the vertical and transverse offsets across the pipelines were approximately 300 mm. The 100-mm and 50-mm-diameter lines on Maclay and MacNeil Streets, respectively, were replaced. The two 25-mm-diameter lines on Chippewa and Newton Streets were not replaced, even though extensive damage to houses, streets, and sidewalks were recorded on both streets in the zone of fault movement (Weber, 1975 and Youd and Olsen, 1971). Apparently, the small diameter pipelines were able to sustain the permanent differential movements caused by faulting.

The deformation of 50-mm-diameter pipelines at points A and B shown in Figure 5.6 were studied by Sharp (1981) when the pipelines were excavated a few days after the earthquake. At point A, substantial

beam buckling of the 50-mm-diameter pipeline was observed, with a downward direction of buckling into the soil bedding beneath the pipe. At this location the total longitudinal shortening of the pipe was approximately 460 mm. Point B is located where a tee connection joined the pipelines on MacNeil Street and Gladstone Avenue. The 50-mm-diameter pipeline on Gladstone Avenue was deflected out of line approximately 230 mm at the tee by the 50-mm-diameter pipe on MacNeil Street. Substantial thrust displacement was apparently transmitted over a distance of 85 m from the location of surface faulting on MacNeil Street.

Figure 5.7 shows a plan view of the western end of the Sylmar segment. The inset in the figure indicates the location of this area with respect to the main portion of the fault zone. Prominent ground ruptures and surface displacements south of the intersection of Glenoaks Boulevard and Hubbard Street are shown relative to locations of breaks in Line 115 (410-mm-diameter steel pipeline). The displacements are those reported by Kamb, et al. (1971) and Weber (1975). The ground ruptures are based on field mapping by M. M. Clark and R. V. Sharp of the U.S. Geological Survey, supplemented by air photo interpre-

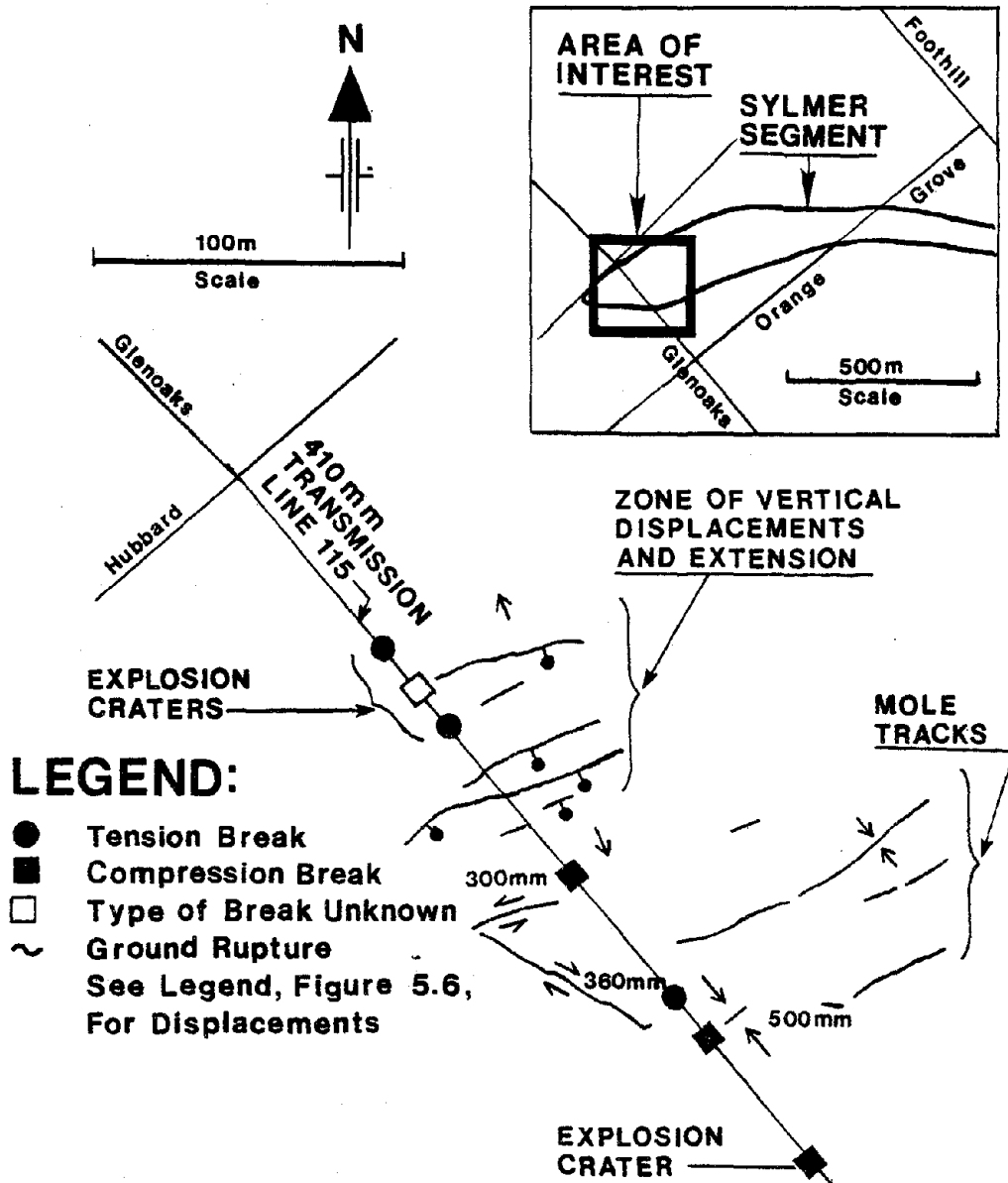


Figure 5.7. Plan view of ground ruptures and pipeline damage in the western Sylmar segment.

tation. The breaks in Line 115 were located by reference to aerial photographs and repair records summarized by the Southern California Gas Company. The identification of compression and tension breaks is based on repair records and discussion with field personnel who repaired the breaks.

Two zones of ground movement were evident. One zone was located at the southern boundary of the surface faulting and extended a distance of approximately 80 m along Glenoaks Boulevard from the front edge of the fault. This zone was characterized by compressive ground movements and is shown as the zone containing mole tracks, or compression ridges. At three locations in this zone, severe compressive wrinkling of the pipeline occurred at the points noted in the figure. At the break approximately 180 m south along Glenoaks Boulevard from Hubbard Street, a compressive shortening of approximately 100 mm was recorded across the damaged pipe (U.S. Geological Survey Staff, 1971). This section of the 410-mm-diameter (wall thickness 8 mm) pipe was also ruptured. A second distinct zone of movement was located along Glenoaks Boulevard between 90 to 160 m from Hubbard Street. This zone was characterized by prominent tensile ground movements as is

shown as the zone containing vertical displacements and extension. Several explosion craters occurred at locations of tensile failure across oxyacetylene pipe welds within this zone.

Line 115 was oriented in a northwest direction and therefore subjected to extension caused by left-lateral slip of the fault. The effects of left-lateral slip are well documented on Glenoaks Boulevard, where a net 0.6-m-extension of the road was measured between Hubbard Street and Orange Grove Avenue (U.S. Geological Survey Staff, 1971). The severe compressive strains in Line 115 are difficult to explain unless the fault thrust was applied to the pipe on a local basis. Figure 5.7 shows a ground rupture with 360 mm of right-lateral slip that intersects the pipeline at a subparallel orientation near a compression break in the pipe. This local displacement was apparently responsible for part of the compressive wrinkling observed in Line 115.

The repair records for the gas distribution system are not detailed enough to determine whether both compression and extension failures occurred on other northwest oriented pipelines. Nevertheless, excellent records of observed damage exist for a 3.6-m-high by

5.5-m-wide box culvert, known as the Wilson Canyon Channel, that crossed the center of the Sylmar segment in a northwest orientation (Hradilek, 1972). Although the culvert showed deformation from axial extension and bending, there was no clear evidence of compressive shortening anywhere within or adjacent to the fault zone. Apparently, the net extension caused by left-lateral slip was able to offset the influence of thrust on this structure.

#### 5.6 EFFECTS OF PIPELINE ORIENTATION

The general effects of pipeline orientation relative to a reverse fault with left-lateral strike slip are shown in Figure 5.8. Movement along the plane of fault rupture can be resolved into a displacement component parallel to the strike of the fault, known as strike slip, and a component parallel to the dip of the fault, known as dip slip. As shown in Figure 5.8a, left-lateral strike slip will impose tension in a pipeline that intersects the fault at an angle,  $\beta$ , provided that the angle is less than 90 degrees. As shown in Figure 5.8b, the dip slip will impose compression in the pipeline. If the tension imposed by strike slip,  $S_s$ , equals the compression caused by dip slip,  $S_d$ , the following equation holds:

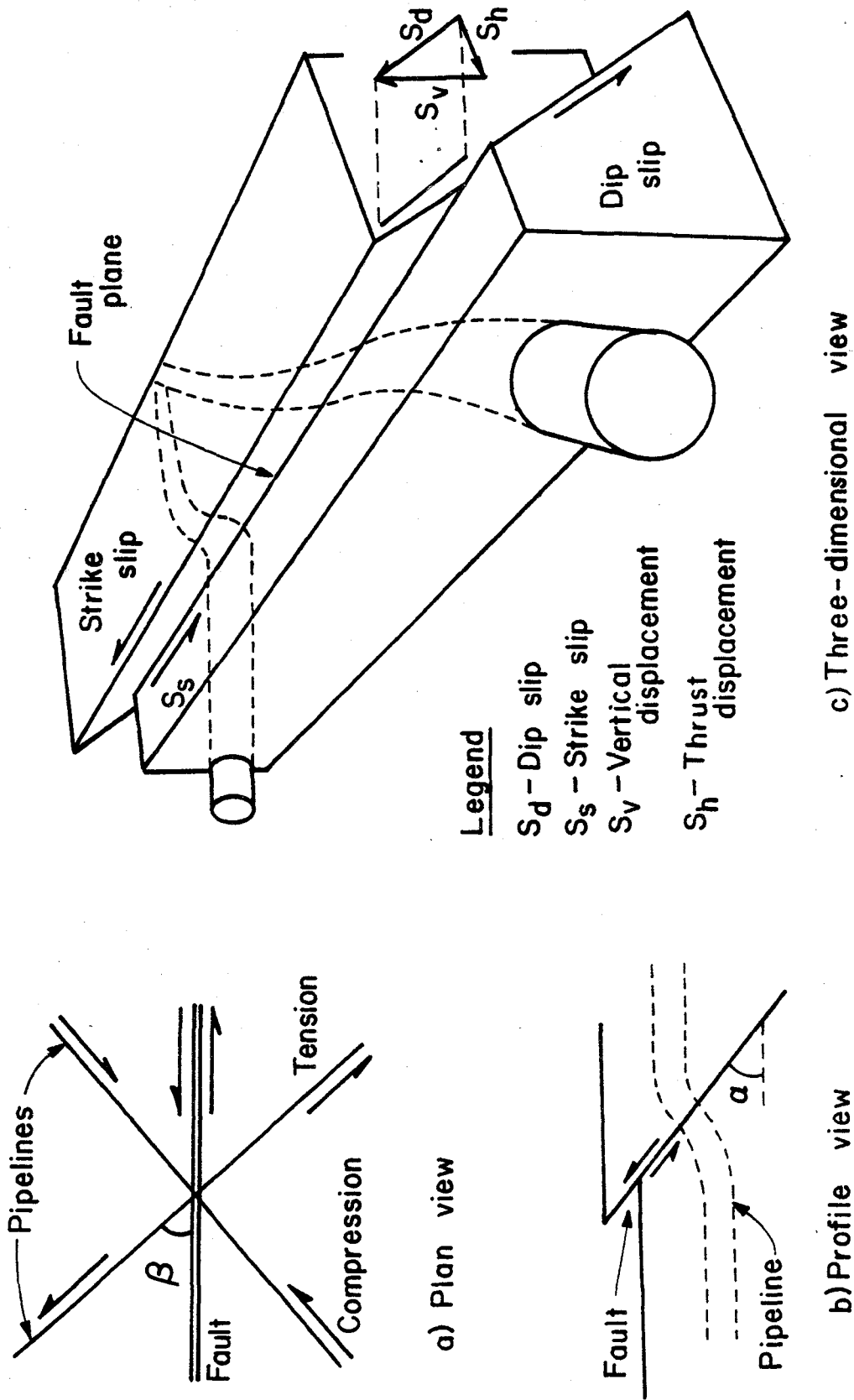


Figure 5.8. Three and two-dimensional views of pipeline deformation from reverse faulting with strike slip movement.

$$S_d \cos \alpha \sin \beta = S_s \cos \beta \quad (5.1)$$

where  $\alpha$  is the angle of inclination of the reverse fault with respect to the horizontal. By rearranging the terms in Equation 5.1:

$$\frac{S_s}{S_d} = \cos \alpha \tan \beta. \quad (5.2)$$

Equation 5.2 can be used to estimate the angle of pipeline/fault intersection at which there would be zero net axial strain. This equation can also be related to Figure 2.3 which describes the fault type as a function of the ratio  $S_s/S_d$ . Figure 5.9 shows a plot of the optimum angle of pipeline/fault intersection as a function of the ratio of strike slip to dip slip for reverse fault inclinations of 30 and 60 degrees. As the dip slip increases with respect to strike slip, the optimum angle of intersection decreases rapidly.

When siting a pipeline in an area of potential reverse faulting, the orientation of the pipe should be chosen, if possible, on the basis of the anticipated fault movements. When the dip slip component of faulting predominates, the angle of pipeline fault in-

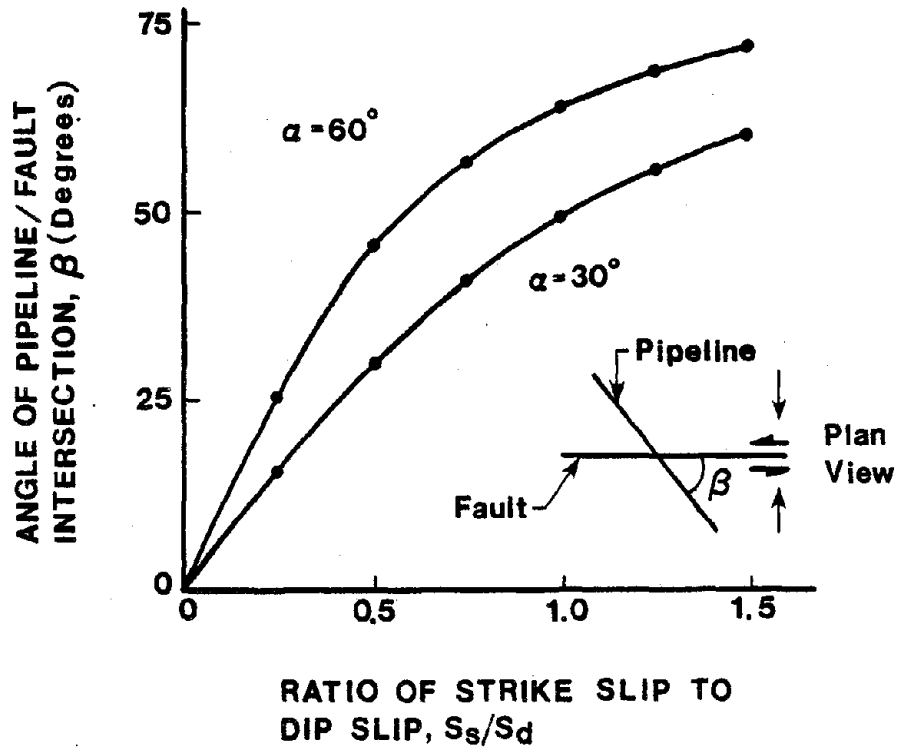


Figure 5.9. Optimal pipeline orientation as a function of the ratio of fault slip components for a reverse fault.

tersection should be small. When strike slip components will accompany the faulting, the intersection angle should be chosen to prevent excessive tension and compression. In these instances, Figure 5.9 can be helpful in choosing an optimal orientation for left-lateral displacements, and a similar line of reasoning can be applied to right-lateral movements. It should be noted, however, that pipeline performance during the 1971 San Fernando earthquake indicates that local compressive forces can be imposed by reverse faulting despite a favorable orientation of the pipeline.

#### 5.7 SUMMARY

Surface faulting associated with the 1971 San Fernando earthquake extended a distance of 15 km along three principal zones of surface faulting, including the Mission Wells, Sylmar, and Tujunga segments. The three segments showed different characteristics of ground movement. The Mission Wells segment had smaller magnitudes of displacement and ruptures which occurred in a narrow zone of shorter length compared to the other segments. The Sylmar segment was characterized by a broad zone of discontinuous ruptures. Displacements on the Tujunga segment generally oc-

curred on a single scarp with branch and secondary ruptures common. Left-reverse-oblique fault displacement produced regional uplift, shortening and lateral offset of 2 m, for each component of movement. The components of maximum displacements on a single fracture were about one-half of the maximum components across the rupture zone.

Damage to gas distribution and transmission pipelines during the 1971 San Fernando earthquake show consistent patterns with respect to surface faulting. The highest concentration of pipeline damage occurred within the zones of permanent fault displacement. Sixty-seven percent of the total length of gas distribution pipelines within the Sylmar segment of the San Fernando fault zone was replaced. Damage to northeast oriented pipelines was consistently higher than damage to northwest oriented pipelines because the left-lateral strike slip component of fault movement added to the compressive strains imposed on the northeast lines. Pipeline damage on the upthrown block of the reverse fault was higher than that on the downthrown block at distances greater than 200 m from the fault centerline.

Most of the damage to gas transmission lines was

caused by tensile failures across oxy-acetylene welded joints in an area of net ground extension. It is unlikely that these failures were related to the type of weld, but rather to the quality of the welds.

A simplified model has been proposed for choosing an optimal pipeline/fault intersection angle for reverse faults with left-lateral strike slip, and a similar model can be used for evaluating the effects of right-lateral strike slip. It should be noted that pipeline performance during the 1971 San Fernando earthquake indicates that local compressive forces can be imposed by reverse faulting despite a favorable orientation of the pipeline.

## CHAPTER 6

### CONCLUSIONS AND RECOMMENDATIONS

In this chapter, conclusions are made regarding the characteristics of surface fault rupture. Conclusions and recommendations are drawn from the work of the previous four chapters and have been subdivided according to the following topics: the characteristics of surface faulting, strike-slip faulting, the long-term performance of pipelines in areas of fault creep, and pipeline response to reverse faulting.

#### 6.1 CHARACTERISTICS OF SURFACE FAULTING

Although there is no clear threshold of earthquake magnitude at which surface faulting is initiated, historic evidence indicates that surface faulting is not likely to occur at earthquake magnitudes less than about 5.5. Generally, the length of surface displacement is only a fraction of the total fault length. For example, historic fault ruptures in California have varied typically from 20 to 50% of the total fault length.

Simplified models based on abrupt, planar displacement offer the most useful means of classifying faults with respect to their influence on pipelines.

The three principal types of fault are strike-slip, normal, and reverse faults. The movements on normal and reverse faults tend to impose tensile and compressive strains, respectively, in buried pipelines. Strike-slip displacements may impose either tensile or compressive strains, depending on the angle of the pipeline/fault intersection. Faults with oblique displacements, involving a combination of strike slip and either normal or reverse slip, require special geometric analyses to determine the optimal angle of pipeline/fault intersection with respect to pipeline strains imposed during faulting.

Fault displacements may occur in the form of coseismic slip, afterslip, and creep. Coseismic slip occurs within a period of several seconds. It represents the most damaging type of movement for buried pipelines because it allows little chance for stress relaxation or redistribution of soil pressures. Both afterslip and creep develop gradually. Observations of historic surface faulting indicate that afterslip generally amounts to less than 30% of coseismic slip, with movements accumulating at a decreasing rate for a period of several days to several months. It is recommended that pipeline design for differential move-

ment at fault crossings be based on coseismic slip. Afterslip should be considered when planning post-earthquake repair and maintenance. The timely excavation of a buried pipeline after fault movement not only provides a measure of stress relief from coseismic slip but minimizes additional deformation from afterslip. Creep should be considered when developing long-term maintenance plans for fault segments affected by creep.

Data are summarized in Chapter 2 pertaining to historic U.S. surface faulting events, for which published information on Richter magnitude, length of faulting, and maximum displacement were available. These data are supplemented with information pertaining to worldwide, reverse faulting events. The data for strike-slip and normal faulting are associated with a common regional setting, which includes the California and Nevada fault systems. Moreover, the data were reviewed with special care, particularly with respect to displacement and length measurements at low earthquake magnitudes.

Linear regression equations developed in this study for strike-slip and normal faulting events show a relatively high level of statistical compliance with

the data. For example, coefficients of determination of 0.83 and 0.91 were found for correlations of strike-slip fault length and maximum displacement, respectively, with Richter magnitude. These coefficients indicate that 83 and 91% of the data variation are explained by the linear regression equations. The correlations in this study show significantly smaller maximum surface displacements than those of other studies for Richter magnitudes less than 6.5. Larger displacements are indicated for Richter magnitudes greater than 8.0.

The linear regressions with the highest degree of statistical significance pertain to strike-slip faulting. In contrast, the regression analyses for reverse faulting indicate a substantial variation between the data and regression equations.

The regression plots and equations developed in Chapter 2 for strike-slip and normal faulting can be used to estimate lengths of faulting and maximum displacements for western U.S. earthquakes. However, any use of these regression analyses for predictive purposes should be made after recognizing two limitations. First, there are relatively few data so that the population selection has had a strong influence on

the results. The analyses should only be used for faults in similar tectonic settings with characteristics similar to those of the data. In addition, the regression analyses should be extended as new data for the western U.S. become available. Second, the regressions have been developed as logarithmic functions. This implies that the length of faulting and maximum displacement are log normally distributed for a given earthquake magnitude. Predictive limits determined by standard statistical methods will be biased toward large arithmetic values of fault length and displacement. Moreover, these values will increase substantially as the confidence limits increase.

The second limitation is perhaps the most significant with respect to applying the regression analyses. There are insufficient data to substantiate the assumption of log normal distribution. Accordingly, the regression equations and plots should be considered as a convenient means of mapping trends. They should be used only as estimates of fault length and maximum displacement, and applied cautiously when extrapolating the data trends with regard to additional statistical evaluations.

## 6.2 STRIKE-SLIP FAULTING

Surface fault ruptures are generally associated with active global plate boundaries. The most active boundaries are recognized by concentrations of seismic activity. Strike-slip faults are typically associated with continental plate boundaries which show parallel movement.

Active faults may be identified by the special geomorphic features produced by repetitive surface faulting. The most prominent geomorphic features are linear valleys and scarps. These lineaments may be recognized by remote sensing techniques, in particular, aerial photography. Geomorphic features associated with strike-slip faults are summarized in Chapter 3 in the form of a table and accompanying three-dimensional illustration.

The fault trace on which coseismic slip or creep was most recently observed is the most likely location of future strike slip movements. Accordingly, zones of fault creep can be used to locate areas of probable coseismic slip. Trenching perpendicular to the fault trace can be used to locate planes of recent rupture and thereby identify areas of future displacement. Trenching provides some of the most positive and de-

tailed evidence of fault activity. It can be used as a site exploration tool and as a vehicle for feedback and design confirmation during pipeline construction. Observations during pipeline construction can result in changes to accommodate true conditions. Examples of design changes at the location of a fault crossing include alteration of backfill material and compaction, and application of coatings aimed at reducing the pipe/soil friction to minimize pipe stress from fault offset.

In Chapter 3, the distributions of strike slip displacement along the length of surface faulting are reviewed for four strike-slip events, including the 1857 Fort Tejon, 1906 San Francisco, 1968 Borrego Mountain, and the 1979 Imperial Valley earthquakes. All displacements are expressed as fractions of maximum fault movement and plotted as a function of the distance normalized with respect to total surface rupture length. The fractions of maximum displacement are summarized such that they represent the largest displacements occurring along 0.95, 0.90, 0.75, and 0.50 of the total fault length. Each fractional displacement is, in effect, the probability that movement generated along the length of faulting will be less

than or equal to the fraction of the maximum displacement associated with it. The probability that a pipeline will be intercepted by some fraction of the maximum offset is approximately equal to that fraction, for displacements equal to or greater than 0.75 times the maximum offset.

The measured displacements along strike-slip faults show a skewed distribution with respect to the length of rupture. The pattern of movement can be represented by an expression that combines both linearly increasing and exponentially decaying functions of the fault distance in the form:

$$\frac{D}{D_{\max}} = \frac{x}{l} e^{(1 - \frac{x}{l})} \quad (6.1)$$

in which  $D$  is the displacement along the surface rupture at a distance,  $x$ ,  $D_{\max}$  is the maximum displacement, and  $l$  is the minimum distance along the length of surface faulting to the point of maximum displacement. This model tends to give conservative estimates of displacement for fractional fault lengths exceeding 0.75.

Historical evidence from strike-slip fault displacement has shown that, across the surface fault

rupture width, most of the displacement has been concentrated as abrupt movement in zones less than 15 m wide, with some displacement distributed in a zone of distortion generally less than 50 m wide. It is recommended that fault movement be modeled as a planar displacement for purposes of analyzing pipeline/soil interaction. This is consistent with the worst conditions observed in the field and sets an upper bound on the severity of deformation. This modeling assumption generally will provide a moderate degree of conservatism in the analysis.

### 6.3 LONG-TERM PERFORMANCE OF PIPELINES IN AREAS OF FAULT CREEP

The Hayward fault is a good location for studies regarding the long-term performance of pipelines subject to fault creep. It is located in a highly populated area where it is crossed by numerous pipelines over a relatively long distance. The average rate of creep on the Hayward fault is 5 mm/yr, although rates as high as 7 mm/yr have been observed on a local basis. The widths of the zones in which creep movements occur are usually more than 1 m but less than 10 m, with 5 m common.

Repair records were studied for a section of the

East Bay Municipal Utility District (EBMUD) involving 76 linear km of water distribution pipelines crossing and adjacent to the Hayward fault. The frequency of repair for cast iron and asbestos cement pipe within 60 m of the centerline of the Hayward fault zone was from three to four times higher than that for the same types of pipe beyond a distance of roughly 150 m from the fault zone centerline. Steel pipelines, which can accommodate significant differential movement by virtue of their ductility, do not show appreciable differences in repair frequency with distance from the fault trace.

A hyperbolic tangent function was found to provide a statistically good representation of the pattern of ground displacement in zones of fault creep, as described in Chapter 4. Using this function, recurrence intervals for damage to a 150-mm-diameter cast iron pipeline were estimated at approximately 18 to 73 years.

Although the likelihood of pipeline damage increases at fault crossings, the actual number of repairs caused by fault creep is a relatively low number when considered on an annual basis. Utility companies should be able to accommodate this level of damage

within the normal course of their maintenance programs. A more significant source of weakening is corrosion. Adobe soils, with a high clay content, are commonly found in the vicinity of the Hayward fault. This type of soil is often associated with a corrosive environment. It is more likely that corrosion rather than fault creep will reduce the capacity of cast iron and steel pipelines to resist permanent earthquake displacements and seismic ground waves in this area.

#### 6.4 PIPELINE RESPONSE TO REVERSE FAULTING

The 1971 San Fernando earthquake provides an excellent case history of pipeline response to permanent ground movements. Approximately 17,000 customers were without gas service as a result of pipeline damage. More than 500 leaks were repaired in gas distribution pipelines, and more than 10 km of line were replaced. This disruption of utility services raises significant questions with regard to seismic performance of life-line systems, including how pipeline damage was distributed with respect to the location of fault movement, and what orientations, soil conditions, and mechanical features had the most significant impact on performance.

Damage to gas distribution and transmission pipe-

lines show consistent patterns with respect to surface faulting. The highest concentration of pipeline damage occurred within the zones of permanent fault displacement. Sixty-seven percent of the total length of gas distribution pipelines within the Sylmar segment of the San Fernando fault zone was replaced. Damage to northeast oriented pipelines was consistently higher than damage to northwest oriented pipelines because the left-lateral strike slip component of fault movement added to the compressive strains imposed on the northeast lines. Pipeline damage on the upthrown block of the reverse fault was higher than that on the downthrown block at distances greater than 200 m from the fault centerline. This concentration of damage correlates with the relatively high levels of seismic intensity that have been documented for the upthrown as opposed to downthrown blocks of reverse faults.

Most of the damage to gas transmission pipelines was caused by tensile failures across oxy-acetylene welded joints. It is unlikely that these failures were related to the type of weld, but rather to the quality of the welds. Toe undercutting was observed at several of the welds during repair. The tensile failures were reported at locations of explosion

craters. Within a 1-km-distance across the Sylmar segment of the San Fernando fault zone, there were 11 explosion craters caused by rupture of the high pressure transmission line on Glenoaks Boulevard.

Both beam buckling and compressive wrinkling of pipelines were observed. At one location, thrust was transmitted over 85 m along a 50-mm-diameter distribution pipeline to a tee connection, where severe bending deformation of the intersected line occurred. In another area of compressive ground movements, wrinkling of a 410-mm-diameter pipeline (wall thickness of 8 mm) was observed at three locations. The pipeline was ruptured at one location where approximately 100 mm of longitudinal shortening occurred across the deformed section.

An abrupt change in the direction of thrust as well as severe local compression was observed near the western end of the Sylmar segment. At this location, there was a rapid decrease in displacement along the western projection of the fault and a corresponding increase in the width of the fault zone. As a result of these end conditions, severe compressive wrinkling was imposed on the 410-mm-diameter gas transmission pipeline in addition to tensile ruptures in a zone of

net extension behind the fault front.

When siting a pipeline in an area of potential reverse faulting, the orientation of the pipeline with respect to the fault should be determined, if possible, on the basis of the anticipated movement patterns. When the dip slip component of faulting predominates, the angle of pipeline/fault intersection should be small. When strike slip components will accompany the faulting, the intersection angle should be chosen to prevent excessive tension as well as compression. A simplified model has been proposed for choosing an optimal orientation for reverse faults with left-lateral strike slip, which is described in Chapter 5. A similar model can be used for evaluating the effects of right-lateral strike slip.

## REFERENCES

- Adams, R. D., and Lowry, M. A., "The Inangahua Earthquake Sequence, 1968," Recent Crustal Movements, Bulletin 9, Royal Society of New Zealand, Wellington, New Zealand, 1971, pp. 129-135.
- Albee, A. L., and Smith, J. L., "Earthquake Characteristics and Fault Activity in Southern California," Engineering Geology in Southern California, Special Publication, Association of Engineering Geologists, Oct., 1966, pp. 9-33.
- Allen, C. R., Grantz, A., Brune, J. N., Clark, M. M., Sharp, R. V., Theodore, T. G., Wolfe, E. W., and Wyss, M., "The Borrego Mountain, California, Earthquake of 9 April 1968: A Preliminary Report," Seismological Society of America, Bulletin, Vol. 58, No. 3, Jun., 1968, pp. 1183-1186.
- Allen, C. R., Hanks, T. C., and Whitcomb, J. H., "Seismological Studies of the San Fernando Earthquake and their Tectonic Implications," San Fernando, California, Earthquake of 9 February 1971, Bulletin 196, California Division of Mines and Geology, Sacramento, California, 1975, pp. 257-262.
- Ambraseys, N. N., "The Buyin-Zara (Iran) Earthquake of September, 1962, A Field Report," Seismological Society of America, Bulletin, Vol. 53, No. 4, Jul., 1963, pp. 705-740.
- Ambraseys, N. N., "An Earthquake Engineering Study of the Buyin-Zahra Earthquake of September 1st, 1962 in Iran," Proceedings of the Third World Conference on Earthquake Engineering, Auckland and Wellington, New Zealand, 22 January - 1 February 1965, New Zealand National Committee on Earthquake Engineering, Vol. 3, 1965, pp. V7-V26.
- Ambraseys, N. N., "Some Characteristic Features of the Anatolian Fault Zone," Tectonophysics, Vol. 9, No. 2/3, Mar., 1970, pp. 143-165.

- Ang, A. H-S. and Mohammadi, J., "Fault Rupture Hazard of Lifeline Systems," Proceedings of the Specialty Conference on Probabilistic Mechanics and Structural Reliability, Tucson, Arizona, January 10-12, 1979, American Society of Civil Engineers, New York, 1979, pp. 322-329.
- Armstrong, C. F., Wagner, D. L., and Bortugno, E. J., "Movement Along the Southern Calaveras Fault Zone as Shown by Fence Line Surveys," Special Report 140, California Division of Mines and Geology, Sacramento, California, 1980, pp. 29-39.
- Audibert, J. M. E., and Nyman, K. J., "Soil Restraint Against Horizontal Motion of Pipes," Journal of the Geotechnical Engineering Division, ASCE, Vol. 103, No. GT10, Oct., 1977, pp. 1119-1142.
- Babcock, E. A., "Detection of Active Faulting Using Oblique Infrared Aerial Photography in the Imperial Valley, California," Geological Society of America, Abstracts with Programs, Vol. 3, No. 2, Feb., 1971, p. 77.
- Barrows, A. G., Kahle, J. E., Weber, F. H., and Saul, R. B., "Map of Surface Breaks Resulting From the San Fernando, California, Earthquake of February 9, 1971," San Fernando, California, Earthquake of February 9, 1971, U.S. Department of Commerce, National Oceanic and Atmospheric Administration, Washington, D.C., Vol. 3, 1973, pp. 127-135.
- Beeby, D. J., and Hill, R. L., "Galway Lake Fault, A Previously Unmapped Active Fault in the Mojave Desert, San Bernadino County, California," California Geology, Vol. 28, No. 10, Oct., 1975, pp. 219-221.
- Billings, M. P., Structural Geology, 3rd ed., Prentice-Hall, Inc., Englewood Cliffs, New Jersey, 1972, 606 p.
- Bolt, B. A., "Causes of Earthquakes", Earthquake Engineering, Wiegel, R. L., ed., 1st ed., Prentice-Hall, Inc., Englewood Cliffs, New Jersey, 1970, pp. 21-45.

- Bolt, B. A., and Miller, R. D., Catalogue of Earthquakes in Northern California and Adjoining Areas, 1 January 1910 to 31 December 1972, Seismographic Stations, University of California, Berkeley, California, 1975, 567 p.
- Bonilla, M. G., "Deformation of Railroad Tracks by Slippage on the Hayward Fault in the Niles District of Fremont, California," Seismological Society of America, Bulletin, Vol. 56, No. 2, Apr., 1966, pp. 281-289.
- Bonilla, M. G., "Historic Surface Faulting in Continental United States and Adjacent Parts of Mexico," National Center for Earthquake Research, U.S. Geological Survey, Washington, D.C., 1967, (Paper TID-24124).
- Bonilla, M. G., "Surface Faulting and Related Effects," Earthquake Engineering, Wiegel, R. L., ed., 1st ed., Englewood Cliffs, New Jersey, Prentice-Hall, 1970, pp. 47-74.
- Bonilla, M. G., "Historic Surface Faulting-Map Patterns, Relation to Subsurface Faulting, and Relation to Pre-existing Faults" Proceedings of Conference VIII, Analysis of Actual Fault Zones in Bedrock, 1-5 April 1979, Open-File Report 79-1239, U.S. Geological Survey, Washington, D.C., 1979, pp. 36-65.
- Bonilla, M. G., "Evaluation of Potential Surface Faulting and Other Tectonic Deformation," NUREG/CR-2991, U.S. Nuclear Regulatory Commission, Washington, D.C., 1982, 58 p.
- Bonilla, M. G. and Buchanan, J. M., "Interim Report on Worldwide Historic Surface Faulting," Open File Report, U.S. Geological Survey, Washington, D.C., 1970, 32 p.
- Bornyakov, S. A., "The Modeling of Strike-Slip Zones in Elastic-Viscous Materials," Soviet Geology and Geophysics, Vol. 21, No. 11, 1980, pp. 64-71.

- Brogan, G. E., Cluff, L. S., Korringa, M. K., and Slemmons, D. B., "Active Faults of Alaska," Tectonophysics, Vol. 29, No. 1-4, Dec. 1975, pp. 73-85.
- Brown, J. S., "Fault Features of Salton Basin, California," Journal of Geology, Vol. 30, No. 3, May, 1922, pp. 217-226.
- Brown, I. R., Brekke, T. L., and Korbin, G. E., "Behavior of the Bay Area Rapid Transit Tunnels Through the Hayward Fault," Report No. UMTA-CA-06-0120-81-1, U.S. Department of Transportation, Washington, D.C., Jun., 1981, 208 p.
- Brown, R. D. and Vedder, J. G., "Surface Tectonic Fractures Along the San Andreas Fault," The Parkfield-Cholame California, Earthquake of June-August 1966 - Surface Geologic Effects, Water-Resources Aspects, and Preliminary Seismic Data, Professional Paper 579, U.S. Geological Survey, Washington, D.C., 1967, pp. 2-22.
- Brown, R. D., Jr. and Wallace, R. E., "Current and Historic Fault Movement Along the San Andreas Fault Between Paicines and Camp Dix, California," Proceedings of Conference on Geologic Problems of San Andreas Fault System, Geological Sciences, Stanford University Publications, Vol. 11, May, 1968, pp. 22-41.
- Brune, J. N. and Allen C. R., "A Low-Stress-Drop Low-Magnitude Earthquake with Surface Faulting, The Imperial, California, Earthquake of March 4, 1966", Seismological Society of America, Bulletin, Vol. 57, No. 3, 1967, pp. 501-514.
- Buchanan, D., Personal Communication, Southern California Gas Company, Newhall District, 1982.
- Bucknam, R. C., Plafker, G., and Sharp, R. V., "Fault Movement (Afterslip) Following the Guatemala Earthquake of February 4, 1976," Geology, Vol. 6, Mar., 1978, pp. 170-173.

- Burford, R. O. and Harsh, P. W., "Slip on the San Andreas Fault in Central California from Alinement Array Surveys," Seismological Society of America, Bulletin, Vol. 70, No. 4, Aug., 1980, pp. 1233-1261.
- Burford, R. O., Harsh, P. W., and Espinosa, A. F., "7.3 Quake in Algeria Reviewed," Geotimes, Vol. 26, No. 5, May, 1981, pp. 18-20.
- Burk, C. A. and Moores, E. M., "Problems of Major Faulting at Continental Margins, with Special Reference to the San Andreas Fault System," Proceedings of Conference on Geologic Problems of San Andreas Fault System, Geological Sciences, Stanford University Publications, Vol. 11, May, 1968, pp. 358-374.
- Buwalda, J. P., "Shutteridges, Characteristic Physiographic Features of Active Faults," Geological Society of America, Proceedings, 1937, p. 307.
- Buwalda, J. P. and Richter, C. F., "Imperial Valley Earthquake of May 18, 1940," Geological Society of America, Bulletin, Vol. 52, No. 12, 1941, pp. 1944-1945.
- Buwalda, J. P. and St. Amand, P., "Geological Effects of the Arvin-Tehachapi Earthquake," Earthquakes in Kern County, California, During 1952, Bulletin 171, California Division of Mines and Geology, San Francisco, California, Nov., 1955, pp. 41-56.
- California Division of Mines and Geology, "State of California Special Studies Zones Revised Official Map of the Hayward Quadrangle," California, California Division of Mines and Geology 7.5 Minute Quadrangle Map, 1982, scale 1: 24,000.
- Callaghan, E. and Gianella, V. P., "The Earthquake of January 30, 1934, At Excelsior Mountains, Nevada," Seismological Society of America, Bulletin, Vol. 25, No. 2, Apr., 1935, pp. 161-168.

- Cheng, I. K., "Report on the 1951 Earthquake in Taiwan," Proceedings of the Second World Conference on Earthquake Engineering, Tokyo and Kyoto, Japan, July 11-18, 1960, Science Council of Japan, Vol. 1, 1960, pp. 397-408.
- Chinnery, M. A., "Earthquake Magnitude and Source Parameters," Seismological Society of America, Bulletin, Vol. 59, No. 5, Oct., 1969, pp. 1969-1982.
- Clark, M. M., "Surface Rupture Along the Coyote Creek Fault," The Borrego Mountain Earthquake of April 9, 1968, Professional Paper 787, U.S. Geological Survey, Washington, D.C., 1972, pp. 55-86.
- Clark, W. B. and Hauge, C. J., "When the Earth Quakes," California Geology, Vol. 24, No. 11, Nov., 1971, pp. 203-216.
- Cluff, L. S., "Urban Development within the San Andreas Fault System," Proceedings of Conference on Geologic Problems of San Andreas Fault System, Geological Sciences, Stanford University Publications, Vol. 11, 1968, pp. 55-69.
- Cluff, L. S. and Steinbrugge, K. V., "Hayward Fault Slippage in the Irvington-Niles District of Fremont, California," Seismological Society of America, Bulletin, Vol. 56, No. 2, Apr., 1966, pp. 257-279.
- Cohn, S. N., Allen, C. R., Gilman, R., and Goulty, N. R., "Preearthquake and Postearthquake Creep on the Imperial Fault and the Brawley Fault Zone," The Imperial Valley, California, Earthquake of October 15, 1979, Professional Paper 1254, U.S. Geological Survey, Washington, D.C., 1982, pp. 161-167.
- Davis, J. F., Bennett, J. H., Borchardt, G. A., Kahle, J. E., Rice, S. J., and Silva, M. A., "Earthquake Planning Scenario for a Magnitude 8.3 Earthquake on the San Andreas Fault in the San Francisco Bay Area," Special Publication 61, California Division of Mines and Geology, Sacramento, California, 1982, 160 p.

- De La Beche, H. T., Geological Observer, Longman, Brown, Green, and Logmans, London, England, 1851, p. 745.
- Der Kiureghian, A. and Ang, A. H-S., "A Fault-Rupture Model for Seismic Risk Analysis," Seismological Society of America, Bulletin, Vol. 67, No. 4, Aug., 1977, pp. 1173-1194.
- Deza, E., "The Pariahuanca Earthquakes, Huancayo, Peru: July-October 1969," Recent Crustal Movements, Bulletin 9, Royal Society of New Zealand, Wellington, New Zealand, 1971, pp. 77-83.
- Dickinson, W. R. and Grantz, A., "Tectonic Setting of the San Andreas Fault System," Proceedings of Conference on Geologic Problems of San Andreas Fault System, Geological Sciences, Stanford University Publications, Vol. 11, May, 1968, pp. 290-291.
- Eguchi, R. T., Philipson, L. L., Legg, M. R., Wiggins, J. H., and Slosson, J. E., "Earthquake Vulnerability of Water Supply Systems," The Current State of Knowledge of Lifeline Earthquake Engineering, American Society of Civil Engineers, 1981, pp. 277-292.
- Everingham, I. B., Gregson, P. J., and Doyle, H. A., "Thrust Fault Scarp in the Western Australian Shield," Nature, Vol. 223, No. 5207, Aug., 1969, pp. 701-703.
- Florensov, N. A. and Solonenko, V. P., The Gobi-Altai Earthquake, 1st ed., U.S. Department of Commerce, Washington, D.C., 1965, 424 p.
- Fyfe, H. E., "Movement on White Creek Fault, New Zealand, During the Murchison Earthquake of 17th June, 1929," New Zealand Journal of Science and Technology, Wellington, New Zealand, Vol. 11, No. 3, Oct., 1929, pp. 192-197.
- Gianella, V. P., "Earthquake and Faulting, Fort Sage Mountains, California, December, 1950," Seismological Society of America, Bulletin, Vol. 47, No. 3, Jul., 1957, pp. 173-177.

- Gianella, V. P. and Callaghan, E., "The Cedar Mountain, Nevada, Earthquake of December 20, 1932," Seismological Society of America, Bulletin, Vol. 24, No. 4, Oct., 1934, pp. 345-384.
- Gordon, F. R. and Wellman, H. W., "A Mechanism for the Meckering Earthquake," Recent Crustal Movements, Bulletin 9, Royal Society of New Zealand, Wellington, New Zealand, 1971, p. 95-96.
- Gutenberg, B. and Richter, C. F., Seismicity of the Earth and Associated Phenomena, 2nd ed., Princeton University Press, Princeton, New Jersey, 1954, 310 p.
- Hamilton, W. B., "Geology of the Colorado Desert (Salton Trough), Mineral Information Service, California Division of Mines and Geology, Vol. 22, No. 6, Jun., 1969, pp. 96-98.
- Hamilton, W. B. and Myers, W. B., "Cenozoic Tectonic Relationships Between the Western United States and the Pacific Basin," Proceedings of Conference on Geologic Problems of San Andreas Fault System, Geological Sciences, Stanford University Publications, Vol. 11, May, 1968, pp. 342-357.
- Harris, C. W. and O'Rourke, T. D., "Response of Jointed Cast Iron Pipelines to Parallel Trench Construction," Geotechnical Engineering Report 83-5, School of Civil and Environmental Engineering, Cornell University, Ithaca, New York, Mar., 1983, 158 p.
- Hart, E. W., "Ground Rupture Associated with Faulting," California Geology, Vol. 28, No. 12, Dec., 1975, pp. 274-276.
- Hart, E. W., "Fault-Rupture Hazard Zones in California," Special Publication 42, California Division of Mines and Geology, Sacramento, California, Mar., 1980, 25 p.
- Hart, E. W. and Rapp, J. S., "Ground Rupture Along the Cleveland Hill Fault," Special Report 124, California Division of Mines and Geology, Sacramento, California, Aug., 1975, pp. 61-72.

- Hays, W. W., "Procedures for Estimating Earthquake Ground Motions," Professional Paper 1114, U.S. Geological Survey, Washington, D.C., 1980, 77 p.
- Henderson, J., "The Geological Aspects of the Hawke's Bay Earthquakes," New Zealand Journal of Science and Technology, Wellington, New Zealand, Vol. 15, No. 1, Jul., 1933, pp. 38-75.
- Hileman, J. A., Allen, C. R., and Nordquist, J. M., Seismicity of the Southern California Region, 1 January 1932 to 31 December 1972, Seismological Laboratory, California Institute of Technology, Pasadena, California, 1973, 397 p.
- Hill, R. L., and Beeby, D. J., "Surface Faulting Associated with the 5.2 Magnitude Galway Lake Earthquake of May 31, 1975: Mojave Desert, San Bernardino County, California," Geological Society of America, Bulletin, Vol. 88, Oct., 1977, pp. 1378-1384.
- Hobbs, W. H., "The Earthquake of 1872 in the Owens Valley, California," Beiträge zur Geophysik, Vol. 10, 1910, p. 379.
- Housner, G. W. and Jennings, P. C., "The San Fernando California Earthquake," The International Journal of Earthquake Engineering and Structural Dynamics, Vol. 1, May, 1972, pp. 5-31.
- Howard, J. H., "Recent Deformation at Buena Vista Hills, California," American Journal of Science, Vol. 266, Nov., 1968, pp. 737-757.
- Hradilek, P. J., "Behavior of Underground Box Conduits in the San Fernando Earthquake of 9 February 1971," Technical Report E-72-1, Jan., 1972, U.S. Army Engineer District, Corps of Engineers, Los Angeles, California, 123 p.
- Iida, K., "Earthquake Energy and Earthquake Fault," Journal of Earth Sciences, Nagoya University, Japan, Vol. 7, No. 2, Dec., 1959, pp. 98-107.
- Iida, K., "Earthquake Magnitude, Earthquake Fault, and Source Dimensions," Journal of Earth Sciences, Nagoya University, Japan, Vol. 13, No. 2, Dec., 1965, pp. 115-132.

- Jones, J. C., "The Pleasant Valley, Nevada, Earthquake of October 2, 1915," Seismological Society of America, Bulletin, Vol. 5, No. 4, Dec., 1915, pp. 190-205.
- Kamb, B., Silver, L. T., Abrams, M. J., Carter, B. A., Jordan, T. H., and Minster, J. B., "Pattern of Faulting and Nature of Fault Movement in the San Fernando Earthquake," The San Fernando California Earthquake of February 9, 1971, Professional Paper 733, U.S. Geological Survey, Washington, D.C., 1971, pp. 41-54.
- Kanamori, H. and Regan, J., "Long-Period Surface Waves," The Imperial Valley, California, Earthquake of October 15, 1979, Professional Paper 1254, U.S. Geological Survey, Washington, D.C., 1982, pp. 55-58.
- Keefer, D. K., Wilson, R. C., and Tannaci, N. E., "Reconnaissance Report on Ground Failures and Ground Cracks Resulting from the Coyote Lake, California, Earthquake of August 6, 1979," Open-File Report 80-139, U.S. Geological Survey, Washington, D.C., Jan., 1980, 14 p.
- Kennedy, R. P., Chow, A. W., and Williamson, R. A., "Fault Movement Effects on Buried Oil Pipeline," Transportation Engineering Journal, American Society of Civil Engineers, Vol. 103, No. TE5, Sep., 1977, pp. 617-633.
- King, C. and Knopoff, L., "Stress Drop in Earthquakes," Seismological Society of America, Bulletin, Vol. 58, No. 1, Feb., 1968, pp. 249-257.
- Koch, T. W., "Analysis and Effects of Current Movement on an Active Fault in Buena Vista Hills Oil Field, Kern County, California," American Association of Petroleum Geologist, Bulletin, Vol. 17, Jun., 1933, pp. 694-712.
- Krinitzsky, E. L., "Fault Assessment in Earthquake Engineering," State-of-the-Art for Assessing Earthquake Hazards in the United States, Miscellaneous Paper S-73-1, Report 2, U.S. Army Engineer Waterways Experiment Station, Vicksburg, Mississippi, May, 1974.

- Lawson, A. C., et al., The California Earthquake of April 18, 1906, The State Earthquake Investigation Commission, The Carnegie Institution of Washington, Washington, D.C., Vol. 1, 1908, 451 p.
- Leeds, D. J., ed., "Reconnaissance Report, Imperial County, California, Earthquake, October 15, 1979," Earthquake Engineering Research Institute, Berkeley, California, Feb., 1980.
- Leeds, A., ed., "El-Asnam, Algeria Earthquake, October, 10, 1980," Earthquake Engineering Research Institute, Berkeley, California, Jan., 1983.
- Lensen, G. J. and Otway, P. M., "Earthshift and Post-Earthquake Deformation Associated with the May 1968 Inangahua Earthquake New Zealand," Recent Crustal Movements, Bulletin 9, Royal Society of New Zealand, Wellington, New Zealand, 1971, pp. 107-116.
- LePire, J. L., Personal Communications, Southern California Gas Company, San Fernando District, 1982.
- Lind, R. J., "What Earthquake Did to 34-in. Line," Gas Age, Vol. 114, No. 3, Jul., 29, 1954, pp. 29-50.
- McNorgan, J., Personal Communication, Southern California Gas Company, Los Angeles District, 1982.
- Miller, W. J., "Recognition of Faults in Southern California," Journal of Geology, Vol. 49, No. 1, Jan.-Feb., 1941, pp. 87-100.
- Moran, D. F., and Duke, C. M., "An Engineering Study of the Behavior of Public Utilities Systems in the San Fernando Earthquake of February 9, 1971," San Fernando, California, Earthquake of 9 February 1971, Bulletin 196, California Division of Mines and Geology, Sacramento, California, 1975, pp. 407-429.

Murphy, L. M. and Brazee, R. J., "Seismological Investigations of the Hebgen Lake Earthquake," Professional Paper 435-C, U.S. Geological Survey, Washington, D.C., 1964, pp. 13-17.

Myers, W. B. and Hamilton, W., "Deformation Accompanying the Hebgen Lake Earthquake of August 17, 1959," Professional Paper 435-I, U.S. Geological Survey, Washington, D.C., 1964, pp. 55-98.

NASA, "Application of Space Technology to Crustal Dynamics and Earthquake Research," NASA Technical Paper 1464, NASA Scientific and Technical Information Branch, Washington, D.C., Aug., 1979, 275 p.

Nason, R. D., "Investigation of Fault Creep Slippage in Northern and Central California," Ph.D. Thesis, University of California, San Diego, University Microfilms No. 72-12,785, Ann Arbor, Michigan, 1971a, 232 p.

Nason, R. D., "Measurements and Theory of Fault Creep Slippage in Central California," Recent Crustal Movements, Bulletin 9, The Royal Society of New Zealand, Wellington, New Zealand, 1971b, pp. 181-187.

Nason, R. D., "Increased Seismic Shaking Above a Thrust Fault," San Fernando, California, Earthquake of February 9, 1971, Vol. 3, U.S. Department of Commerce, Washington, D.C., 1973, pp. 123-126.

Nason, R. D., Philippsborn, F. R., and Yamashita, P. A., "Catalog of Creepmeter Measurements In Central California from 1968 to 1972," Open-File Report 74-31, U.S. Geological Survey, Menlo Park, California, 1974, 224 p.

Naugler, F. P. and Wageman, J. M., "Gulf of Alaska: Magnetic Anomalies, Fracture Zones, and Plate Interaction," Geological Society of America, Bulletin, Vol. 84, No. 5, May, 1973, pp. 1575-1584.

- Neuman, F., "The Utah Earthquake of March 12, 1934," United States Earthquakes, 1934, Serial No. 593, U.S. Coast and Geodetic Survey, Washington, D.C., 1936, pp. 43-48.
- Newby, A. B., "Pipelines Ride the Shock Waves," Proceedings of the Pacific Coast Gas Association, Pacific Coast Gas Association, San Francisco, California, Vol. 45, 1954, pp. 105-109.
- Newmark, N. M. and Hall, W. J., "Pipeline Design to Resist Large Fault Displacement," presented at the June, 1975, U.S. National Conference on Earthquake Engineering, held in Ann Arbor, Michigan, (Paper UILU-ENG-75-2011), pp. 416-425.
- Oakeshott, G. B., "The Kern County Earthquakes in California's Geologic History," Earthquakes in Kern County California During 1952, Bulletin 171, California Division of Mines and Geology, Sacramento, California, Nov., 1955, pp. 15-22.
- Oakeshott, G. B., "Patterns of Ground Ruptures in Fault Zones Coincident with Earthquakes: Some Case Histories," Geology Seismicity, and Environmental Impact, Special Publication, Association of Engineering Geologists, Oct., 1973, pp. 287-312.
- Oil and Gas Journal, "Alyeska Now Moving Peak Prudhoe Bay Oil Flow," Oil and Gas Journal, Vol. 75, No. 8, Feb., 1980, p. 70-78.
- Oliver, H. W., Robbins, S. L., Grannell, R. B., Alewine, R. W., and Biehler, S., "Surface and Subsurface Movements Determined by Remeasuring Gravity," San Fernando, California, Earthquake of 9 February 1971, Bulletin 196, California Division of Mines and Geology, Sacramento, California, 1975, pp. 195-211.
- O'Rourke, T. D. and Trautmann, C. H., "Analytical Modeling of Buried Pipeline Response to Permanent Earthquake Displacements," Geotechnical Engineering Report 80-4, Cornell University, School of Civil and Environmental Engineering, 1980a, 85 p.

- O'Rourke, T. D. and Trautmann, C. H., "Buried Pipeline Response to Permanent Earthquake Ground Movements," Presented at August, 1980, American Society of Mechanical Engineers, Century 2, Pressure Vessels and Piping Conference, held at San Francisco, California, 1980b, (Preprint 80-C2/PVP-78), 12 p.
- O'Rourke, T. D. and Trautmann, C. H., "Earthquake Ground Rupture Effects on Jointed Pipe," Lifeline Earthquake Engineering, Proceedings of the Second Specialty Conference of the Technical Council on Lifeline Earthquake Engineering, American Society of Civil Engineers, Aug., 1981, pp. 65-80.
- Otsuka, M., "Earthquake Magnitude and Surface Fault Formation," Journal of Physics of the Earth, Vol. 12, No. 1, May, 1964, pp. 19-24.
- Page, B. M., "Basin-Range Faulting of 1915 In Pleasant Valley, Nevada," Journal of Geology, Vol. 43, No. 7, Oct.-Nov., 1935, pp. 690-707.
- Plafker, G., "Surface Faults on Montague Island Associated with the 1964 Alaska Earthquake," Professional Paper 543-G, U.S. Geological Survey, Washington, D.C., 1967, 42 p.
- Plafker, G., "Tectonics of the March 27, 1964 Alaska Earthquake," Professional Paper 543-I, U.S. Geological Survey, Washington, D.C., 1969, 74 p.
- Plafker, G. and Brown, R. D., "Surface Geologic Effects of the Managua Earthquake of December 23, 1972," Proceedings, Conference on Managua, Nicaragua Earthquake of Dec. 23, 1972, Earthquake Engineering Research Institute, Berkeley, California, Vol. 1, 1973, pp. 115-142.
- Radbruch, D. H. and Bonilla, M. G., "Tectonic Creep in the Hayward Fault Zone, California," Circular 525, U.S. Geological Survey, Washington, D.C., 1966, 13 p.
- Radbruch, D. H. and Lennert, B. J., "Damage to Culvert Under Memorial Stadium, University of California, Berkeley, Caused by Slippage in the Hayward Fault Zone," Seismological Society of America, Bulletin, Vol. 56, No. 2, 1966, pp. 295-304.

- Richter, C. F., Elementary Seismology, W. H. Freeman & Co., San Francisco, California, 1958, 768 p.
- Rowan, L. C. and Wetlauffer, P. H., "Relation Between Regional Lineament Systems and Structural Zones in Nevada," American Association of Petroleum Geologists, Bulletin, Vol. 65-8, Aug., 1981, pp. 1414-1432.
- Scholz, C. H., "A Comparison of the San Andreas Fault with the Alpine Fault," Proceedings of the Conference on Tectonic Problems of the San Andreas Fault System, Geological Sciences, Stanford University Publications, Vol. 13, Sep., 1973, pp. 186-191.
- Segall, P. and Pollard, D. D., "Mechanics of Discontinuous Faults," Journal of Geophysical Research, Vol. 85, No. B8, Aug., 1980, pp. 4337-4350.
- Sharp, R. P., "Physiographic Features of Faulting in Southern California," Geology of Southern California, Bulletin 170, California Division of Mines and Geology, Sacramento, California, Sep., 1954, pp. 21-28.
- Sharp, R. V., Lienkaemper, J. J., Bonilla, M. G., Burke, D. B., Fox, B. F., Herd, D. G., Miller, D. M., Morton, D. M., Ponti, D. J., Rymer, M. J., Tinsley, J. C., Yount, J. C., Kahle, J. E., Hart, E. W., and Sieh, K. E., "Surface Faulting in the Central Imperial Valley," The Imperial Valley, California, Earthquake of October 15, 1979, Professional Paper 1254, U.S. Geological Survey, Washington, D.C., 1982, pp. 119-143.
- Sherard, J. L., Cluff, L. S., and Allen, C. R., "Potentially Active Faults in Dam Foundations," Geotechnique, London, Vol. 24, No. 3, Sep., 1974, pp. 367-428.
- Sieh, K. E., "Slip Along the San Andreas Fault Associated with the Great 1857 Earthquake," Seismological Society of America, Bulletin, Vol. 68, No. 5, Oct., 1978, pp. 1421-1448.

- Slemmons, D. B., "Geological Effects of the Dixie Valley-Fairview Peak, Nevada, Earthquakes of December 16, 1954," Seismological Society of America, Bulletin, Vol. 47, No. 4, Oct., 1957, pp. 353-375.
- Slemmons, D. B., "Faults and Earthquake Magnitude," State-of-the-Art for Assessing Earthquake Hazards in the United States, Miscellaneous Paper S-73-1, Report 6, U.S. Army Engineer Waterways Experiment Station, Vicksburg, Mississippi, May, 1977, 166 p.
- Slemmons, D. B., "Determination of Design Earthquake Magnitude for Microzonation," Proceedings, Third International Earthquake Microzonation Conference, National Science Foundation, Vol. 1, Jun.-Jul., 1982, pp. 119-130.
- Snedecor, G. W. and Cochran, W. G., Statistical Methods, 7th ed., The Iowa State University Press, Ames, Iowa, 1980, 507 p.
- Southern California Gas Company, "Earthquake Effects on Southern California Gas Company Facilities," San Fernando, California, Earthquake of February 9, 1971, Vol. 2, U.S. Department of Commerce, Washington, D.C., 1973, pp. 59-63.
- Steinbrugge, K. V., Zacher, E. G., Tocher, D., Whitten, C. A., and Claire, C. N., "Creep on the San Andreas Fault," Seismological Society of America, Bulletin, Vol. 50, No. 3, Jul., 1960, p. 389-415.
- Steinbrugge, K. V., Schader, E. E., Bigglestone, H. C., and Weers, C. A., "San Fernando Earthquake, February 9, 1971," Pacific Fire Rating Bureau, San Francisco, California, 1971, 93 p.
- Taber, S., "Some Criteria Used in Recognizing Active Faults," Geological Society of America, Bulletin, Vol. 34, Dec., 1923, pp. 661-668.

- Taylor, C. L., "Geologic Studies Conducted for the Alameda County Fairmont Hospital-Juvenile Hall Complex," Proceedings, Conference on Earthquake Hazards in the Eastern San Francisco Bay Area, Special Publication 1982, California Division of Mines and Geology, Sacramento, California, 1982, pp. 299-308.
- Taylor, G. C. and Bryant, W. A., "Surface Rupture Associated with the Mammoth Lakes Earthquakes of 25 and 27 May, 1980," Mammoth Lakes, California Earthquake of May 1980, Special Report 150, California Division of Mines and Geology, Sacramento, California, 1980, pp. 49-67.
- Taylor, C. L. and Cluff, L. S., "Fault Activity and its Significance Assessed by Exploratory Excavation," Proceedings, Conference on Tectonic Problems of the San Andreas Fault System, Geological Sciences, Stanford University Publications, Vol. 13, Sep., 1973, pp. 239-247.
- Taylor, C. L. and Cluff, L. S., "Fault Displacement and Ground Deformation Associated with Surface Faulting," Lifeline Earthquake Engineering, Proceedings, Specialty Conference of the Technical Council on Lifeline Earthquake Engineering, American Society of Civil Engineers, Aug., 1977, pp. 338-353.
- Taylor, C. L., Cummings, J. C., and Ridley, A. P., "Discontinuous En Echelon Faulting and Ground Warping Portola Valley, California," Studies of the San Andreas Fault Zone in Northern California, Special Report 140, California Division of Mines and Geology, Sacramento, California, 1980, pp. 59-70.
- Tchalenko, J. S., "Similarities Between Shear Zones of Different Magnitudes," Geological Society of America, Bulletin, Vol. 81, No. 5, Jun., 1970, pp. 1625-1639.
- Tocher, D., "Movement on the Rainbow Mountain Fault," The Fallon-Stillwater Earthquakes of July 6, 1954 and August 23, 1954, Seismological Society of America, Bulletin, Vol. 46, No. 1, Jan., 1956, pp. 10-14.

- Tocher, D., "Earthquake Energy and Ground Breakage," Seismological Society of America, Bulletin, Vol. 48, No. 2, Apr., 1958, pp. 147-153.
- Tocher, D., "The Alaska Earthquake of July 10, 1958: Movements on the Fairweather Fault and Field Investigation of Southern Epicentral Region," Seismological Society of America, Bulletin, Vol. 50, No. 2, Apr., 1960, pp. 267-292.
- Tugend, T., "Lifeline Earthquake Engineering: An Interview with C. Martin Duke," Earthquake Information Bulletin, U. S. Geological Survey, Washington, D.C., Vol. 12, No. 3, May-Jun., 1980, pp. 104-107.
- U.S. Geological Survey, "Borrego Mountain Earthquake, April 9, 1968," Professional Paper 787, U.S. Geological Survey, Washington, D.C., 1972, 207 p.
- U.S. Geological Survey Staff, "Surface Faulting," The San Fernando, California, Earthquake of February 9, 1971, Professional Paper 733, U.S. Geological Survey, Washington, D.C., 1971, pp. 55-76.
- Wallace, R. E., "Earthquakes of August 19, 1966, Varto Area, Eastern Turkey," Seismological Society of America, Bulletin, Vol. 58, No. 1, Feb., 1968a, pp. 11-45.
- Wallace, R. E., "Notes on Stream Channels Offset by the San Andreas Fault, Southern Coast Ranges, California," Proceedings, Conference on Geologic Problems of San Andreas Fault System, Geological Sciences, Stanford University Publications, Vol. 11, May, 1968b, pp. 7-21.
- Wallace, R. E. and Roth, E. F., "Rates and Patterns of Progressive Deformations," The Parkfield-Cholame, California Earthquakes of June-August 1966, Surface Geologic Effects, Water-Resources Aspects, and Preliminary Seismic Data, Professional Paper 579, U.S. Geological Survey, Washington, D.C., 1967, pp. 23-40.

- Weber, F. H., "Surface Effects and Related Geology of the San Fernando Earthquake in the Sylmar Area," San Fernando, California, Earthquake of 9 February 1971, Bulletin 196, California Division of Mines and Geology, Sacramento, California, 1975, pp. 71-96.
- Wesson, R. L., Helley, E. J., LaJoie, K. R., and Wentworth, C. M., "Faults and Future Earthquakes," Studies for Seismic Zonation of the San Francisco Bay Region, Professional Paper 941-A, U.S. Geological Survey, Washington, D.C., 1975, pp. A5-A30.
- Wilt, J. W., "Measured Movement Along the Surface Trace of an Active Thrust Fault in the Buena Vista Hills, Kern County California," Seismological Society of America, Bulletin, Vol. 48, No. 2, Apr., 1958, pp. 169-176.
- Witkind, I. J., "Reactivated Faults North of Hebgen Lake," Professional Paper 435-G, U.S. Geological Survey, Washington, D.C., 1964, pp. 37-50.
- Woodward-Clyde Consultants, "Geologic/Seismic Hazards Evaluation, Fairmont Hospital-Juvenile Hall, San Leandro, California," prepared for the Alameda County Public Works Agency, Hayward, California, Dec., 1978, 118 p.
- Youd, T. L., and Olsen, H. W., "Damage to Constructed Works Associated with Soil Movements and Foundation Failures," The San Fernando, California, Earthquake of February 9, 1971, Professional Paper 733, U.S. Geological Survey, Washington, D.C., 1971, pp. 126-132.

